MINIMUM ORDER LINEAR SYSTEM IDENTIFICATION AND PARAMETER ESTIMATION WITH APPLICATION

A THESIS SUBMITTED TO
THE GRADUATE SCHOOL OF NATURAL AND APPLIED SCIENCES
OF
MIDDLE EAST TECHNICAL UNIVERSITY

BY

ONUR CEM ERDOĞAN

IN PARTIAL FULFILLMENT OF THE REQUIREMENTS
FOR
THE DEGREE OF MASTER OF SCIENCE
IN
MECHANICAL ENGINEERING

SEPTEMBER 2014

Approval of the thesis:

MINIMUM ORDER LINEAR SYSTEM IDENTIFICATION AND PARAMETER ESTIMATION WITH APPLICATION

submitted by **ONUR CEM ERDOĞAN** in partial fulfillment of the requirements for the degree of **Master of Science in Mechanical Engineering Department, Middle East Technical University** by,

Prof. Dr. Canan Özgen
Dean, Graduate School of **Natural and Applied Sciences** _____

Prof. Dr. Suha Oral
Head of Department, **Mechanical Engineering** _____

Prof. Dr. Tuna Balkan
Supervisor, **Mechanical Engineering Dept., METU** _____

Prof. Dr. Bülent E. Platin
Co-supervisor, **Mechanical Engineering Dept., METU** _____

Examining Committee Members:

Assist. Prof. Dr. Buğra Koku
Mechanical Engineering Dept., METU _____

Prof. Dr. Tuna Balkan
Mechanical Engineering Dept., METU _____

Prof. Dr. Bülent E. Platin
Mechanical Engineering Dept., METU _____

Assist. Prof. Dr. Yiğit Yazıcıoğlu
Mechanical Engineering Dept., METU _____

M.Sc. Burak Gürcan
Manager of SSTT Dep., ASELSAN Inc. _____

Date: 02/09/2014

I hereby declare that all information in this document has been obtained and presented in accordance with academic rules and ethical conduct. I also declare that, as required by these rules and conduct, I have fully cited and referenced all material and results that are not original to this work.

Name, Last name : ONUR CEM ERDOĞAN
Signature :

ABSTRACT

MINIMUM ORDER LINEAR SYSTEM IDENTIFICATION AND PARAMETER ESTIMATION WITH APPLICATION

Erdoğan, Onur Cem

M.S., Department of Mechanical Engineering

Supervisor : Prof. Dr. Tuna Balkan

Co-Supervisor : Prof. Dr. Bülent E. Platin

September 2014, 172 pages

Design, control, and investigation of complex systems require a tool to understand and model system behavior. This tool is the system identification, which convert the system response to a mathematical formulation. During the identification phase, the utilized model is important to convey system behavior. In this study, a number of minimum order and non-parametric system identification algorithms are implemented for the identification of linear time invariant mechanical systems. For this purpose, impulse response determination methods are investigated to obtain system behavior. State space modeling and special models used in the identification process of physical systems are investigated. Two system realization algorithms implementing minimum order non-parametric linear system identification are presented. A transformation based method for the extraction of physical system parameters from a real system model is represented. The suggested methods are implemented on both simulation and test data for different system models to investigate their effectiveness and performance.

Keywords: Linear System Identification, State Space Modeling, Minimum Order System Identification, Inverse Vibration Problem, Wavelet Analysis, Parameter Estimation in Physical Systems

ÖZ

DOĞRUSAL SİSTEMLERİN EN AZ DERECELİ MODELLER İLE UYGULAMALI OLARAK TANILANMASI VE PARAMETRELERİNİN TAHMİNİ

Erdoğan, Onur Cem

Yüksek Lisans, Makina Mühendisliği Bölümü

Tez Yöneticisi : Prof. Dr. Tuna Balkan

Ortak Tez Yöneticisi : Prof. Dr. Bülent E. Platin

Eylül 2014, 172 sayfa

Karmaşık sistemlerin tasarımı, kontrolü ve incelenmesi sistem davranışını anlayacak ve modelleyecek bir aracı gerektirmektedir. Sistem tepkilerini matematiksel bir formülasyona çevirecek bu araç sistem tanılamasıdır. Sistem tanılamasında kullanılacak model, tanılama işleminin performansında en önemli role sahiptir. Bu çalışmada, doğrusal ve parametreleri zamanla değişmeyen mekanik sistemler için en az mertebeli ve parametrik olmayan tanılama yöntemleri kullanılmıştır. Bu amaçla, sistemin dürtü yanıtını bulan yöntemler incelenmiştir. Fiziksel sistemlerin durum uzayında modellenmesi incelenmiş ve tanılamaya özel kullanılan modellere yer verilmiştir. Doğrusal sistemler için en az mertebeli ve parametrik olmayan sistem tanılaması gerçekleştiren iki yöntem sunulmuştur. Gerçek bir sistemin parametrelerini dönüşüm matrisleri yardımıyla saptayan bir yöntem önerilmiştir. tanıtılmıştır. Önerilen yöntemlerin etkinlikleri ve başarımları değişik sistem modellerinin benzetim ve test verilerine uygulanarak değerlendirilmiştir.

Anahtar kelimler: Doğrusal Sistem Tanılaması, Durum Uzayında Modelleme, En Az Mertebeli Tanılama, Ters Titreşim Problemi, Dalgacık Analizi, Fiziksel Sistemlerde Parametre Kestirimi

To my lovely family and,

To Gizem ,

ACKNOWLEDGEMENTS

First, I would like thank to my advisor, Prof. Dr. Tuna BALKAN and my co-advisor, Prof. Dr. Bülent Emre PLATİN for their guidance, support and suggestions throughout this study.

I would like to express my gratitude to Dr. Murat Gültekin and Mr. Burak GÜRCAN for providing valuable guidance and support during this study.

I would also like to express my appreciation to Eyyüp Sincar, Boran Kılıç, Özgüler Mine Azgın and Akın Dalkılıç for their valuable support, motivation and help.

I would also like to thank TÜBİTAK for providing financial support during this study.

I would like to express my deepest gratitude to my family, for their endless understanding, support and motivation during this study.

TABLE OF CONTENTS

LIST OF TABLES

TABLES

LIST OF FIGURES

FIGURES

LIST OF SYMBOLS AND ABBREVIATIONS

A	:	State transition matrix
B	:	Input-state influence matrix
C	:	State-output influence matrix
D	:	Direct input-output influence matrix
P_{α}	:	Observability matrix
Q_{β}	:	Controllability matrix
Y	:	Markov Parameters
H	:	Hankel Matrix
$\aleph$	:	Correlated Hankel Matrix
Φ	:	Mass normalized undamped eigenvectors
Ω	:	Mass normalized undamped eigenvalues
Ξ	:	Modal damping matrix
ζ	:	Modal damping ratio
w_{ni}	:	Undamped natural frequencies
Ψ	:	Complex eigenvectors
Λ	:	Complex eigenvalues

X	:	Complex mode shapes
S	:	Scaling matrix
ϕ	:	Wavelet scaling function
ψ	:	Mother wavelet function
e_t	:	Distributed normalized random variable
$A(z), B(z), C(z)$	:	Polynomials
$u(t)$	:	Input signal
$y(t)$	:	Output signal
λ	:	Selected variable
a_0	:	Scaling constants
b_0	:	Shifting constants
z	:	Shifting operator
m, j	:	Level of wavelet transform
u^{DWT}	:	Discrete wavelet transform of the input signal
D	:	Diagonal scaling matrix
W	:	Wavelet transformation matrix
k	:	Shifting operator
$g[n]$	:	Highpass filter

$h[n]$	:	Lowpass filter
$x[n]$	:	Discrete signal
$x(t)$	:	Continuous signal
N	:	Number of samples of a signal
$h(\theta)$	:	Temporal impulse response
θ	:	Normalized time variable
n	:	Number of states
m	:	Number of outputs
r	:	Number of inputs
M	:	Mass matrix
D	:	Damping matrix
K	:	Stiffness matrix
$\hat{B}_m$	:	Estimated modal input state matrix
$\hat{C}_m$	:	Estimated modal output state matrix
$\hat{q}$	:	Identified modal time history
$\overline{q}$	:	Actual modal time history
σ_i	:	Real part of the characteristic system root
w_i	:	Imaginary part of the characteristic system root

I_γ	:	Identity matrix of order γ
O_γ	:	Null matrix of order γ
R	:	Left unitary matrix
Σ	:	Diagonal eigenvalue matrix
S	:	Right unitary matrix
P_ξ	:	Block correlation observability matrix
Q_ζ	:	Block correlation controllability matrix
MRA	:	Multi resolution analysis
DWT	:	Discrete wavelet transform
FFT	:	Fast Fourier transform
PDV	:	Physical displacement velocity model
MDV	:	Modal displacement velocity model
ERA	:	Eigensystem realization algorithm
ERA/DC	:	Eigensystem realization algorithm with data correlation
MAC	:	Modal amplitude coherence
MSV	:	Mode singular value
IR	:	Impulse response
CBSI	:	Common basis normalized structural identification
FRF	:	Frequency response function

SVD	:	Singular value decomposition
DOF	:	Degrees of freedom
PEM	:	Prediction error method

CHAPTER 1

INTRODUCTION

Mechanical design, construction, investigation, and control of complex systems always become the main objective of engineering practice. Moving objects always attracted the engineers' attention and their will to manipulate them is getting more and more demanding. During this course, engineers try to understand static and dynamic characteristics of the plant of their interest. Understanding the system, provides engineers to better optimize system parameters according to the design requirements which derives design for lighter, smaller and more agile systems. In addition to that, understanding real system provides a feedback and a mathematical model to the design engineer about how good their initial design meets the requirements and enables them to predict system behavior under different operating conditions. Additionally, monitoring system behavior under operational conditions conveys information about the health of the system.

System identification is the name given to the process devoted to mathematically representing real system behavior and it is defined by Juang as "Identification is the course of developing mathematical models for physical system by using experimental data" [1]. In the literature, there are various methods and implementations of system identification techniques and their growth followed a similar progress with the demand on control action. Although for structural design considerations, the finite element method provides accurate models and these models can be further improved by implementing static and dynamic testing, this traditional approach to obtain system models generally is not accurate enough to be

used in the control design application. This is why system realization became a key component in the system identification application.

Identification procedures are generally dependent on the purpose of the identification application. Different requirements like control implementation, finite element model correction/updating and health monitoring/damage detection may require different identification schemes and additional procedures.

Identification problem also incorporates the model selection criteria and there are some techniques that work with pre-defined models during system identification application. However as defining model for a complex system is a complicated and tedious task, non-parametric modeling is generally preferred depending on the type of the identification problem.

1.1 AIM OF THESIS

This study is resulted from the identification and modeling requirement of the stabilized gun platforms developed at ASELSAN. Those stabilized machine gun platforms are designed for remote control of machine guns to compensate the disturbances resulting from the motion of the hull vehicles. Some examples of such platforms are shown in Figure 1.1. Those platforms are capable to move in the azimuth and elevation directions and have gyroscopes as inertial speed measuring sensors on the both axes of their line of fire such that they can counteract against the disturbances coming from the base platform movements. Those base platforms can be naval or land vehicles as well.

In order for these stabilized platforms to counteract against disturbances coming from their base, they require a mean of control action. For this reason, the degree of control action directly determines the performance of those systems and in order to make these stabilized platforms more agile and precise, more compact designs and better control implementations are the key requirements. For this purpose, by finding mass and stiffness distribution of the system, the best possible sensor locations and

effective control action over the lumped masses can be determined. In addition to that, model based design can be implemented on those systems by realizing a state space system model as nearly whole modern control techniques utilize state space system representation. Finally, the identified models can be used to monitor the health of the system by repeating realization application over time and comparing results with the initial realization results.

Figure 1.1 Stabilized Machine Gun Platforms Developed by ASELSAN [2]

For the reasons stated above, a system identification procedure is required in the development of such stabilized platforms. The main objective is to find minimum order system model, so that the physical system will be represented mathematically and physical system parameters are obtained from the measured system input and

output data in terms of the mass, stiffness, and damping matrices. During developing those models, the main assumption is the linear time-invariant (LTI) system characteristics. In order to conserve physical system interpretation and minimize the requirement on the user expertise, non-parametric and deterministic modeling approaches will be implemented. Non-parametric modeling means that the physical domain of the system is known, which is the mechanical system represented by second order differential equations. However, in this study, the actual order or model length is unknown in non-parametric modeling and the order of the system should also be determined during the identification implementation. In addition to that, deterministic modeling approaches will be utilized in this study in order to simplify the identification process and decrease dependence on statistical analysis. By implementing deterministic identification approach, the system order can be determined in a more analytical and systematic way.

1.2 HISTORY OF SYSTEM IDENTIFICATION

The term system identification was first coined by Lotfi Zadeh in 1962. His definition for system identification was that, "Identification is the determination, on the basis on input and output of a system within a specified class of systems, to which the system under test is equivalent" [3]. This definition was implying high dependency on the system under test and it does not convey the statistical content of system identification. However, it became the standard terminology in the control community since then. Additionally, the terminology and methods of identification spread out of control community to other fields like, statistics, econometrics, geophysics, signal processing, etc.

Starting with Gauss (1809) up to 1960s, explicit parametric models, in which a pre-determined model is utilized, were the major concern of the control community.

Several methods in system identification rely on variants of time series analysis, and further development on spectral and parametric methods for time series was started

by Yule (1927) [3]. During this period of time, nearly all the essential statistical concepts used in system identification had appeared. Linear regression, least squares method (Wald 1943), and maximum likelihood methods (Fisher 1912), (Wald 1949), (Cramer 1946) constitute the foundations of modern system identification theory [3]. According to Ljung, stochastic approximation, (Robbins and Monro 1951) was developed in the beginning of 1950s and then it gave inspiration to recursive identification techniques [3]. Up until late 1950's much of control design relied on classical methods like Bode, Nyquist or Ziegler-Nichols charts, or on step response analyses. Also these methods were only limited to single input single output (SISO) systems.

Number and depth of system identification studies have grown with the demand and development of feedback control applications over time. Around 1960, the demand for control activities increased significantly so that, parametric modeling and estimation activities gain acceleration [4]. Around 1960's Kalman introduced the state-space realization and stated the foundations of state-space based optimal filtering and optimal control theory with Linear Quadratic (LQ) optimal control as a cornerstone of the model based control design [4].

At the third IFAC (International Federation of Automatic Control) Congress in London in 1966, a survey paper on the current status of system identification was presented by Eykhoff et al. [3]. A year later, in 1967, the first IFAC Symposium on system identification was organized in Prague. Since then, system identification has been an important subject of automatic control with regular sessions at all general control meetings like the CDC and IFAC Congress.

The status of identification field was described by Åström and Eykhoff (1971) in their survey paper by the following quotation [5] : "The field of identification is at the moment rather bewildering, even for the so-called experts. Many different methods are being analyzed and treated. 'New Methods' are suggested en masse, and, on the surface, the field looks more like a bag of tricks than a unified subject. "

The reason why there was not much improvement and comparison between the models was because there was not enough computing power and access to other methods. In addition to that, there were no common models used in various identification algorithms. Each researcher was using their own model sets with varying noise and distortion models, and after they implement their own model structure and find good results, their own suggested algorithms were being superior among all the other identification schemes. However, there were not enough evidence and comparison between the model structures and their implementations such that, most of the suggested methods could not go further than implementing different noise models and model structures on specific problems rather than being different methods.

In the year 1965 there appeared two landmark papers of Åström and Bohlin (1965) [6], and Ho and Kalman (1965) [7], which gave birth to two main streams of research areas that dominated the development of system identification in the control community even until today.

Åström and Bohlin (1965) revealed the foundations of maximum likelihood methods based on parametric single input, single output models in their paper [6]. Their theory depends on the analysis of time series for estimation of parameters included in the difference equations. In the statistical literature, they are known as ARMA (Auto Regressive Moving Average) or ARMAX (Auto Regressive Moving Average with eXogeneous input) models. These models and the maximum likelihood methods later evolved into the successful prediction error identification framework, which relies on the statistical aspect of the identification implementation [4].

In their paper Åström and Bohlin (1965) introduced the maximum likelihood method for parameter estimation of models in ARMAX form as follows [4].

$$A(z^{-1})y_t = B(z^{-1})u_t + \lambda C(z^{-1})e_t \tag{1.1}$$

where e_t is a sequence of identically distributed normalized $(0,1)$ random variable, where z denotes the shifting operator. The maximum likelihood method has been extensively examined and studied in statistics for its application to various time series models [4]. Beyond the success of this methodology, Åström and Bohlin (1965) gave the complete algorithmic derivations and development of the maximum likelihood method for ARX and ARMAX models. In addition to that, they performed and presented the whole asymptotic consistency, efficiency, and normality analyses for the validation of the estimated parameters with model order.

Furthermore, the concepts and notations used by Åström and Bohlin (1965) were accepted by the whole identification community, so that they are even used in today's analyses in the same form. Therefore, Åström and Bohlin (1965) constructed the foundation for the parametric identification. They gave the fundamentals of maximum likelihood approach and the foundations of prediction error framework with slight improvements in the noise models. However, as this approach is concentrated on representing the system model with the best approximation, the real system parameters do not have any significance. As the main objective of this thesis is determination of the actual system parameters, the maximum likelihood and prediction error like methodologies are not appropriate in this manner.

Whereas in 1965 Ho and Kalman introduced the first solution to the challenging minimum order realization concept in the complete contrast to maximum likelihood framework [7]. In their analysis, the state space representation of the input-output model is given by the following general expression.

$$\begin{aligned} x_{t+1} &= Ax_t + Bu_t \\ y_t &= Cx_t \end{aligned} \tag{1.2}$$

The above expression was simplified by using the shifted impulse response history matrix, called as *Hankel matrix* , H_k as the following.

$$y_t = \sum_{k=1}^{\infty} H_k u_{t-k} \tag{1.3}$$

where

$$H(z) = \sum_{k=1}^{\infty} H_k z^{-k} \tag{1.4}$$

The problem here is to replace the infinite description of $H_k \in \mathbb{R}^{p\times m}$ with the expression for A, B, and C matrices where $A \in \mathbb{R}^{n\times n}, B \in \mathbb{R}^{n\times m}, C \in \mathbb{R}^{p\times n}$ providing that

$$H(z) = C(zI - A)^{-1}B \tag{1.5}$$

with the dimension of A being minimal. They separated the problem into two parts, first part is finding the McMillan degree of $H(z)$, which then provides the minimum dimension for matrix A. Second problem is the computation of A, B, and C matrices.

Here, the solution brought by Ho and Kalman is the utilization of the Hankel matrix, and its factorization into the product of controllability and observability matrices as follows.

$$\begin{aligned} H &= \begin{bmatrix} H_1 & H_2 & H_3 & \cdots \\ H_2 & H_3 & H_4 & \cdots \\ H_3 & H_4 & H_5 & \cdots \\ \vdots & \vdots & \vdots & \ddots \end{bmatrix} \\ H &= \begin{bmatrix} C \\ CA \\ CA^2 \\ \vdots \end{bmatrix} \begin{bmatrix} B & AB & A^2B & \cdots \end{bmatrix} \end{aligned} \tag{1.6}$$

If the McMillan degree of $H(z)$ is determined as n, then, the $rank(H) = n$, and there exist a solution for A, B, and C matrices such that $H_k = CA^{k-1}B$.

Although Ho and Kalman introduced the theory underneath the minimum order system realization algorithm in 1965, researchers could understand their theory years later. With their approach, Ho and Kalman formed the basis for linear system identification and realization theory. The solution of the minimum order realization problem was then extended by Akaike (1974) [8] and others to be used in stochastic realization, where a Markovian model is utilized for a purely random process. This methodology then extended in the early 90's to also include control input and became known as the subspace identification [4]. In this thesis as the major concern is to find the model of the "true system", therefore minimum order realization algorithms that are further improved versions of Ho and Kalman's algorithm will be utilized.

Box and Jenkins published a book in 1970 [9], which provided momentum on the real life application of identification. In fact, that book explained the whole identification process starting from the initial data analysis up to the estimation of a model. The methodology involved in that book is mainly based on the time series methods and correlation analysis for determination of the model structures. The book remained as a major reference book in the identification area for about two decades. In addition to the book of Box and Jenkins, the other references were the survey paper published by Åström and Eykhoff in 1971 [5] and a paper by Akaike involving other special topics on system identification and time series analysis published in 1974 [8].

According to Gevers from the middle seventies, the prediction error framework dominated identification theory and its applications. The main concern was the identifiability problem for both multivariable and closed loop systems. Again, nearly all the focus was concentrated on the search of "true system" [4].

As Gevers stated, in the seventies, around 1978, Anderson et al, Ljung and Caines were started research on the best possible approximation of the "true system", rather than searching for the "true system" [4]. This concept guided the identification community searching from "true system" to characterization of the best possible approximation. Therefore, the error utilized in the identification process became the main research objective. Later in 1986, Ljung and Wahlberg [10] provided a theory for investigating model bias and variance, which guided researchers to move on to the transfer function errors rather than dealing with bias and variance errors. During this period of time, Ljung's one of the major contribution was eliminating vast majority of identification techniques suggested by different researchers. Ljung also separated and pointed two major concepts as the choice of parametric model structure and the choice of an identification criterion. After Ljung's approach, most of the existing parametric identification techniques were found out to be the particular cases of the prediction error framework.

The work on bias and variance analysis lead researchers to a new concept of considering identification as a "design problem". Starting from the experiment design, the choice of model structure, the criteria for choosing model and other parameters became design criterion so that one can adjust those parameters in the objective of identification [11].

In the year 1984, Juang and Pappa [12] improved the minimum order state space realization technique, which was originally developed by Ho and Kalman so that, they revealed the eigensystem realization algorithm (ERA). They also presented application of ERA to Galileo spacecraft. In the preceding years, Juang proposed further improvements for ERA with other researchers [13].

A book published by Ljung [11] in 1987 made a major impact on the identification community by emphasizing the view of system identification as a design problem, where selected models plays the crucial role. In this book, the statistical and system

identification point of views are clearly differentiated by pointing the main objective that, the model must explain the data in hand as accurate as possible.

Being able to design system identification, model qualities were improved significantly so that a model based identification concept had appeared starting from the beginning of 90's [11]. In the preceding years, in addition to the model based robust controller design, the concept of designing system identification opened new research areas as closed-loop identification, frequency domain identification and uncertainty analysis [4].

As Gevers stated, around 90's, the identification of multiple input multiple output (MIMO) systems became the major concern. With the development of numerically robust procedures based on singular value decomposition (SVD) and least squares techniques, subspace based algorithms could manage to solve identification for MIMO systems. In the early 90's, different research groups (Larimore,1990; Van Overschee and De Moor 1994; Verhaegen,1994; Viberg,1995) provided closely related methodologies for Subspace identification algorithms [4]. Subspace algorithms started from the minimum order realization concept coined by Ho and Kalman (1965) [7], then they evolved by incorporating the stochastic methodologies. Until today, subspace algorithms continued their improvement with various other improved versions like the famous numerical algorithms for subspace state space system identification (N4SID) algorithm. However, the order determination became less straightforward over the development of subspace methods, such that oversized model structures generally results from subspace identification techniques, because of their stochastic implementation, so that subspace identification techniques are not utilized in this study.

1.3 RELEVANT IDENTIFICATION TECHNIQUES AND THEIR IMPLEMENTATIONS

In this study the main objective is to find a minimum order system realization so that, physical system parameters can be obtained from this representation. For this reason, when the history of system identification is investigated, Ho and Kalman's minimum order realization theory best suits to the solution of stated problem. However, due to vulnerability of Ho and Kalman's theory to measurement noise, an improved version of their original theory is required. At this point, the eigensystem realization algorithm (ERA) which is developed by Juang and Pappa, seems like the best solution as their implementation of minimum order realization problem is capable to suppress measurement noise. In addition to that, Juang and Pappa revealed real life implementation of ERA on Galileo spacecraft, which proves effectiveness of their algorithm. To sum up, since ERA has a straightforward implementation and it is a numerically robust algorithm, it will be implemented as the main realization algorithm in this study.

1.3.1 Eigensystem Realization Algorithm (ERA)

In 1984, Jer-Nan Juang and Richard Pappa [12], as researchers at NASA Langley Research Center, working on large space structures developed ERA by adopting and improving the state space formulation given by Ho and Kalman. Their main focus was to develop an algorithm to accurately determine modal parameters and identify reduced system model in order to better interact structures with the control discipline. They observed that, Ho and Kalman's algorithm is susceptible to noise on the analyzed data, and noise can adversely affect the order of the realized system model. Juang and Pappa incorporated SVD into the Ho and Kalman's algorithm to determine the true order of the system and to improve noise suppression and accuracy in the realized system models. The computational details of ERA are given in Chapter 4.

In addition to the ERA, Juang and Pappa [12] developed performance measures of the realized model by using modal amplitude coherence (γ) and modal phase collinearity (μ) as will be discussed in the Chapter 4.

In order to verify their algorithm, Juang and Pappa, used Galileo spacecraft shown in Figure 1.2, which was later sent to Jupiter's orbit. All the appendages including SXA (S-/X-Band Antenna) were fixed to the vehicle at their stowed positions. In addition to that, all the structure was cantilevered from its base by bolting its bottom adapter ring to a massive seismic block. In order to give dynamic excitation, several shakers all with 100 N capacity were attached to many different locations. In addition to that responses were recorded from 162 accelerometers that were distributed over the whole test structure.

In order to compare test data, a finite element model of the Galileo Spacecraft was constructed and from the identified model, 45 modes of vibration below 50 Hz were obtained with the lowest frequency at about 13 Hz. However, according to the amplitude and collinearity considerations, only about 15 modes were major contributors, the others did not contribute significantly to the dynamic behavior of the spacecraft in its launch configuration.

The excitation given to the system was limited to the frequency interval of 10 to 45 Hz, and at each measurement, two output data sets for both vehicle axes were recorded. The sampling frequency of the measurement system was at 102.4 Hz and each test approximately took 5 seconds. Therefore at each test approximately 500 free response data was recorded.

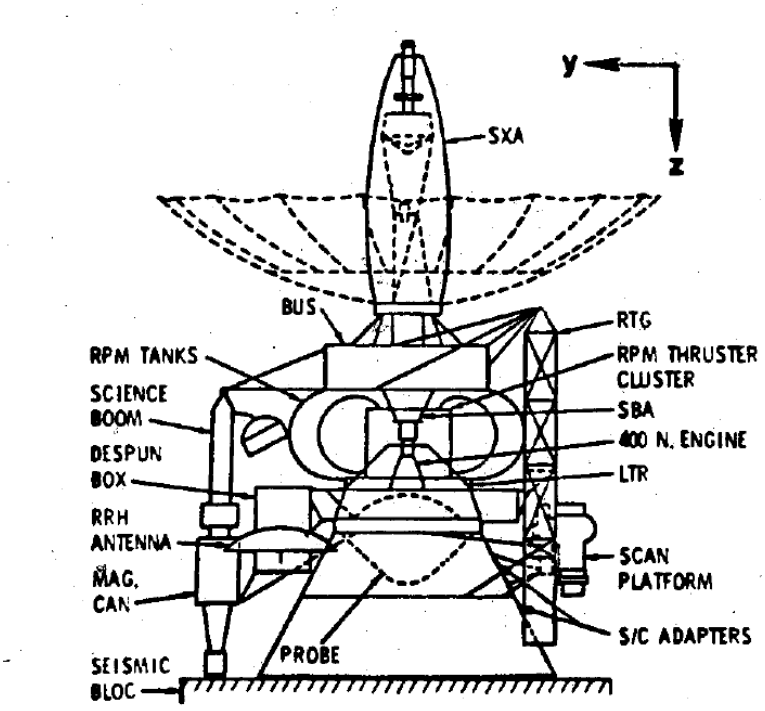

Figure 1.2 Galileo Spacecraft in the launch configuration [12]

After the tests were completed, an ERA analysis were conducted using all 162 response measurements and one initial condition for each test run. In this configuration the Hankel matrix (H_{rs}) was formed by 324 rows and 500 columns of data in the analysis. The summary of the test results for x axis can be found in Table 1.1. Identified frequencies, damping factors and accuracy indicators for each mode are given in Table 1.1. According to the authors, the identified results closely agree with the other experimental identification techniques.

In the ERA implementation, the major accuracy indicator was stated as the model amplitude coherence (γ) which is also given in Table 1.1. The modal amplitude coherence represents the purity of each individual modal amplitude time history. For each identified eigenvalue, a corresponding modal amplitude time sequence is obtained depending on each initial condition. The obtained time sequence of modal amplitudes provide a direct indication of the strength of identification for each mode

in the ERA analysis. For strongly identified modes, the modal amplitude history becomes an exponentially decaying function over time, however for the weakly identified modes, the history becomes distorted. Examples of modal amplitude history for strongly and weakly identified mode were given in the study of Juang and Pappa. To sum up, Juang and Pappa visualized the dynamic response of the reconstructed system model and verified that the identified system exhibited a good agreement as shown in Figure 1.3.

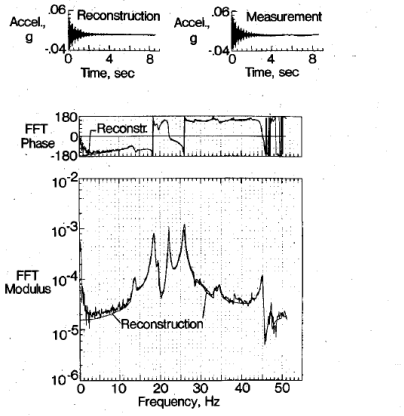

Figure 1.3 ERA Reconstruction Comparison with Test Data [12]

Table 1.1 X Axis ERA Results for Galileo Spacecraft [12]

Mode No.	Frequency, Hz	Damping factor, %	Accuracy indicators			
			γ[a]	μ[b]	Max.[c]	No.[d]
1	13.613[e]	3.301	98.6[e]	99.0	0.104	6
2	14.153[e]	1.645	99.8[e]	94.2	0.063	5
3	18.369[e]	1.409	99.7[e]	98.7	0.270	59
4	18.680[e]	1.086	99.7[e]	79.8	0.068	17
5	19.516[e]	0.659	96.5[e]	99.1	0.090	23
6	22.040	8.311	50.7	43.1	0.009	0
7	22.047[e]	0.777	98.9[e]	97.7	0.122	58
8	22.132[e]	0.356	97.5[e]	99.3	0.088	45
9	22.640[f]	1.282	93.1[f]	86.6	0.018	4
10	25.126[e]	1.515	99.8[e]	89.8	0.239	27
11	25.751[g]	5.569	80.2[g]	56.2	0.043	15
12	25.871[e]	0.806	98.6[e]	99.4	0.279	67
13	28.517[e]	0.835	97.7[e]	98.0	0.121	10
14	29.659[f]	1.723	91.7[f]	61.2	0.010	1
15	30.940[e]	3.003	98.2[e]	77.1	0.059	5
16	32.828	6.668	67.9	52.8	0.015	2
17	33.288[f]	2.894	93.4[f]	44.0	0.012	4
18	33.613[e]	1.326	98.1[e]	59.8	0.024	3
19	34.402[e]	1.057	98.2[e]	98.4	0.047	15
20	36.890[f]	1.633	93.3[f]	73.1	0.020	2
21	37.631	5.957	50.0	76.2	0.041	2
22	38.019[f]	0.575	94.1[f]	44.9	0.008	0
23	39.551	4.048	75.5	99.2	0.240	5
24	41.021[f]	2.038	92.4[f]	89.8	0.123	17
25	42.169	3.737	65.2	89.1	0.022	6
26	42.273[f]	1.124	92.9[f]	68.5	0.011	3
27	43.758[f]	1.614	94.2[f]	57.7	0.019	3
28	44.892[e]	0.394	99.4[e]	99.1	0.513	24
29	45.173	4.188	79.6	67.0	0.021	6
30	45.174	0.835	78.5	78.7	0.041	3
31	47.191[g]	2.126	84.3[g]	50.8	0.008	0
32	48.311[f]	1.214	94.4[f]	78.3	0.034	5
33	48.414	3.300	59.2	57.0	0.014	3
34	50.385[g]	1.143	89.5	40.2	0.027	3

[a] γ%: Modal amplitude coherence.
[b] μ%: Modal phase collinearity.
[c] Maximum modal participation in g's among the 162 components identified. (The measurement noise floor was approximately 0.002 g.)
[d] Number of mode shape components of 162 with initial response amplitude >0.01 g. Indicator of local or global response.
[e] $95\% \leq \gamma \leq 100\%$.
[f] $90\% \leq \gamma < 95\%$.
[g] $80\% \leq \gamma < 90\%$.

1.3.2 Eigensystem Realization Algorithm with Data Correlation (ERA/DC)

After a successful application of ERA, in order to improve noise suppression of the methodology, a data correlation improvement was obtained by Juang [1]. In the data correlated version, the auto and cross correlations over a defined number of lag values was considered on the system output data. ERA/DC also requires a pulse-response history as its primary input about system characteristics.

In order to verify the success of the suggested data correlation procedure, Lew, Juang, and Longman [14] conducted a comparison study among four different identification techniques including both ERA and ERA/DC. The comparison was made on the simulated model of mini mast structure obtained from a finite element analysis [14]. The mini mast structure which is shown in Figure 1.4, is a benchmark problem on which both European and American researchers tested different identification algorithms.

On their comparison, Lew, Juang and Longman tested different algorithms for analyzing the system data with the addition of different noise characteristics. In addition to the characteristics of the algorithms, comparison is also made on their computational performances.

According to their test results, ERA and ERA/DC gave the best and close results for the noise free case. With the addition of noise, ERA/DC outperformed ERA and the other two algorithms as expected.

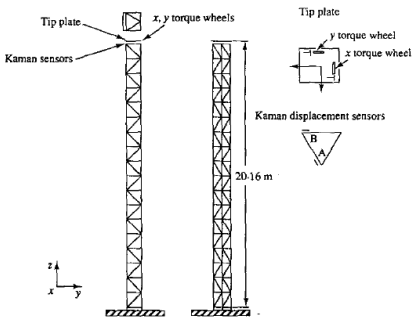

Figure 1.4 Mini-Mast Structure [14]

After Juang and Pappa had exhibited a superior performance of their ERA for non-parametric minimum order system realization, lots of researchers investigated performance of their realization algorithm on both simulation and test data. Chuang, Chen and Tsuei [15] investigated performance of both ERA and ERA/DC on both 2 DOF and 7 DOF simulation models and they performed a modal test on an acrylic beam. Their simulation models are shown in Figure 1.5 and Figure 1.6.

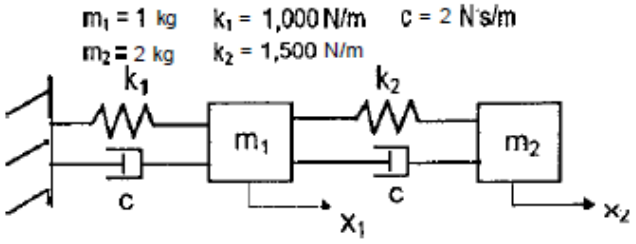

Figure 1.5 2DOF Simulation Model [15]

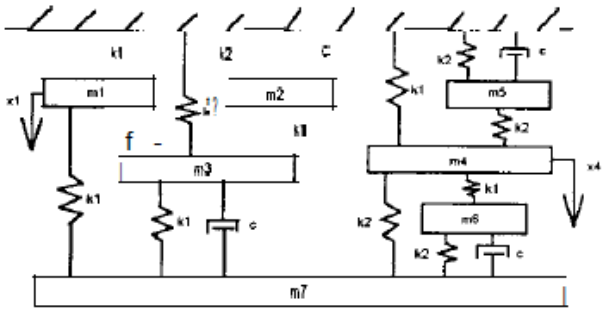

Figure 1.6 7DOF Simulation Model [15]

They presented results of identified natural frequencies and modal damping values from both realization algorithms, as tabulated in Table 1.2 and Table 1.3, respectively.

Table 1.2 Realization Results for 2 DOF Simulation System [15]

ω_i(Hz)/ζ_i(%)	Exact	ERA-DC			ERA
		$\mathcal{R}_{16,16}$	$\mathcal{R}_{8,8}$	$\mathcal{R}_{4,4}$	$H_{2\times229\times2}$
1	2.52 1.44	2.52 1.41	2.52 1.41	2.52 1.43	2.53 2.64
2	8.72 4.15	8.71 4.28	8.70 4.28	8.70 4.40	8.68 4.82

(The quantities with shadow mean larger error)

Table 1.3 Realization Results for 7 DOF Simulation System [15]

ω_i(Hz)/ζ_i(%)	Exact	ERA-DC		ERA
		$\mathcal{R}_{144,144}$	$\mathcal{R}_{144,36}$	$H_{18\times2,64\times7}$
1	13.40 1.40	13.40 1.41	13.40 1.41	13.40 1.42
2	22.89 5.05	22.88 5.12	22.88 5.12	22.90 5.31
3	28.15 4.31	28.16 4.38	28.16 4.39	28.27 4.63
4	28.88 4.36	28.95 4.33	28.95 4.34	28.97 4.52
5	40.85 2.21	40.81 2.23	40.81 2.23	40.81 1.96
6	41.38 7.09	41.57 6.97	41.57 7.03	
7	45.99 4.12	46.04 4.01	46.04 4.02	44.84 3.88

(The quantities with shadow mean larger error)

When the results of identification applied are investigated, it is observed that both algorithms are capable to yield good approximation; however, ERA/DC computes slightly improved results, as expected.

In another study, Sanchez-Gasca [16] investigated torsional modes of turbine generator shown in Figure 1.7 by using ERA.

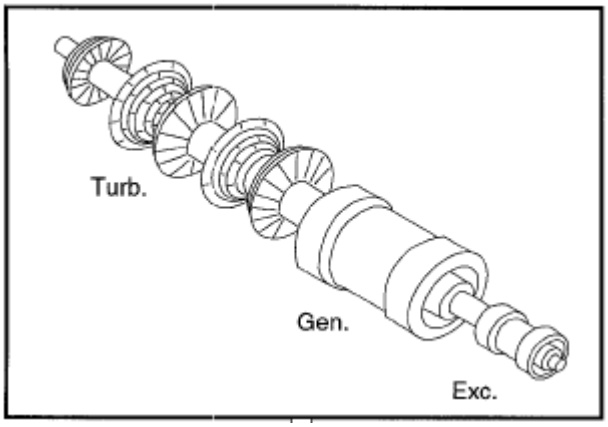

Figure 1.8 Tested Turbine Generator [16]

In his study, Sanchez-Gasca implemented modal testing on the actual generator and he represented torsional modes identified with ERA for 7 different testing and compared them with the torsional modes computed from exponential fitting method as given in Table 1.4.

Table 1.4 Torsional Modes Identified by ERA [16]

Case	Tfrm sec	Np	Δt msec	dim (H)	Telap sec	8.2 Hz mode		14.7 Hz mode		19.5 Hz mode		21.7 Hz mode	
						f	ξ	f	ξ	f	ξ	f	ξ
1	8.0	728	11	256x 600	7	8.18	.0030	14.66	.0014	19.49	.0009	21.71	.0005
2	8.0	1067	7.5	534x 800	46	8.18	.0031	14.66	.0014	19.49	.0009	21.71	.0006
3	7.0	934	7.5	368x 750	19	8.18	.0030	14.66	.0014	19.48	.0009	21.71	.0007
4	7.0	637	11	274x 500	7	8.18	.0030	14.66	.0014	19.48	.0009	21.71	.0007
5	6.0	801	7.5	302x 650	11	8.18	.0031	14.66	.0014	19.48	.0009	21.72	.0007
6	6.0	546	11	192x 450	3	8.18	.0030	14.66	.0014	19.48	.0009	21.71	.0005
7	5.0	667	7.5	334x 500	10	8.18	.0030	14.66	.0014	19.48	.0009	21.72	.0003

Therefore, once again, the superior performance of the ERA is verified in [16].

Another important study is conducted by Petsounis and Fassois [17], in which they compared four stochastic and three deterministic (including ERA) time domain

identification methods, to identify the simplified model of railway vehicle shown in Figure 1.9.

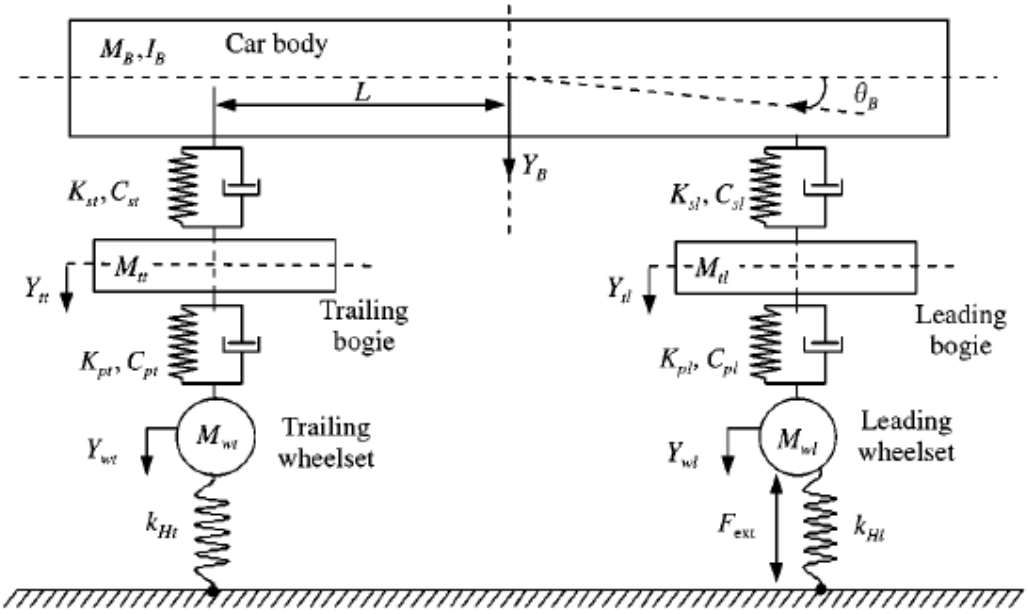

Figure 1.9 Simplified Railway Vehicle Model [17]

In their study, they simulated the response of the railway vehicle and tested identification algorithms with varying noise models. In their study Petsounis and Fassois [17], compared these seven algorithm in terms of model order determination, modal parameter estimation, sensitivity analysis, and computational complexity. Their results are too comprehensive so that they will not be presented here. But in the end of their analysis, as their problem was a parametric one, the prediction error method yielded good results among other stochastic approaches. However, when the ERA was evaluated, it was observed that, it solved the same problem in the non-parametric methodology, which does not require an estimate of model structure. In addition to that ERA was found to be superior in terms of its minimum order system identification capability and its computational simplicity.

On the other hand, in recent years, the application of ERA and ERA/DC in civil engineering structures became more popular for health monitoring applications and some examples of them can be found in [18], [19], [20], and [21].

1.4 OUTLINE OF THE THESIS

In Chapter 1, the aim of this study brief history of the system identification is presented and significant publications are briefly mentioned. In addition to that, relevant applications in the literature and their results are briefly mentioned.

In Chapter 2, the impulse response determination by utilizing direct time domain approaches, Fourier transforms and Wavelet transforms are presented. These methods are compared in terms of their performances. Improvements on them developed to enhance the extraction of system impulse response data are given. Details of wavelet transforms and their algorithmic implementations are presented.

In Chapter 3, a second order mechanical system representation is presented and the transformation from second order system models into first order state space models is given. In those first order representations, special cases are constructed and their special use is explained.

In Chapter 4, fundamental concepts in system realization are introduced, and controllability and observability properties of linear time invariant systems are investigated. Two realization methods implementing minimum order state space realization is introduced and their formulations are investigated.

In Chapter 5, the inverse vibration problem is solved using first order realized state space models via transformation based methodology. The physical system parameters like mass, stiffness, and damping matrices are obtained as a result of this analysis.

In Chapter 6, simulation and test results are given. The realization and physical system parameter extraction methodologies explained in the previous chapters are

applied on the two different simulation models. These results also evaluated regarding performances of the selected methods. The test setup is introduced and same identification procedure is applied to the input and output data of the test setup.

In Chapter 7, a general summary of the present work is presented. Conclusions and comments on the performance obtained from the applied identification methods are stated. Intended future improvements on the identification process are suggested.

CHAPTER 2

IMPULSE RESPONSE DETERMINATION

The identification of modal parameters from the measurements of input and output data is a must in a system realization process. This complex extraction can be whether performed in the frequency domain or in the time domain. In the frequency domain, modal parameters can be determined by using frequency response functions (FRF). Equivalently in the time domain, the modal parameters can be extracted by using impulse response functions in the system identification applications.

Dynamic properties of a linear time invariant (LTI) system can be described by its impulse response function $h(t)$ in continuous time domain. For any applied input $u(t)$, the output of the system $y(t)$ can be computed by using the following convolution integral.

$$y(t) = \int_{-\infty}^{\infty} h(\tau)u(t-\tau)\mathrm{d}\tau \tag{2.1}$$

Traditional realization methods generally utilize FRFs in order to obtain system characteristics because of its ease to represent system behavior and the existence of various frequency domain identification schemes. For this purpose FRFs are obtained by using the ratio of discrete Fourier transform of the input and output data. The continuous Fourier transform $X(f)$ of a continuous signal $x(t)$ is obtained as

$$X(f) = F\left[x(t)\right] = \int_{-\infty}^{\infty} x(t)e^{-j2\pi ft}dt \tag{2.2}$$

The discrete counterpart of the continuous Fourier transform is given as follows.

$$X(f_k) = \sum_{n=0}^{N-1} x_n . e^{-i2\pi kn/N} \tag{2.3}$$

where $X(f_k)$ is the discrete Fourier transform of a discrete signal $x_n(k)$ and N is the length of the discrete signal.

In order to solve Equation (2.1), Fourier transforms $Y(f)$ and $U(f)$ of the input and output signals are used, which are related in the frequency domain as follows.

$$Y(f) = H(f)U(f) \tag{2.4}$$

where $H(f)$ is the FRF. Therefore, the convolution integral in time domain, becomes simply a multiplication in the frequency domain in term of extracting FRF by a simple division. However, due to the noise involved in the measurement data, Equation (2.4) is slightly changed by introducing new correlation variables $G_{uu}(f_k, r)$ and $G_{yu}(f_k, m, r)$ as follows.

$$\begin{aligned} G_{uu}(f_k, r) &= \hat{u}(f_k, r).\hat{u}^*(f_k, r) \\ G_{yu}(f_k, m, r) &= \hat{y}(f_k, m).\hat{u}^*(f_k, r) \end{aligned} \tag{2.5}$$

where $\hat{u}(f_k, r)$ and $\hat{y}(f_k, m)$ are the discrete Fourier transforms of the input and output signals, respectively, and, $\hat{u}^*(f_k, r)$ and $\hat{y}^*(f_k, m)$ are their complex conjugate pairs. After correlated variables are obtained, the FRF of the system can simply be obtained by dividing the output correlation variable to input correlation variable as follows.

$$H(f_k, m, r) = \frac{G_{yu}(f_k, m, r)}{G_{uu}(f_k, r)} \tag{2.6}$$

The discrete impulse response of the system can then be obtained by using inverse discrete Fourier transform to return back to time domain, which is simply denoted by

$$h_n = F^{-1}(H(f_k, m, r)) \tag{2.7}$$

The determination of discrete impulse response function using Fourier transform is a computationally efficient method as described above. However, in order to catch the whole system behavior, the input signal must span the entire frequency range of interest, which makes the data in hand impractically large. Besides large data processing, there are other drawbacks of frequency domain analysis as well. One of them is the leakage, which is the corruption of spectral densities due to forward and inverse Fourier transforms. The leakage occurs due to the non-periodicity of the signal and this disturbs the Fourier transform of the signal. This problem can be eliminated with the implementation of windowing, which smoothens the ends of the signal so that the signal is forced to behave like periodic. Introducing windows in the Fourier analysis called short time Fourier transform (STFT) and it is the most widely utilized Fourier based analysis tool on the finite interval discrete signals. However, the windowing itself also adversely affects the damping properties of the system estimate because of the phase lags introduced by the windowing filters. Another disadvantage of using FRFs is that, during the identification procedure, the input signal should be rich in terms of frequency content, otherwise sparse input signals cause ill conditioning in the analysis. For online system identification, the input signal becomes the disturbance itself and generally its frequency content is at a single frequency or in limited range, which makes frequency analysis impractical. Another disadvantage of implementing Frequency Domain identification scheme is the requirement of an inverse Fourier transform to go back to time domain representation.

Due to stated problems with the discrete forward and inverse Fourier transforms, researchers seek for direct time domain methods which solve the deconvolution

problem by using matrix algebra. For this purpose, the convolution equation is represented in matrix form in time domain as follows.

$$Y = hU \tag{2.8}$$

where, U is the convolution operation applied to input matrix, Y is the output matrix, and h is the time domain impulse response matrix. They can also be explicitly expressed as

$$\begin{aligned} Y &= \begin{bmatrix} y(0) & y(1) & \dots & y(s-1) \end{bmatrix}_{(m \times s)} \\ h &= \begin{bmatrix} h(0) & h(1) & \dots & h(rp) \end{bmatrix}_{(m \times r(p+1))} \\ U &= \begin{bmatrix} u(0) & u(1) & \dots & u(p) & \dots & u(s-1) \\ 0 & u(0) & \dots & u(p-1) & \dots & u(s-2) \\ 0 & 0 & \dots & u(p-2) & \dots & u(s-3) \\ 0 & 0 & \ddots & \ddots & \ddots & \vdots \\ 0 & 0 & 0 & u(0) & \dots & u(s-p-1) \end{bmatrix}_{(r(p+1) \times s)} \end{aligned} \tag{2.9}$$

where m, r, s, and p are the number of output signals, number of input signals, number of output measurement samples and the desired length of impulse response function respectively.

A direct method for solving Equation (2.8) is the multiplication of both sides with U^{-1}. However, depending on the type of input used, the matrix U may become ill conditioned, such that impulse response cannot be obtained directly. For this reason mostly pseudo inverse of U is used in order to obtain impulse response function. Another improvement on the direct time domain methods is the utilization of auto and cross correlated variables like in the case of frequency domain approach described in the preceding section. The correlated variables are defined as following.

$$\begin{aligned} R_{UU} &= UU^T \\ R_{YU} &= Y U^T \end{aligned} \tag{2.10}$$

By using Equation (2.10), the impulse response function h can be obtained as follows.

$$h = R_{YU} R_{UU}^{-1} \tag{2.11}$$

which is analytically equivalent to the pseudo inverse implementation.

In order to solve the ill conditioned deconvolution matrix problem, least square techniques and observer based techniques are suggested by different researchers. However, due to noise and distortions, the identified system response again could not meet the requirements of the researchers.

In order to cope with most of the problems stated in the preceding section, another method called wavelet transform is suggested [22]. The wavelet transform processes the data only in time domain as opposed to frequency domain approaches and it was originated from analysis requirement of finite interval signals with varying spectral properties [23]. Its implementation involves forward and inverse discrete wavelet transform and an inversion operation, which is preferable in certain cases. In addition to that, its unique property is being able to catch the whole response properties even under a single frequency input. All these make the use of wavelets as a primary tool in the health monitoring applications, where disturbances with single frequency content are acting on the system.

In 1970s J. Morlet, who is a geophysical engineer, was faced with analyzing signals which had low frequency components with long time intervals and high frequency components with short time periods [20]. In such analysis, the problem associated with using Fourier transform is the use of same basis function over the whole signal. In order to solve this problem, Morlet came up with the idea of using different window functions for analyzing different frequency bands. In addition to that, these windows were generated by dilation and compression of a selected Gaussian function, which later Morlet named it as *wavelets of constant shape* [20]. After his ingenious idea, Morlet and several mathematicians improved wavelet theory with

revealing orthogonal wavelet basis functions, which had good frequency and time localization characteristics. Later in the late 1980's, Ingrid Daubechies, developed the wavelet frames for discretization of time and scale parameters. After the arrival of wavelet frames, there appeared more options on the selection of basis functions.

Daubechies with Mallat, developed the basis for the transformation from continuous to discrete signal analysis [24]. Later on, Mallat introduced the multi resolution analysis for the discrete wavelet transform [21]. His idea was breaking up a discrete signal into its frequency bands by using series of lowpass and highpass filters to compute discrete wavelet transform of the signal at different levels. His theory later called as *Mallat's pyramid*.

In order to better understand wavelets, its comparison with Fourier transform will be beneficial. Wavelet and Fourier transforms both represent any selected signal through linear combinations of their basis functions. In the case of Fourier transforms, basis functions are dilations of sinusoidal functions sine and cosine. In addition to that, in the Fourier analysis these basis functions spans the entire time interval, which means they are assumed to be infinite in length. In the case of wavelet transforms, basis functions are translations and dilations of the selected basis function called as the *mother wavelet*. Also in the wavelet analysis, each basis function spans logarithmically reduced subintervals making them finite in length. Additionally, the dilations of both mother wavelet and scaling function is possible, and due to their frequency localization, information about the frequency content of the analyzed signal can be obtained directly. This enables the time localization and as a matter of fact this is the most important difference between the Fourier analysis and wavelet analysis. Sine and cosine functions as the basis functions of Fourier transform, are not finite; however, basis functions of the wavelet transform are compact and finite in time. This enables wavelet transforms to obtain both time and frequency information of the analyzed signal.

Although, a direct implementation of Fourier transform does not convey time localization information, it can be obtained when a windowing is applied in the STFT analysis. The window is a square wave which is applied to the basis sine or cosine function to fit the signal into the particular width of the time interval. In the STFT, the same square window is used for all frequencies, which results in the same resolution over the whole time and frequency ranges, and this is again not appropriate to the solution of Morlet's problem. On the other hand, the discrete wavelet transform (DWT) has a window size which is getting smaller with increasing frequencies. A comparison of the STFT and DWT in terms of their windowing characteristics is visualized in Figure 2.1. As seen in Figure 2.1, by increasing the scale of DWT, the window size gets smaller, as opposed to STFT where the window size remains constant.

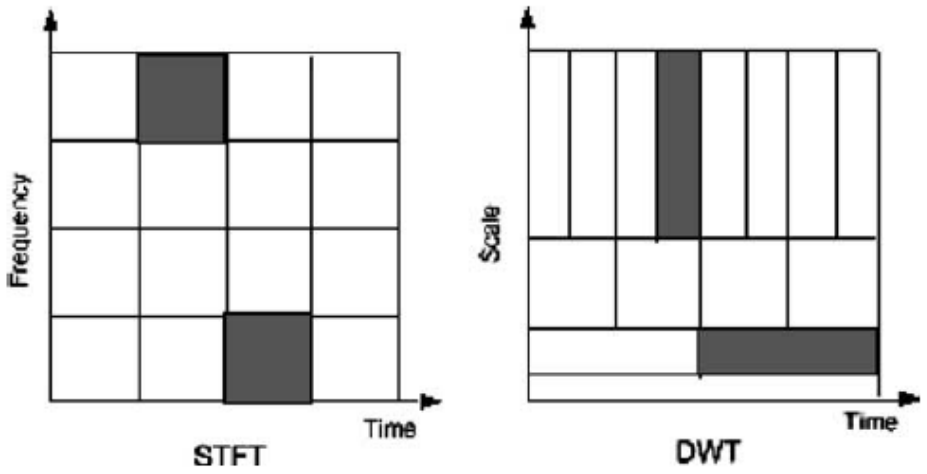

Figure 2.1. STFT and DWT Time Frequency Windowing [22]

This property of DWT analysis makes it advantageous when analyzing signals including both discontinuities and smooth components as encountered mostly in real life applications. Note that short length and high frequency range basis functions are required for analyzing discontinuities, but long length and low frequency range ones are required for the analysis of smooth components. Because of its prescribed advantages, the DWT is an appropriate tool to analyze system response data.

A function $f(t)$ can be approximated by using DWT as [26]

$$f(t) = a_0^{-m/2} \sum_{m,n} f_{(m,n)}^{wav} \cdot \psi(a_0^{-m} t - n b_0) \tag{2.12}$$

where $f_{(m,n)}^{wav}$ is the wavelet transform coefficients, $\psi(a_0^{-m} t - n b_0)$ is the wavelet basis function, a_0 and b_0 are the scaling and shifting constants, respectively, and m and n are the constants representing level of wavelet transform and shifting respectively. An examination of Equation (2.12) reveals, that $\psi(a_0^{-m} t - n b_0)$ consists of orthogonal basis functions based on the specific choice of mother wavelet functions. However, these basis functions cannot be explicitly expressed; rather they are computed as a part of the transformation process.

In the selection of basis functions, although there are a number of choices, for the analysis of physical system response, the basis function should satisfy certain properties like conservation of area, accuracy, orthogonality, and so on. Among these properties, the most important one is the orthogonality; because, most other properties are satisfied by nearly all basis functions. Considering the orthogonality property, for a vibration analysis, generally Daubechies basis functions are selected among various options as they both satisfy orthogonality and second order or higher accuracy when representing signals [25].

The scaling function $\phi(t)$ for Daubechies' N coefficient description can be obtained from the following dilation equation [23].

$$\begin{aligned} \phi(t) &= \sum_{k=0}^{N-1} c_k \phi(2t - k) \\ \phi_{m,k}(t) &= 2^{-m/2} \phi(2^{-m} t - k) \end{aligned} \tag{2.13}$$

where m and k are the level of wavelet transform and shifting operation. By using the scaling functions in Equation (2.13), the wavelet functions can be expressed as

$$\psi(t) = \sum_{k=0}^{N-1} (-1)^k c_k \phi(2t + k - N + 1)$$
$$\psi_{m,k}(t) = 2^{-m/2} \psi(2^{-m} t - k) \tag{2.14}$$

The above scaling and wavelet functions satisfy normalization and orthogonalization constraints. In order to better understand the nature of the wavelet transform, f^{wav} can be explicitly shown as follows [21]

$$f^{wav}(t) = a_0 \phi(t) + a_1 \psi(t) + \begin{bmatrix} a_2 & a_3 \end{bmatrix} \begin{Bmatrix} \psi(2t) \\ \psi(2t-1) \end{Bmatrix} + \begin{bmatrix} a_4 & a_5 & a_6 & a_7 \end{bmatrix} \begin{Bmatrix} \psi(4t) \\ \psi(4t-1) \\ \psi(4t-2) \\ \psi(4t-3) \end{Bmatrix} \tag{2.15}$$
$$+ \cdots + a_{(2^j+k)} \psi(2^j t - k)$$

where a_0,..., $a_{(2^j+k)}$ are the wavelet transform coefficients, which are computed as

$$a_0 = \int_0^1 f(t)\phi(t)dt \qquad \text{and} \qquad a_{(2^j+k)} = 2^j \int_0^1 f(t)\psi(2^j t - k)dt \tag{2.16}$$

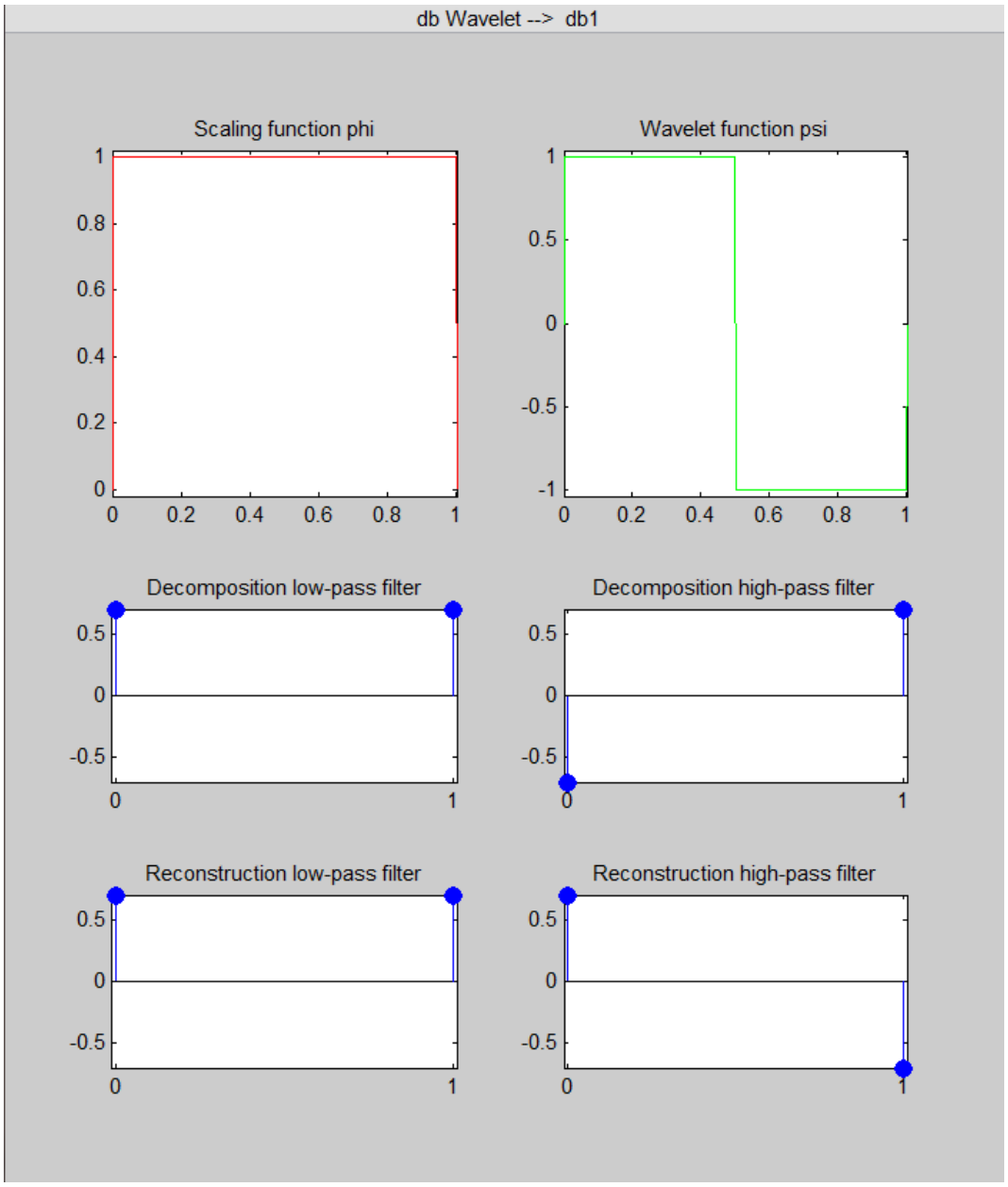

Figure 2.2 Daubechies-1 Wavelet (a.k.a Haar Wavelet)

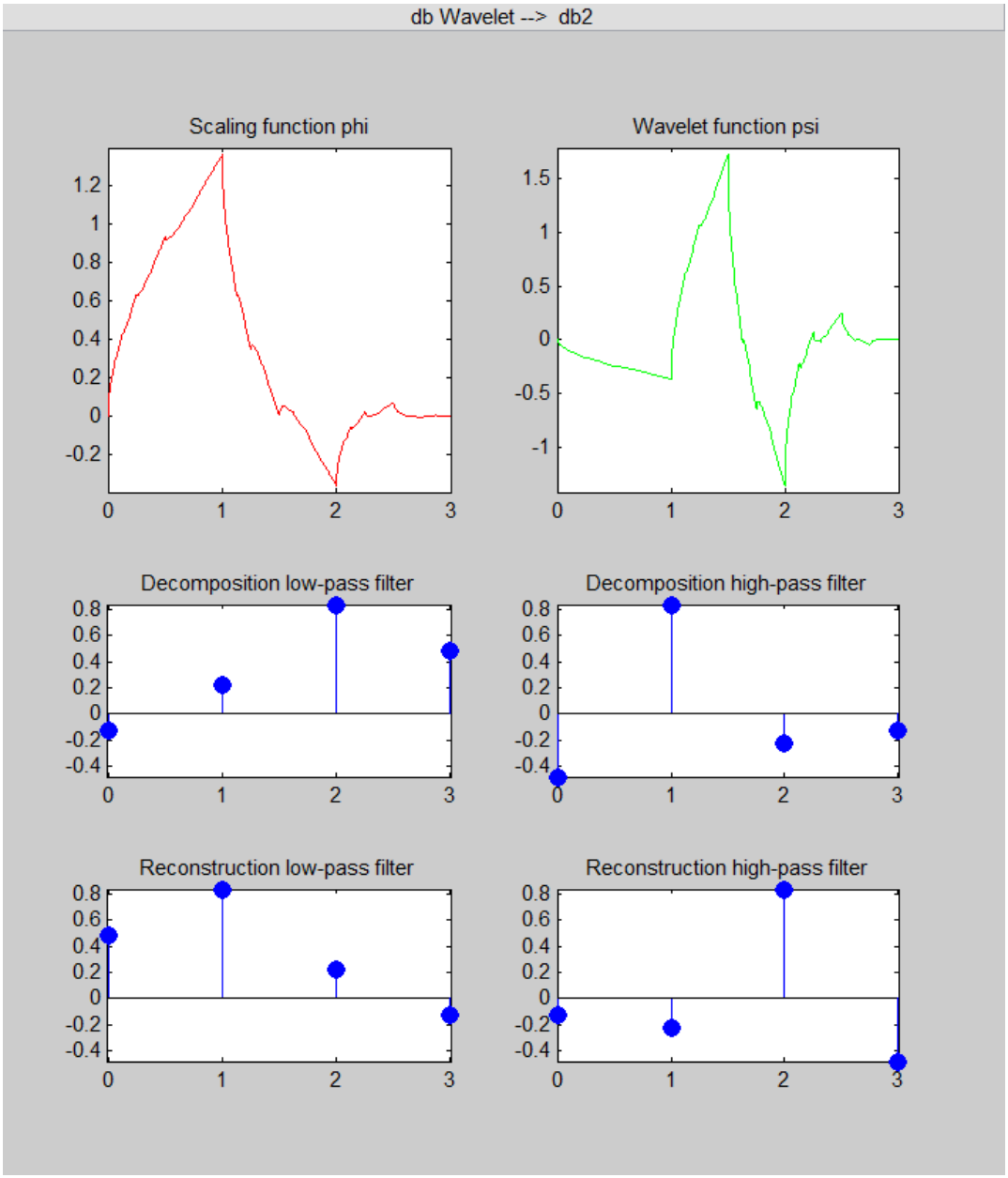

Figure 2.3 Daubechies-2 Wavelet

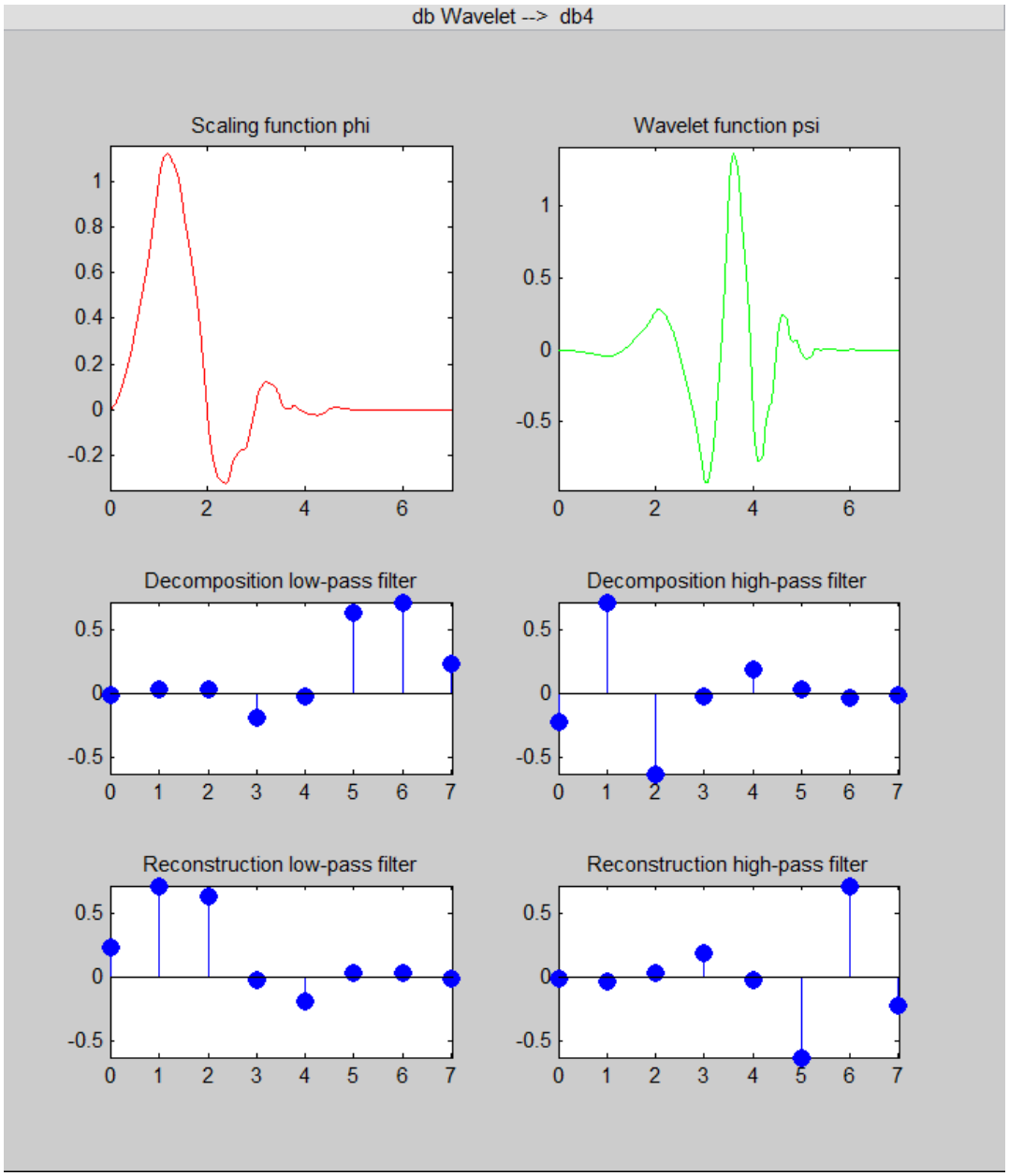

Figure 2.4 Daubechies-4 Wavelet

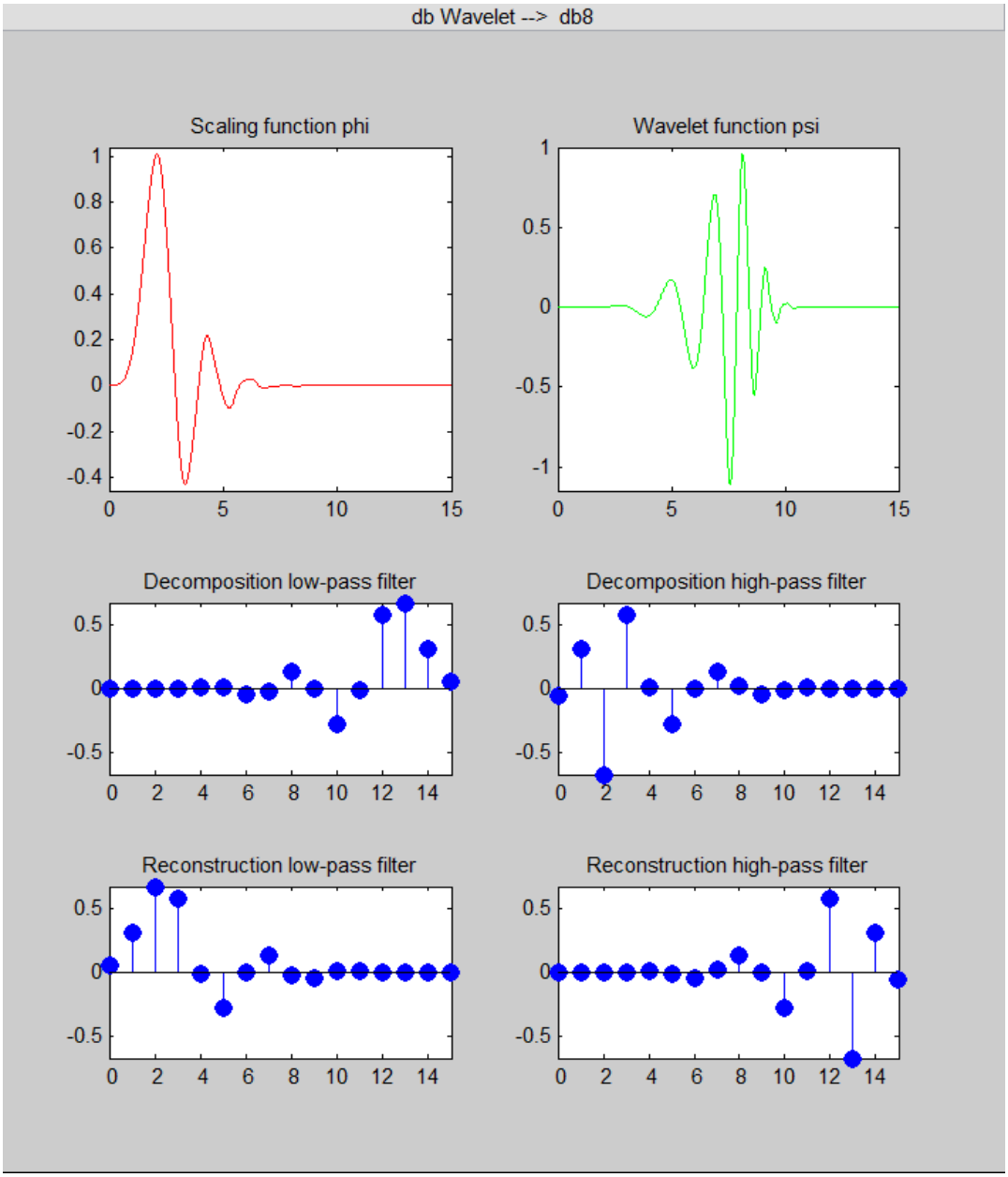

Figure 2.5 Daubechies-8 Wavelet

From Figure 2.2 to Figure 2.5 the Daubechies-1, 2 , 4, and 8 wavelets are given by using Matlab's Wavelet Toolbox [24] to better illustrate forms and properties of the Daubechies wavelet functions. In those figures, scaling and wavelet functions belonging to each Daubechies wavelet forms are given together with the decomposition and reconstruction filter coefficients. Here in the above figures, a

Daubechies-N form wavelet has $2N$ number of filter coefficients shown with blue dots.

Here it should be noted that in Equation (2.15), the first two terms associated with the scaling function $\phi(t)$ and the mother wavelet function $\psi(t)$ spans the entire time interval $0 \le t \le 1$. Similarly the functions associated with the next two terms $\psi(2t)$ and $\psi(2t-1)$ span the intervals $0 \le t \le \frac{1}{2}$ and $\frac{1}{2} \le t \le 1$ respectively and, in the same manner, each subsequent term spanning smaller and smaller intervals without overlapping as a result of the orthogonality property for the local bases.

At this point, Mallat considered frequency information of each term given in Equation (2.15) in the multi resolution analysis (MRA). Then MRA is developed to obtain discrete wavelet transform of a discrete signal iteratively applying lowpass and highpass filters and down sampling them by 2 after each step. In Figure 2.6, the schematic representation of the MRA is shown, here $g[n]$ and $h[n]$ are the highpass and lowpass filters respectively and in this figure at each level the frequency bands are shown as well.

The numerical procedure at each level can be represented as

$$y_{high}[k] = \sum_n x[n] \cdot g[2k-n]$$
$$y_{low}[k] = \sum_n x[n] \cdot h[2k-n] \qquad (2.17)$$

where,

$$h[N-1-n] = (-1)^n g[n] \qquad (2.18)$$

with N being the total number of samples of signal $x[n]$.

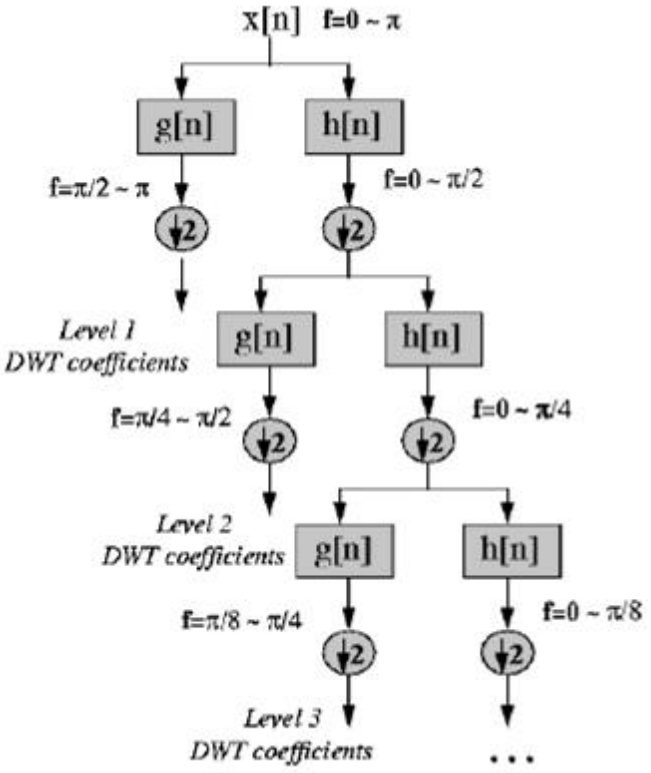

Figure 2.6 Implementation of DWT by MRA [20]

Therefore the original signal can be reconstructed by using outputs of highpass and lowpass filters(y_{high}, y_{low}) in the MRA analysis as follows.

$$x[n] = \sum_{k} (y_{high}[k] \cdot g[2k-n]) + (y_{low}[k] \cdot h[2k-n]) \tag{2.19}$$

2.1 BASIC WAVELET ALGORITHM FOR IMPULSE RESPONSE FUNCTION DETERMINATION

After a short review on the discrete wavelet transform, it can be observed that, the wavelet analysis is an appropriate tool to inspect system response in terms of vibration analysis [21]. Therefore the convolution problem given in the very beginning of this chapter, can be solved with using wavelet transform and the discrete wavelet transform defines the same problem as follows.

$$y(t) = \int_0^T h(\theta)\, u(t-\theta)\, d\theta \tag{2.20}$$

where $h(\theta)$ is the impulse response function. Here the system of interest is assumed to be linear time-invariant so that the at any discrete time t_n the output is only affected by the nature of the input. Therefore the temporal impulse response $h(\theta)$ can be expanded by using wavelet basis functions over the whole response measurement time interval, and θ represent the normalized time variable through the adoption of $\{0 \le t \le T \;\Rightarrow\; 0 \le \theta \le 1\}$ as

$$h(\theta) = h_0^{DWT} + \sum_j \sum_k h_{(2^j+k)}^{DWT} \psi(2^j \theta - k) \tag{2.21}$$

In Equation (2.21), impulse response function $h(\theta)$ is represented by using the wavelet function and in this equation, h^{DWT} is the discrete wavelet transform of the impulse response function. For the similar discrete wavelet transform representation of the term $u(t-\theta)$, first input $u(\theta)$ is reversed in time to obtain $u(-\theta)$, then it is shifted over the positive time axis by t amount where $\{u(\theta) = 0, \text{ for } \theta > t\}$. With the described convention, the discrete wavelet transform(DWT) of $u(t-\theta)$ can be expressed as follows.

$$u(t-\theta) = u_0^{DWT} + \sum_j \sum_k u_{(2^j+k)}^{DWT} \psi(2^j \theta - k) \tag{2.22}$$

where u^{DWT} is the discrete wavelet transform of $u(t-\theta)$. At this point, in order to solve the convolution integral given in Equation (2.20), the discrete wavelet transform of the impulse response function and input signals can be substituted, however, in order to do this, orthogonality condition for the selected mother wavelets must be provided as follows.

$$\int_0^1 \psi(2^j \theta - k)\, d\theta = 0 \tag{2.23}$$

$$\int_0^1 \psi(2^j\theta - k)\psi(2^r\theta - s)d\theta = \begin{cases} \frac{1}{2^j} & \text{when } r = j \text{ and } s = k \\ 0 & \text{otherwise} \end{cases} \tag{2.24}$$

After the substitution of wavelet transform of the input signal and impulse response function with considering the orthogonality property stated in Equation (2.24), response at a specific time t_0 can be computed in the discrete time as follows.

$$y(t_0) = h_0^{DWT} u_0^{DWT} + \sum_j \sum_k \frac{1}{2^j} h_{(2^j+k)}^{DWT} u_{(2^j+k)}^{DWT} \tag{2.25}$$

Combining scaling function and wavelet function coefficients, the Equation (2.25), can be expressed as follows.

$$y(t_0) = h^{DWT} u^{DWT} \tag{2.26}$$

where

$$\begin{aligned} h^{DWT} &= [h_0 \quad h_1 \quad h_2 \quad h_3 \quad \cdots \quad h_{n-1}] \\ (u^{DWT})^T &= [u_0 \quad u_1 \quad \frac{u_2}{2} \quad \frac{u_3}{2} \quad \cdots \quad \frac{u_{n-1}}{2^j}] \end{aligned} \tag{2.27}$$

Here again, h^{DWT} and u^{DWT} are the discrete wavelet transforms of $h(\theta)$ and $u(t-\theta)$ respectively and j is computed as $j = \log_2(n)$, which conveys the level of wavelet transformation.

It should be noted that, Equation (2.26), computes the system response at a particular time instant t_0. In order to compute the whole response series $\{y(t_0) \quad y(t_1) \quad y(t_2) \quad \ldots\}$, the input and output relation can be arranged in the following matrix equation as

$$\tilde{y}_{(m\times s)} = h^{DWT}{}_{(m\times rl)} \cdot U^{DWT}{}_{(rl\times s)} \tag{2.28}$$

where

$$\tilde{y} = \{ y(0) \quad y(1) \quad y(2) \quad \dots \}$$

$$U^{DWT} = \{ u^{DWT}(0) \quad u^{DWT}(1) \quad u^{DWT}(2) \quad \dots \}$$

with m, s, r, and l are the number of measurement points, the number of measurement samples, the number of input signals and the depth of wavelet transform level respectively.

Here solving the discrete wavelet transform of the impulse response function h^{DWT} from Equation (2.28), yields the following expression.

$$h^{DWT} = \tilde{y} \cdot (U^{DWT})^T \cdot \left[U^{DWT} (U^{DWT})^T \right]^{-1} \tag{2.29}$$

Finally the inverse discrete wavelet transform of the h^{DWT} yields the desired impulse response data as follows.

$$h(t) = DWT^{-1} \left\{ h^{DWT} \right\} \text{ for } t = t_0, t_1, \dots t_{(s-1)} \tag{2.30}$$

At this point there are a few remarks to be to pointed out, first the wavelet transformed input coefficients $u^{DWT}(k)$, consist of a set of orthogonal basis functions; therefore, when $rl \le s$ the rank of U^{DWT} becomes rl and this results in that, $(r \times 1)$ input vectors included in the input vector $u(t)$ must be linearly independent. When the input vectors are linearly independent, the $\left[U^{DWT} (U^{DWT})^T \right]^{-1}$ expression in Equation (2.29) is invertible. On the other hand, when $rl \ge s$, which may be the case for a higher or full depth wavelet resolution analysis, $\left[U^{DWT} (U^{DWT})^T \right]^{-1}$ cannot be inverted directly and least square solution implementing pseudo-inverse shall be applied to solve Equation (2.29).

The second and final remark can be done on the major drawback of the discrete wavelet transform which is the computation time and resource requirement. During

the solution of the impulse response function, each row of the input U matrix must be transformed with total of rl times. Besides this transformation takes time, it also requires large storage space depending on the size of rl , as it makes operations on a $rl \times rl$ square matrix. However, in the system identification implementation, the time required for discrete wavelet transformation is not significantly large when the whole identification process time is taken into consideration. In terms of the resource requirement, thanks to the ability of wavelet transform to determine impulse response even under a single tone input signal, data length can be kept minimum without compromising from the determined system response.

2.2 IMPROVEMENTS ON WAVELET ALGORITHM VIA ENSEMBLE AVERAGING

The impulse response determination via discrete wavelet transform, explained in the preceding section can be referred as the basic wavelet algorithm as the collected input and output signals are not conditioned in any sense. On the other hand, in the case of traditional impulse response determination methods like the spectral methods explained previously, they rely heavily on the data conditioning by implementing both filtering and ensemble-averaging. Considering these extensions for the spectral methods, implementing ensemble averaging to the basic wavelet algorithm can result in similar improvement as stated in [19].

Although the main interest is focused on linear time-invariant systems, most of the real-life systems do not posses these properties exactly, rather they are assumed to behave under specific conditions. The ensemble averaging is a method of recording repetitive input and output series over time and averaging them together to find an averaged system response. Each time series used in the ensemble procedure are either recorded in a one long input/output time history or they are obtained as a result of multiple tests. In the wavelet analysis process, there are various ways to include ensemble averaging on the actual or correlated matrices.

The starting point for extending the basic wavelet method with ensemble averaging is the description of the wavelet transformed matrices as follows.

$$\begin{aligned} h &= h^{DWT} \cdot W^T \\ U &= W \cdot U^{DWT} \end{aligned} \tag{2.31}$$

where W and W^T are the wavelet transformation matrix that is applied to the columns and rows of the selected matrices respectively. As these matrices perform the wavelet transform, their rows or columns consists of the basis functions of the selected wavelets. Descriptions of these matrices can be substituted into the convolution integral in Equation (2.20) to obtain the system response as follows.

$$\tilde{y} = h^{DWT} \cdot W^T \cdot W \cdot U^{DWT} = h^{DWT} \cdot D \cdot U^{DWT} \tag{2.32}$$

This equation is the same with Equation (2.28), with D being a diagonal matrix composed of scaling values which are resulted from the multiplication of $W^T \cdot W$. This diagonal matrix results when the wavelet matrix is orthogonal, but not orthonormal. Ensemble averaging procedure then start with Equation (2.32), by multiplying both sides of the equation by the transpose of the input matrix $\left(U^{DWT}\right)^T$ to create auto $\left\{U^{DWT} \cdot (U^{DWT})^T\right\}$, and cross $\left\{\tilde{y} \cdot (U^{DWT})^T\right\}$ correlation matrices as

$$\tilde{y} \cdot \left(U^{DWT}\right)^T = h^{DWT} \cdot D \cdot U^{DWT} \cdot \left(U^{DWT}\right)^T \tag{2.33}$$

Again this equation gives the correlation functions for response at a specific time, and in order to obtain the whole response series, they are summed together as

$$\sum\left[\tilde{y} \cdot \left(U^{DWT}\right)^T\right] = h^{DWT} \cdot D \cdot \sum\left[U^{DWT} \cdot \left(U^{DWT}\right)^T\right] \tag{2.34}$$

Therefore the wavelet generated impulse response h can be calculated as follows.

$$h^{DWT} = \left\{\sum\left[\tilde{y}.\left(U^{DWT}\right)^{T}\right]\right\}.\left\{\sum\left[U^{DWT}.\left(U^{DWT}\right)^{T}\right]\right\}^{-1} \cdot D^{-1} \qquad (2.35)$$

$$\text{therefore, } h = DWT^{-1}(h^{DWT})$$

As noted before, representation of the time correlation function in the wavelet domain is not unique and there are other possibilities like, transforming $\tilde{y}$ in place of transforming either input matrix U or impulse response history h; or there exists two dimensional transformations, or wavelet transformations of the auto and cross correlations directly.

2.2.1 Auto And Cross Correlation Approach

The final improvement on the wavelet analysis is the utilization of auto and cross correlations directly in the time domain by multiplying both sides of the direct time relation by U^T as follows [19].

$$\begin{aligned} \tilde{y} &= h \cdot U \\ \tilde{y} \cdot U^T &= h \cdot U \cdot U^T \end{aligned} \qquad (2.36)$$

Here implementation of wavelet transform to the auto and cross correlations in the wavelet domain results in as

$$\begin{aligned} \tilde{y} \cdot U^T &= \left[\tilde{y} \cdot U^T\right]^{DWT} \cdot W^T \\ U \cdot U^T &= \left[U \cdot U^T\right]^{DWT} \cdot W^T \end{aligned} \qquad (2.37)$$

Then the wavelet transformed auto and cross correlation variables can be substituted back into the Equation (2.36) , to obtain system response as

$$\begin{aligned} \left[\tilde{y} \cdot U^T\right]^{DWT} \cdot W^T &= h \cdot \left[U \cdot U^T\right]^{DWT} \cdot W^T \\ \left[\tilde{y} \cdot U^T\right]^{DWT} &= h \cdot \left[U \cdot U^T\right]^{DWT} \end{aligned} \qquad (2.38)$$

Finally the ensembling process can also be applied to the response obtained in Equation (2.38), as follows.

$$\sum \left[\tilde{y} \cdot U^T \right]^{DWT} = h \cdot \sum \left[U \cdot U^T \right]^{DWT}$$
$$h = \left\{ \sum \left[\tilde{y} \cdot U^T \right]^{DWT} \right\} \cdot \left\{ \sum \left[U \cdot U^T \right]^{DWT} \right\}^{-1} \tag{2.39}$$

Here, when the results are examined, it is noted that no scaling matrix D appears in this case since there exists the multiplication of $W^T \cdot (W^T)^{-1}$, not the $W^T \cdot W$ term. Although, these two methods converge to the same result for infinitely large ensembling, results of these two methods may differ slightly in the case of a few ensembling application.

In this study, the selected system realization algorithms are all working on the time-domain. Which makes impulse response as the key tool to analyze the response of the system under test. In the following section, ERA and ERA/DC are explained in details and their primary input is described to be the impulse response function. Therefore, the Fourier and wavelet analyses will be utilized to determine impulse response functions of the systems of interest.

CHAPTER 3

STATE SPACE FORMULATION FOR LINEAR STRUCTURAL SYSTEM IDENTIFICATION

In this study, the structural system identification will be performed by using state space representation of the system dynamics. The state space or the first order equation form is the fundamental tool to uniquely express damped structural behavior of the realized system model by using experimental data. In this chapter, theoretical basis for the equations of motion for structures and their transformation to first order state space forms will be explained [25].

3.1 STATE SPACE FORMULATIONS OF STRUCTURAL DYNAMICS

For a typical linear time invariant mechanical system, the equilibrium conditions can be discretized through finite spatial displacement variables, which results in a n dimensional set of second order linear differential equations in the matrix form.

$$\begin{aligned} M\,\ddot{q}(t) + D_{amp}\,\dot{q}(t) + K\,q(t) &= \hat{B}\,u(t) \\ y(t) &= H_d\,q(t) + H_v\,\dot{q}(t) + H_a\,\ddot{q}(t) \end{aligned} \tag{3.1}$$

where M, D, and K are the mass, damping, and stiffness matrices respectively; q is the n number of state vector, u is the r number of input force vector, and y is the m number of sensor output vector, which can either be displacement, velocity or

acceleration; $\hat{B}$ is the input state influence matrix whereas H_d, H_v, and H_a are state output influence matrices for displacement, velocity and acceleration respectively. Here $\hat{B}$, H_d, H_v, and H_a consists of binary value (0 or 1) because they map the input and output locations to the physical degrees of freedom. For simplified analysis, the undamped portion of the second order equation (3.1), can be decoupled through and eigenvector change of basis $q(t) = \Phi\eta(t)$, which results in as follows.

$$\begin{aligned} \ddot{\eta}(t) + \Phi^T D_{amp} \Phi \dot{\eta}(t) + \Omega\eta(t) &= \Phi^T \hat{B} u(t) \\ y(t) = H_d \Phi \eta(t) + H_v \Phi \dot{\eta}(t) + H_a \Phi \ddot{\eta}(t) & \end{aligned} \tag{3.2}$$

where Ω represents the normal eigenvalues and Φ is the mass normalized eigenvector, which is orthogonal and satisfy the following generalized undamped eigenproblem as

$$K\Phi = M\Phi\Omega \tag{3.3}$$

where

$$\begin{aligned} &\Phi^T M \Phi = I_{n\times n} \\ &\Phi^T K \Phi = \Omega = \begin{bmatrix} w_{n1}^2 & & & 0 \\ & w_{n2}^2 & & \\ & & \ddots & \\ 0 & & & w_{ni}^2 \end{bmatrix} \\ &\Phi^T D_{amp} \Phi = \Xi \end{aligned} \tag{3.4}$$

Here w_{ni} is the undamped natural frequency for mode i and Ξ is the *modal damping matrix* in the case of proportional Rayleigh damping ($D = \alpha M + \beta K$ or more generally $D = \alpha M^p + \beta K^s$) and it can be expressed as

$$\Xi = \begin{bmatrix} 2\zeta_1 w_{n1} & & & 0 \\ & 2\zeta_2 w_{n2} & & \\ & & \ddots & \\ 0 & & & 2\zeta_i w_{ni} \end{bmatrix} \tag{3.5}$$

Here ζ_i is the *modal damping ratio* for mode i. The modal damping ratio varies from 0% for undamped system response up to 100% for critically damped system response.

Here it should be noted that the second order system representations in Equation (3.1) and (3.2) have different coordinate bases, but they are equivalent representations of the same mechanical system. In order to examine the equivalent realization concept, a general solution to Equation (3.1) can be considered by implementing the Laplace transform.

$$\begin{aligned} [M s^2 + D_{amp} s + K] q(s) &= \hat{B} u(s) \\ [H_d + H_v s + H_a s^2] q(s) &= y(s) \end{aligned} \tag{3.6}$$

Therefore the input output relationship in the s-domain can be expressed in matrix form as

$$y(s) = H(s)\, u(s) \tag{3.7}$$

$$H(s) = (H_d + H_v s + H_a s^2)(M s^2 + D_{amp} s + K)^{-1} \hat{B}$$

$$u(s) = \int_0^\infty u(t) e^{-st} dt$$

$$y(s) = \int_0^\infty y(t) e^{-st} dt$$

here $H(s)$ is the transfer function matrix from input to output. By using Laplace transform again, the transfer function relationship can also be obtained from the modal coordinate model in (3.2) as follows.

$$
\begin{aligned}
y(s) &= (H_d + H_v\, s + H_a\, s^2)\ \Phi\, [\Phi^T (M\, s^2 + D_{amp}\, s + K)\Phi]^{-1}\, \Phi^T \hat{B} u(s) \\
y(s) &= (H_d + H_v\, s + H_a\, s^2)(M\, s^2 + D_{amp}\, s + K)^{-1} \hat{B} u(s) \\
y(s) &= H(s) u(s)
\end{aligned}
\tag{3.8}
$$

Therefore, from Equations (3.8) and (3.7), the *model equivalence* can be defined as the same input output relationship remains regardless of the definition of the internal dynamical states, where in this case the second order model variables are q and η.

3.1.1 General State Space Formulation

As a result of the model equivalence phenomenon defined above, the equation of motion can also be transformed from second order representation into the first order differential form. The general form of a linear, time invariant state space realization is defined as

$$
\begin{aligned}
\dot{x}(t) &= Ax(t) + Bu(t) \\
y(t) &= Cx(t) + Du(t)
\end{aligned}
\tag{3.9}
$$

where x is the $n \times 1$ state vector, A is the $n \times n$ state transition matrix, B is the $n \times m$ input-state influence matrix, C is the $r \times n$ state-output influence matrix, and D is the $r \times m$ direct input output influence matrix. For structural dynamics, input $u(t)$ are generally the externally applied inputs as in the case of Equation (3.1). Similarly, output array $y(t)$ includes the physical sensor measurements like displacement, velocity or acceleration, and C matrix is an array that extracts the outputs from the internal variables $x(t)$. In the special case of $x(t)$ being a subset of physical displacements and velocities of degrees of freedom driven by $u(t)$ and measured by $y(t)$, then vectors B and C are typically consisting of binary values (0 or 1) to map the input and output measurement locations to internal states similar to second order representation.

Here an important property related with the model equivalence concept is the *similarity transformation* [25]. In the application of similarity transformation the basis state vector x can be transformed into a different basis v as follows.

$$x = T v \tag{3.10}$$

where T is a nonsingular transformation matrix. Then using this transformation the state space model in Equation (3.9) becomes as

$$\begin{aligned} T\dot{v} &= ATv + Bu \\ y(t) &= CTv + Du \end{aligned} \tag{3.11}$$

or can be simplified as follows.

$$\begin{aligned} \dot{v} &= T^{-1}ATv + T^{-1}Bu = \breve{A}v + \breve{B}u \\ y(t) &= \breve{C}v + Du \end{aligned} \tag{3.12}$$

where the new variables are expressed as

$$\begin{aligned} \breve{A} &= T^{-1}AT \\ \breve{B} &= T^{-1}B \\ \breve{C} &= CT \end{aligned} \tag{3.13}$$

Therefore Equation (3.12) is a new realization of general state space model given in Equation (3.9), which is obtained by changing the state definition v. The state transformation via utilization of T is termed as the similarity transformation because λ, the eigenvalues of the realization satisfy the following relationship as

$$\left|\lambda I - A\right| = \left|\lambda I - \breve{A}\right| = 0 \tag{3.14}$$

Both representations are the same under this similarity transformation. As the similarity transformation assures model equivalence, the transfer function H from input to output, remains same for both representations and it can be proved by applying Laplace transform to Equation (3.12) as

$$
\begin{aligned}
y(s) &= \breve{C}(sI - \breve{A})^{-1}\breve{B}\,u(s) \\
y(s) &= CT(sT^{-1}T - T^{-1}AT)^{-1}T^{-1}Bu(s) \\
y(s) &= C(sI - A)^{-1}Bu(s)
\end{aligned}
\tag{3.15}
$$

As stated before, the similarity transformation in Equation (3.10), provides an equivalent model realization as well. Therefore, an infinite number of equivalent realization of the general state space model given in Equation (3.9) can be obtained.

3.1.2 State Space Formulation for Structural Dynamics via Physical Variables

A family of state space realizations for the general state space model given in Equation (3.9), can be obtained by using the similarity transformation with generalized momentum variable v which can be defined as

$$
v(t) = E_1 M\,\dot{q}(t) + E_2\,q(t) \tag{3.16}
$$

and the state space basis is transformed as follows.

$$
x(t) = \begin{Bmatrix} q(t) \\ v(t) \end{Bmatrix} \tag{3.17}
$$

At this point, instead of determining the general state space equations for x, there are a number of special alternatives for E_1 and E_2 to be selected accordingly.

Case I is selecting $E_1 = M^{-1}$ and $E_2 = 0$ and in this case $v(t) = \dot{q}(t)$ is the selected state space basis which is also termed as *physical displacement-velocity*(PDV) model [25]. The resultant state space model is obtained as

$$
\begin{aligned}
\dot{x}_I(t) &= A_I x_I(t) + B_I u(t) \\
y(t) &= C_I x_I(t) + Du(t)
\end{aligned}
\tag{3.18}
$$

where

$$
\begin{aligned}
A_I &= \begin{bmatrix} 0 & I \\ -M^{-1}K & -M^{-1}D_{amp} \end{bmatrix} \\
B_I &= \begin{bmatrix} 0 \\ M^{-1}\hat{B} \end{bmatrix} \\
C_I &= \begin{bmatrix} H_d & 0 \end{bmatrix} + \begin{bmatrix} H_v & 0 \end{bmatrix} A_I + \begin{bmatrix} H_a & 0 \end{bmatrix} A_I^{\,2} \\
C_I &= \begin{bmatrix} H_d - H_a M^{-1}K & H_v - H_a M^{-1}D_{amp} \end{bmatrix} \\
D &= H_a M^{-1}\hat{B}
\end{aligned}
\tag{3.19}
$$

Similarly for the case II, selecting $E_1 = I$ and $E_2 = D_{amp}$, the generalized momentum variable becomes $v = M\dot{q} + D_{amp}\, q$ and the state basis definition given in Equation (3.17), results in the physical displacement-momentum(PDM) model. The canonical representation for Case II can be obtained as follows.

$$
\begin{aligned}
\dot{x}_{II}(t) &= A_{II}\, x_{II}(t) + B_{II}\, u(t) \\
y(t) &= C_{II}\, x_{II}(t) + Du(t)
\end{aligned}
\tag{3.20}
$$

where

$$
\begin{aligned}
A_{II} &= \begin{bmatrix} -M^{-1}D_{amp} & M^{-1} \\ -K & 0 \end{bmatrix} \\
B_{II} &= \begin{bmatrix} 0 \\ \hat{B} \end{bmatrix} \\
C_{II} &= \begin{bmatrix} H_d & 0 \end{bmatrix} + \begin{bmatrix} H_v & 0 \end{bmatrix} A_{II} + \begin{bmatrix} H_a & 0 \end{bmatrix} A_{II}^{\,2} \\
D &= H_a M^{-1}\hat{B}
\end{aligned}
\tag{3.21}
$$

Here as previously stated and proved, similarity transformation results in an equivalent model which preserves the same transfer function H for each realization. This is also valid for realizations given in Equations (3.18) and (3.20) which are equivalent state space realizations of the equation of motion given in Equation (3.1).

3.1.3 State Space Formulation for Structural Dynamics via Normal Modal Variables

Equivalent state space realizations are represented in the preceding section and their implementation to second order modal form given in Equation (3.2) is also possible through similarity transform with generalized variable v defined as

$$v(t) = E_1\dot{\eta}(t) + E_2\eta(t) \tag{3.22}$$

and the state basis is similarly defined as follows.

$$x(t) = \begin{Bmatrix} \eta(t) \\ v(t) \end{Bmatrix} \tag{3.23}$$

Two other special state space models of the general form can be obtained, through the following selection of variables.

Case III is obtained through selecting $E_1 = I$, $E_2 = 0$, and in this case $v(t) = \dot{\eta}(t)$ is the selected state space basis which is also termed as modal displacement-velocity(MDV) model. The resultant state space model is obtained as

$$\begin{aligned} \dot{x}_{III}(t) &= A_{III}x_{III}(t) + B_{III}u(t) \\ y(t) &= C_{III}x_{III}(t) + Du(t) \end{aligned} \tag{3.24}$$

where

$$\begin{aligned} A_{III} &= \begin{bmatrix} 0 & I \\ -\Omega & -\Xi \end{bmatrix} \\ B_{III} &= \begin{bmatrix} 0 \\ \Phi^T\hat{B} \end{bmatrix} \\ C_{III} &= \begin{bmatrix} H_d\Phi & 0 \end{bmatrix} + \begin{bmatrix} H_v\Phi & 0 \end{bmatrix} A_{III} + \begin{bmatrix} H_a\Phi & 0 \end{bmatrix} A_{III}^{\,2} \\ C_{III} &= \begin{bmatrix} H_d\Phi - H_a\Phi\Omega & H_v\Phi - H_a\Phi\Xi \end{bmatrix} \\ D &= H_a\,\Phi\,\Phi^T\hat{B} = H_a M^{-1}\hat{B} \end{aligned} \tag{3.25}$$

Finally, Case IV is obtained through selecting $E_1 = I$ and $E_2 = \Xi$ and in this case $v(t) = \dot{\eta}(t) + \Xi\eta(t)$ is the selected state space basis which is also termed as *modal displacement-momentum*(MDM) model. The resultant state space model is obtained as

$$\begin{aligned} \dot{x}_{IV}(t) &= A_{IV}x_{IV}(t) + B_{IV}u(t) \\ y(t) &= C_{IV}x_{IV}(t) + Du(t) \end{aligned} \tag{3.26}$$

where

$$\begin{aligned} A_{IV} &= \begin{bmatrix} -\Xi & I \\ -\Omega & 0 \end{bmatrix} \\ B_{IV} &= \begin{bmatrix} 0 \\ \Phi^T\hat{B} \end{bmatrix} \\ C_{IV} &= \begin{bmatrix} H_d\Phi & 0 \end{bmatrix} + \begin{bmatrix} H_v\Phi & 0 \end{bmatrix} A_{IV} + \begin{bmatrix} H_a\Phi & 0 \end{bmatrix} A_{IV}^{\ 2} \\ C_{IV} &= \begin{bmatrix} H_d\Phi - H_a\Phi\Xi + H_a\Phi\Xi^2 - H\Phi\Omega & H_v\Phi - H_a\Phi\Xi \end{bmatrix} \\ D &= H_a\,\Phi\,\Phi^T\hat{B} = H_a M^{-1}\hat{B} \end{aligned} \tag{3.27}$$

Similarly, the model equivalence of Equations (3.24) and (3.26) with the general modal form in Equation (3.2) is provided by the similarity transformation. Each model among the 2 model and 2 modal equivalent representation family has particular advantages for whether using for simulation, control design, or system identification purposes [25].

3.1.4 State Space Formulation for Non-Proportionally Damped Systems

As stated in the preceding section, modal form is decoupled from the general second order differential equation for proportional (Rayleigh) damping case. This form of damping is either called as diagonal, proportional, classical, or modal damping and in this case modal damping matrix (Ξ) is obtained as diagonal. On the other hand,

most of the real life systems do not have proportional damping characteristics and, the generalized modal damping matrix Ξ, is not diagonal for this case, which is termed as non-classical or non-proportional damping. In this case damping matrix D_{amp} cannot be represented as a proportional combination of M and K. The physical interpretation of the non-proportional damping is that, the modes that decouples the system equations are complex in this case which results from the phase relationship between displacement of each structural mode.

For the non-proportional damping case, because the second order equation of motion cannot be decoupled by normal modes anymore, the governing eigenvalue problem for non-proportional damping must be formulated from equivalent first-order equations of motion. In order to reformulate the expression, the PDV model given in Equation (3.18) with displacement output is stated in a symmetrical companion form as follows.

$$\begin{bmatrix} D_{amp} & M \\ M & 0 \end{bmatrix} \begin{Bmatrix} \dot{q} \\ \ddot{q} \end{Bmatrix} = \begin{bmatrix} -K & 0 \\ 0 & M \end{bmatrix} \begin{Bmatrix} q \\ \dot{q} \end{Bmatrix} + \begin{bmatrix} \hat{B} \\ 0 \end{bmatrix} u$$
$$y_d = \begin{bmatrix} H_d & 0 \end{bmatrix} \begin{Bmatrix} q \\ \dot{q} \end{Bmatrix} \tag{3.28}$$

which leads to the symmetric eigenvalue problem as

$$\begin{bmatrix} -K & 0 \\ 0 & M \end{bmatrix} \begin{bmatrix} X \\ X\Lambda \end{bmatrix} = \begin{bmatrix} D_{amp} & M \\ M & 0 \end{bmatrix} \begin{bmatrix} X \\ X\Lambda \end{bmatrix} \Lambda \tag{3.29}$$

providing the following expression.

$$\begin{bmatrix} X \\ X\Lambda \end{bmatrix}^T \begin{bmatrix} D_{amp} & M \\ M & 0 \end{bmatrix} \begin{bmatrix} X \\ X\Lambda \end{bmatrix} = I$$
$$\begin{bmatrix} X \\ X\Lambda \end{bmatrix}^T \begin{bmatrix} -K & 0 \\ 0 & M \end{bmatrix} \begin{bmatrix} X \\ X\Lambda \end{bmatrix} = \Lambda \tag{3.30}$$

where,

$$\Lambda = \begin{bmatrix} \sigma_1 \pm jw_1 & & & 0 \\ & \sigma_2 \pm jw_2 & & \\ & & \ddots & \\ 0 & & & \sigma_i \pm jw_i \end{bmatrix}$$
$$X = \lfloor \ldots, \Re(X_i) \pm \Im(X_i), \ldots \rfloor \tag{3.31}$$

Here Λ and X are the complex eigenvalues and complex damped mode shapes normalized with respect to the physical properties of the structure.

As the system realization given in Equation (3.28) is a general one for the proportional damping case, the complex mode shapes and eigenvalues can still be obtained; however, for each mode the complex and real mode shapes are directly related to one another as observed in the follows.

$$\begin{aligned} \sigma_i &= -\zeta_i w_{ni} \\ w_i &= w_{ni}\sqrt{1-\zeta_i^2} \\ \Re(X_i) &= \frac{1}{2\sqrt{w_i}}\phi_i \\ \Im(X_i) &= -\frac{1}{2\sqrt{w_i}}\phi_i \end{aligned} \tag{3.32}$$

where ϕ_i and X_i are normalized mode shapes as given in Equations (3.4) and (3.30) respectively. The contributions of real and imaginary parts of the frequency response function to a typical displacement response with two closely spaced modes for both proportionally damped and non-proportionally damped cases are visualized in Figure 3.1 for better understanding.

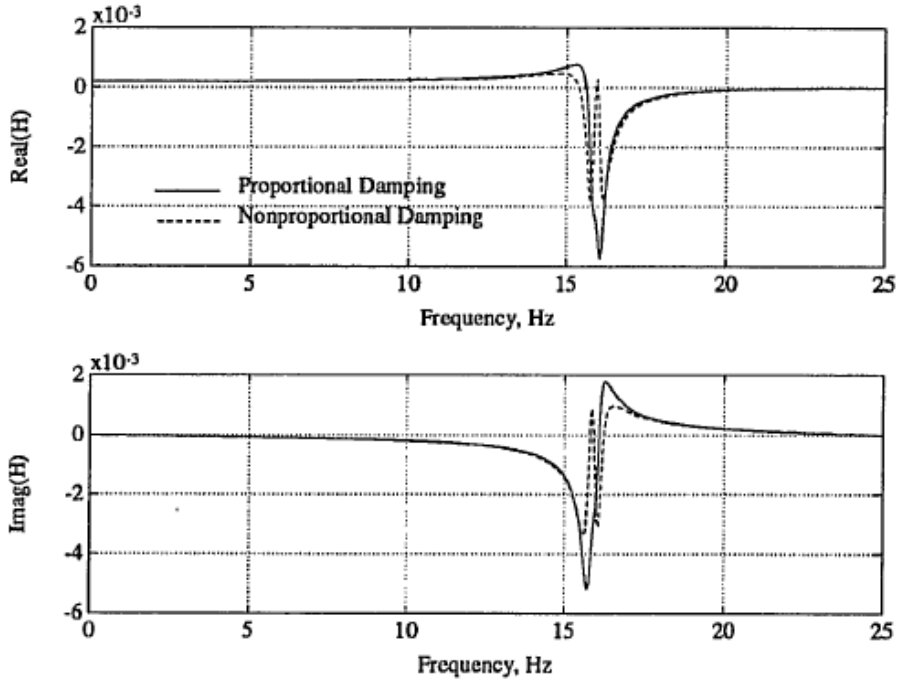

Figure 3.1 Frequency Response Function Components with Proportional and Non-Proportional Damping [28]

Briefly, in this chapter, transformation from second order mechanical system representation, into first order state space model is introduced for realization purposes. Moreover, special cases used for transformation of the state space model and modal forms are presented to be utilized in the realization process.

CHAPTER 4

LINEAR SYSTEM REALIZATION THEORY

System realization is the determination of system characteristics in the state space representation by using the excitation and response data. The basis is formed onto modern state space system theory that enables investigation of complex systems. There are two main approaches which are frequency domain and time domain realization methods. In this study, the main focus is concentrated on time-domain analysis techniques.

System realization property and its effectiveness depends on two fundamental aspects which are, observability and controllability. Observability is the ability of a system to convey its state information involved in its output over a finite time interval. On the other hand, controllability is the ability of a system to get its states controlled by an external input.

The observability and controllability concepts are first introduced by Kalman [26], who then introduced the basis for the minimum order realization concept with Ho [27]. Observability and controllability concepts play important role in the design of control systems as well. In the control implementations, the observability and controllability conditions affect the existence of the complete and unique solution. Although most physical systems are both controllable and observable, their mathematical representations may not possess the same abilities.

When the discrete time state space model of any system is considered as

$$\begin{aligned} x(k+1)_{n\times 1} &= A_{n\times n}\, x(k)_{n\times 1} + B_{n\times r}\, u(k)_{r\times 1} \\ y(k)_{m\times 1} &= C_{m\times n} x(k)_{n\times n} + D_{m\times r} u(k)_{r\times 1} \end{aligned} \tag{4.1}$$

where A is the system state transition matrix, B is the state input matrix, C is the state output matrix and D is the direct input output coupling matrix. In addition to that n is the number of states, m is the number of outputs, and r is the number of inputs applied to the system. Initially, assuming that there is no external excitation except the initial condition, $x(0) \neq 0$, the corresponding output y for the successive discrete time steps, $t = \Delta t, 2\Delta t, 3\Delta t, ..., k\Delta t$ can be expressed as follows.

$$\begin{aligned} y(0) &= C\, x(0) \\ y(1) &= C\, x(1) = C\, A\, x(0) \\ &\vdots \\ y(k-1) &= C\, x(k-1) = C\, A^{k-1}\, x(0) \end{aligned} \tag{4.2}$$

$$\begin{bmatrix} y_0 \\ y_1 \\ y_2 \\ \vdots \\ y_{k-1} \end{bmatrix} = P x_0 \quad , \; where \; P = \begin{bmatrix} C \\ CA \\ CA^2 \\ \vdots \\ CA^{(k-1)} \end{bmatrix}_{mk\times n} \tag{4.3}$$

Where P is the observability matrix with dimensions $mk \times n$ where k is the length of the expressed time series, where it might be truncated at any sufficiently long time duration.

Secondly, if the train of excitations $u(s) = \{u(0), u(1), u(2), ...u(s-1)\}$ is applied, then the internal state variable can be expressed as

$$x_s = A^s x_0 + Q_s \begin{bmatrix} u(s-1) \\ u(s-2) \\ \vdots \\ u(1) \\ u(0) \end{bmatrix}, \quad where\ Q_s = [B \quad AB \quad A^2B \quad \cdots \quad A^{(s-1)}B]_{n \times rs} \qquad (4.4)$$

where Q_s is the controllability matrix.

In a system identification application, in order to obtain the unique solution, again system states must be both controllable and observable. Further details and properties of observability and controllability concepts can be found in [29] and [11].

4.1 CONCEPTS OF REALIZATION

When the basic system characteristics is examined in the discrete time domain, the state space formulation can be obtained as follows.

$$x(k+1) = Ax(k) + Bu(k) \qquad (4.5)$$

$$y(k) = Cx(k) + Du(k) \qquad (4.6)$$

Here, for an impulse input, let $u_i(0) = 1 (i = 1, 2, 3, ..., r)$ and $u_i(k) = 0 (k = 1, 2, 3 \ldots)$ with zero initial conditions($x(0) = [0]$) be substituted into Eqs. (4.5) and (4.6). When the input is substituted into the above equations the outputs can be assembled into the impulse-response matrix Y , with the dimensions $m \times r$ as

$$Y_0 = D, \quad Y_1 = CB, \quad Y_2 = CAB, \ \ldots Y_k = CA^{k-1}B \qquad (4.7)$$

The constant impulse response matrices are also known as Markov parameters. These Markov parameters are used as the building bricks of identification for discrete time models. In Equations (4.5) and (4.6) there are four represented

unknown matrices as A, B, C, and D. In equation (4.7) as $D = Y_0$ is determined, only remaining three matrices A, B, and C are required to be computed.

Computation of the system triplet A, B, and C from Markov parameters, which satisfy Equation (4.7) is called *realization*. It can be predicted that, any system has infinite number of realizations that has the identical impulse-response behavior. This is because with higher order models, same impulse-response characteristics can be obtained as well. However, a unique solution can be obtained by using a minimum order realization. The minimum order realization means the smallest state space model that represents the impulse-response history uniquely. All the minimum order realization models include the same system characteristics which are eigenvalues and modal parameters of the actual system.

Assuming the state transition matrix A has a complete set of linearly independent eigenvectors $\Psi = [\psi_1, \psi_2, \ldots \psi_n]$ and corresponding eigenvalues $\Lambda = \text{diag}(\lambda_1, \lambda_2, \ldots \lambda_n)$ of the order n, then the realization of the system triplet A, B, and C can be transformed to realization of Λ, $\Psi^{-1}B$, and $C\Psi$. In this transformation the diagonal matrix Λ contains the modal damping and damped natural frequency information. Here by transforming Λ from discrete time to continuous time by applying $\Lambda_c = \ln(\Lambda)/\Delta t$, the desired modal damping rate and the damped natural frequency can be found simply from the real and imaginary parts of the eigenvalues Λ_c. Whereas the matrix $\Psi^{-1}B$ defines the initial modal amplitudes and $C\Psi$ matrix defines the mode shapes at the sensor locations which will be discussed in details in the next section.

There is one important thing to noted that, conversion of the eigenvalues from discrete time domain to continuous time domain is not unique. Because the imaginary part of the natural logarithm of a complex number can be adjusted by adding any multiple of 2π, which allows Λ_c to take different values. This is

because of the fact that, when observing from the same sample time, two frequencies that differ by multiples of $2\pi/\Delta t$ are indistinguishable. Therefore avoiding this problem, in order to find natural frequencies of the system, either the sample time Δt must be selected sufficiently short or a filter must be applied to prevent the frequencies beyond the Nyquist frequency from being folded into a lower frequencies in the realization.

The system realization process starts by forming the generalized Hankel matrix which includes Markov parameters from Equation (4.7).

$$H(k-1)=\begin{bmatrix} Y_k & Y_{k+1} & \cdots & Y_{k+\beta-1} \\ Y_{k+1} & Y_{k+2} & \cdots & Y_{k+\beta} \\ \vdots & \vdots & \ddots & \vdots \\ Y_{k+\alpha-1} & Y_{k+\alpha} & \cdots & Y_{k+\alpha+\beta-2} \end{bmatrix} \tag{4.8}$$

For the case when $k=1$, the Hankel matrix can be obtained as follows.

$$H(0)=\begin{bmatrix} Y_1 & Y_2 & \cdots & Y_{\beta} \\ Y_2 & Y_3 & \cdots & Y_{\beta+1} \\ \vdots & \vdots & \ddots & \vdots \\ Y_{\alpha} & Y_{\alpha+1} & \cdots & Y_{\alpha+\beta-1} \end{bmatrix} \tag{4.9}$$

It should be again mentioned that $Y_0=D$, which is previously stated in Equation (4.7), is not included in the $H(0)$. If $\alpha \geq n$ and $\beta \geq n$ (where n is the order of the system), the matrix $H(k-1)$ can be found of rank n. In order to confirm this, Markov parameters in Equation (4.7) can be substituted into Equation(4.8) as

$$H(k-1)=\begin{bmatrix} CA^{k-1}B & CA^{k}B & \cdots & CA^{k+\beta-2}B \\ CA^{k}B & CA^{k+1}B & \cdots & CA^{k+\beta-1}B \\ \vdots & \vdots & \ddots & \vdots \\ CA^{k+\alpha-2}B & CA^{k+\alpha-1}B & \cdots & CA^{k+\alpha+\beta-3}B \end{bmatrix} \tag{4.10}$$

and decomposing $H(k-1)$ into three matrices gives the following expression.

$$H(k-1) = P_\alpha A^{k-1} Q_\beta \tag{4.11}$$

where P_α is the observability matrix and Q_β is the controllability matrices as follows.

$$P_\alpha = \begin{bmatrix} C \\ CA \\ CA^2 \\ \vdots \\ CA^{\alpha-1} \end{bmatrix} \text{ and } Q_\beta = \begin{bmatrix} B & AB & A^2B & \dots & A^{\beta-1}B \end{bmatrix} \tag{4.12}$$

As previously stated for a controllable and observable system of order n, P_α and Q_β matrices must be of rank n as well. Based on the controllability and observability properties of the Hankel matrix, two modal parameter realization methodologies will be discussed in the preceding sections.

4.2 EIGENSYSTEM REALIZATION ALGORITHM (ERA)

The development of state space realization began with the study of the Ho and Kalman [27], who introduced the principles of minimum realization theory. The Ho and Kalman procedure utilize the generalized Hankel matrix in Equation(4.10) to identify modal parameters of a linear system from noise-free measurement data. This methodology was modified and extended by Juang and Pappa [12] to realize modal parameters of a linear system from noisy measurement data.

Unlike the classical system realization methods that utilize the generalized Hankel matrix given in (4.10), the ERA begins by forming a block data matrix which is obtained by deleting some row and columns of the generalized Hankel matrix, by keeping the first block matrix Y_k untouched. In addition to that, the standard ordering of the Markov parameters in the Hankel matrix does not need to be

maintained in the ERA. The schematic representation of the implementation of ERA is shown in Figure 4.1.

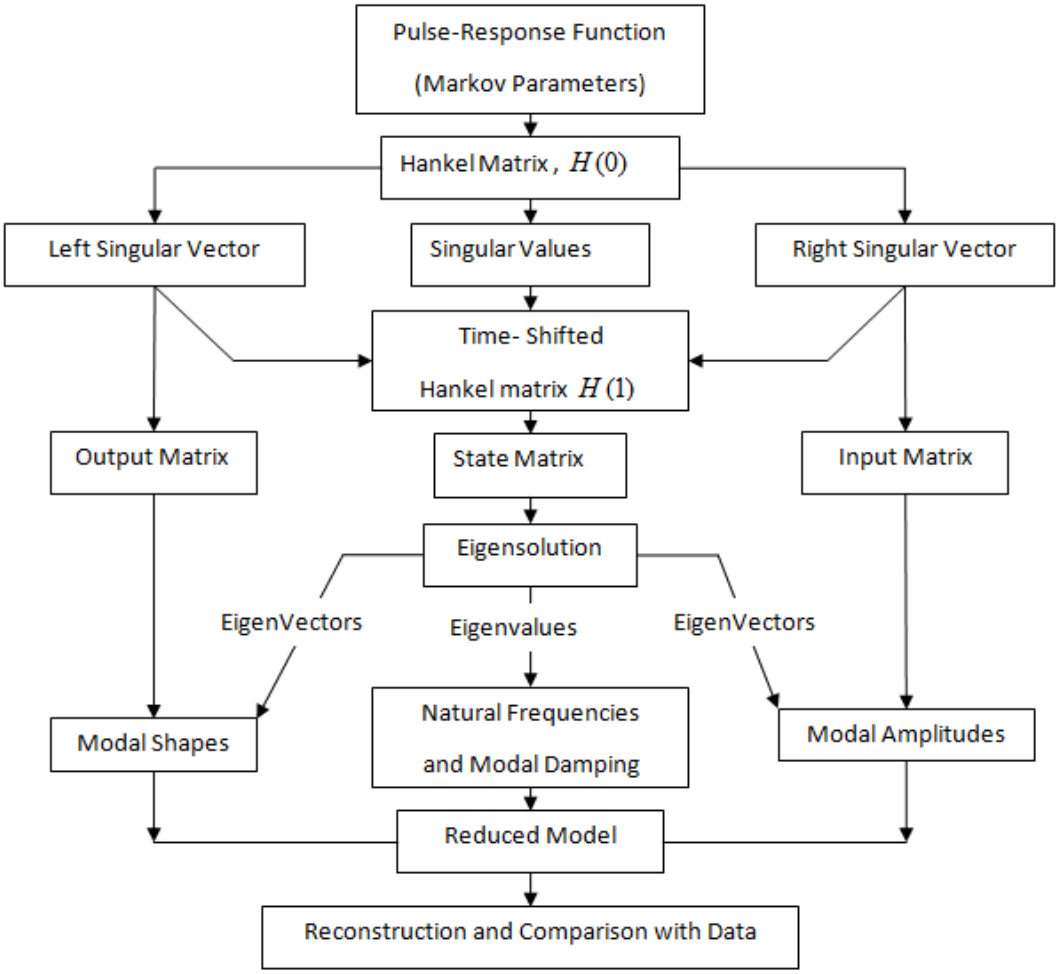

Figure 4.1 ERA Algorithm Flowchart [12]

When r is the number of inputs and m is the number of outputs, the input and output matrices can be defined as

$$B = \begin{bmatrix} b_1 & b_2 & \dots & b_r \end{bmatrix} \text{ and } C = \begin{bmatrix} c_1 \\ c_2 \\ \vdots \\ c_m \end{bmatrix} \tag{4.13}$$

where the column vector b_i is the control influence vector for the ith control input and the row vector c_j is the measurement influence vector for the jth sensor output. In this representation, column submatrices of B can be denoted by $B_i(i = 0,1,...\eta)$ and row submatrices of C can be denoted by $C_j(j = 0,1,...,\xi)$.

Then the ERA data block matrix can be expressed by incorporating the submatrices as follows.

$$H(k-1) = \left[Y_{s_i+k+t_j} \right] \text{ where } Y_{s_i+k+t_j} = C_j A^{s_i+k-1+t_j} B_i \qquad (4.14)$$

Where $s_0 = t_0 = 0$, and s_i and t_j are any arbitrary integers. Although this matrix looks more complex, it represents the matrix shown in Equation (4.10) with some rows and columns are deleted, but the first block Y_1 is maintained the same.

The ERA block data matrix, in Equation (4.14), enables including only good or strongly measured impulse response data without losing any capability if the number of measurement sensors or actuators are sufficiently oversized. This is especially useful when more noisy measurement data or output of malfunctioning sensor data is involved in the test output. The advantage of this capability is minimizing noise distortion on the identified system parameters. Here the columns of $H(k)$ can be formed as independently as possible by properly selecting the data samples to use as entries of the Hankel matrix. This effort substantially decreases the size of the Hankel matrix in dealing with large sized problems. This method also gets the true order of the state matrix A for substantially low noise level. This fact can be obtained by examining the observability and controllability matrices as given blow.

From Equation (4.14) Hankel matrix can be formed as follows.

$$H(k) = P_\alpha A^k Q_\beta \qquad (4.15)$$

where

$$P_\alpha = \begin{bmatrix} C \\ C_1 A^{s_1} \\ \vdots \\ C_\alpha A^{s_\alpha} \end{bmatrix} \text{ and } Q_\beta = \begin{bmatrix} B & A^{t_1}B_1 & \dots & A^{t_\beta}B_\beta \end{bmatrix} \tag{4.16}$$

again s_i and t_j are arbitrary integers. As previously stated P_α and Q_β are generalized observability and controllability matrices, which are slightly different from the ones shown above.

Assuming that there exists a matrix $H^\dagger$,which satisfies the following relation as

$$Q_\beta H^\dagger P_\alpha = I_n \tag{4.17}$$

$$H(0)H^\dagger H(0) = P_\alpha Q_\beta H^\dagger P_\alpha Q_\beta = P_\alpha Q_\beta = H(0) \tag{4.18}$$

where I_n is an identity matrix of order n. Therefore the matrix $H^\dagger$ is thus the pseudo-inverse of the Hankel matrix $H(0)$ in general.

The ERA implementation starts with the factorization of the block Hankel matrix, which is the general case independent of the selection of s_i and t_i, using singular value decomposition, the block Hankel matrix can be partitioned as

$$H(0) = R\Sigma S^T \tag{4.19}$$

where the columns of the left and right unitary matrices R and S are orthonormal and Σ is a rectangular matrix, whose diagonal elements contain the eigenvalues as follows.

$$\Sigma = \begin{bmatrix} \Sigma_n & 0 \\ 0 & 0 \end{bmatrix} \tag{4.20}$$

Where $\Sigma_n = \text{diag}[\sigma_1, \sigma_2, \ldots, \sigma_i, \sigma_{i+1}, \ldots, \sigma_n]$ and $\sigma_i (i = 1, 2, ..., n)$ are monotonically non increasing n (system order) number of eigenvalues as follows.

$$\sigma_1 \geq \sigma_2 \geq \ldots \geq \sigma_i \geq \sigma_{i+1} \ldots \sigma_n \geq 0 \tag{4.21}$$

Next, R_n and S_n matrices can be formed by using the first n columns of R and S matrices. By using the singular value decomposition from the rank of the block Hankel matrix, as the order of the realized system (n) is determined, then the matrix $H(0)$ and its pseudo-inverse can be represented by the smallest sized matrix that contains the same information as follows.

$$H(0) = R_n \Sigma_n S_n^T \text{ where } R_n^T R_n = I_n = S_n^T S_n \tag{4.22}$$

$$H^{\dagger} = S_n \Sigma_n^{-1} R_n^T \tag{4.23}$$

The above reduced matrices convey the same information with the original matrices as, beyond the rank of the block Hankel matrix, the contribution of eigenvalues are insignificant.

Here Equation (4.23) can be easily proven by investigating Equation (4.18). Also when Equation (4.22) and Equation (4.15) are compared with $k = 0$, it can be observed that P_α and Q_β are related to R_n and S_n^T respectively. Therefore one possible choice can be $P_\alpha = R_n \Sigma_n^{1/2}$ and $Q_\beta = \Sigma_n^{1/2} S_n^T$. Also this selection gives a balanced result for both P_α and Q_β. In addition to that from Equation (4.16), it is apparent that first r columns of Q_β, form the input matrix B meanwhile, the first m rows of P_α, constitute the output matrix C. It can be further examined by selecting $k = 1$ in Equation (4.15) as follows.

$$H(1) = P_\alpha A Q_\beta = R_n \Sigma_n^{1/2} A \Sigma_n^{1/2} S_n^T \tag{4.24}$$

Therefore one obvious solution for the state transition matrix A is as follows.

$$A = \Sigma_n^{-1/2} R_n^T H(1) S_n \Sigma_n^{-1/2} \tag{4.25}$$

Defining O_i as a null matrix of order i, I_i as an identity matrix of order i, then construct $E_m^T = [I_m \quad O_m \quad \dots \quad O_m]$ where m is the number of outputs and $E_r^T = [I_r \quad O_r \quad \dots \quad O_r]$ where r is the number of inputs. Then using above equations, a minimum order realization can be found as follows.

$$\begin{aligned}
Y_k &= E_m^T H(k-1) E_r \\
Y_k &= E_m^T P_\alpha A^{k-1} Q_\beta E_r \\
Y_k &= E_m^T P_\alpha [Q_\beta H^\dagger P_\alpha] A^{k-1} [Q_\beta H^\dagger P_\alpha] Q_\beta E_r \\
Y_k &= E_m^T H(0) [S_n \Sigma_n^{-1} R_n^T] P_\alpha A^{k-1} Q_\beta [S_n \Sigma_n^{-1} R_n^T] H(0) E_r \\
Y_k &= E_m^T H(0) S_n \Sigma_n^{-1/2} [\Sigma_n^{-1/2} R_n^T H(1) S_n \Sigma_n^{-1/2}]^{k-1} \Sigma_n^{-1/2} R_n^T H(0) E_r \\
Y_k &= E_m^T R_n \Sigma_n^{1/2} [\Sigma_n^{-1/2} R_n^T H(1) S_n \Sigma_n^{-1/2}]^{k-1} \Sigma_n^{1/2} S_n^T E_r
\end{aligned} \tag{4.26}$$

This is the fundamental formula of realization for the ERA. Therefore the system triplet can be obtained as

$$\hat{A} = \Sigma_n^{-1/2} R_n^T H(1) S_n \Sigma_n^{-1/2}, \quad \hat{B} = \Sigma_n^{1/2} S_n^T E_r, \; \hat{C} = E_m R_n \Sigma_n^{1/2} \tag{4.27}$$

which is the minimum order realization for system triplet . Here the quantities with over head like $\hat{A}$, represents estimated quantities or matrices. Here the order of the $\hat{A}$ matrix is n again, which is the true order of the actual system, determined via singular value decomposition analysis for sufficiently low noise data.

4.3 EIGENSYSTEM REALIZATION ALGORITHM WITH DATA CORRELATION (ERA/DC)

The problem with ERA is that, when the input and output measurements includes higher noise level, determined order of the system gets larger than the true order of the system. In order to overcome this problem, suggested method is to use correlated Hankel Matrices. The computational flowchart for the Eigensystem Realization Algorithm with Data Correlation (ERA/DC) can be seen in Figure 4.2.

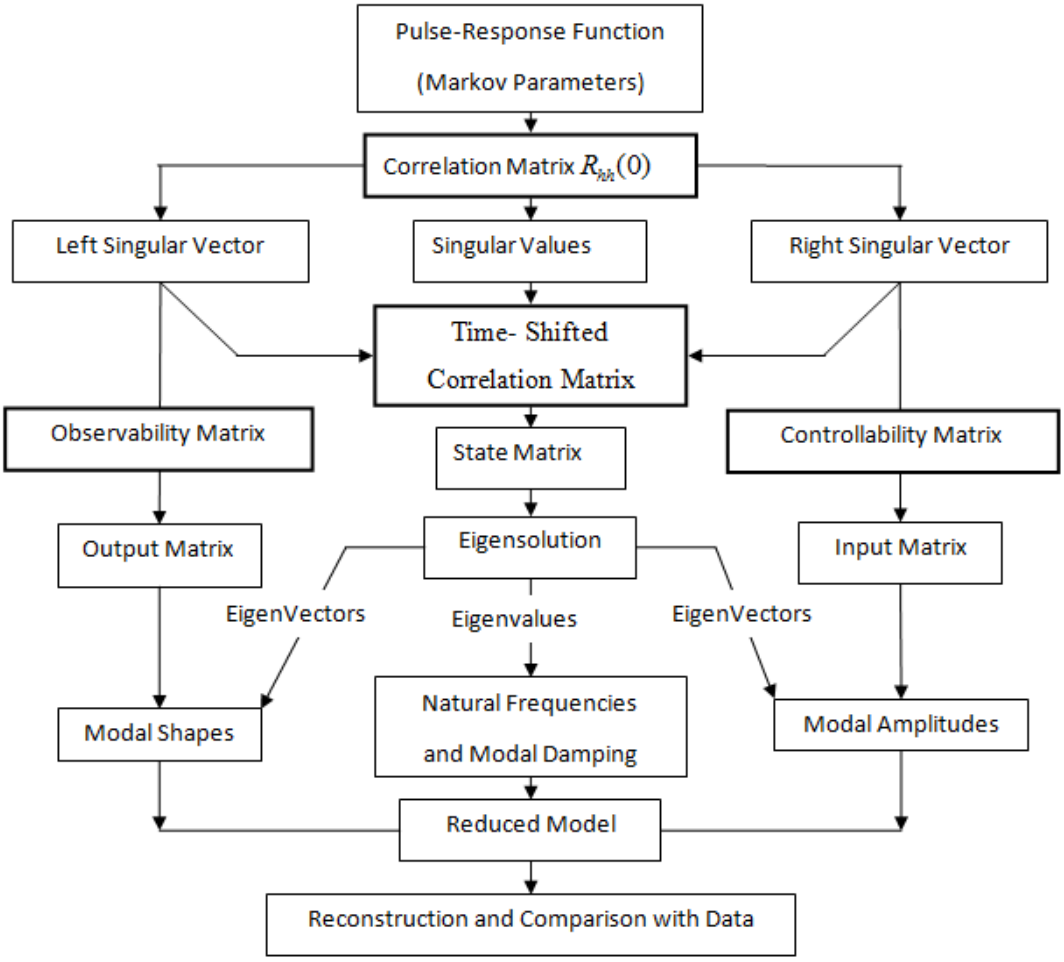

Figure 4.2 ERA / DC Algorithm Flowchart [1]

In order to get benefit from the ERA method with data correlations, the definition of a square matrix of order $\gamma = m\alpha$, where m is the number of outputs and α is the selected number of rows of Hankel matrix, is required as follows.

$$
\begin{aligned}
R_{hh}(k) &= H(k)H^T(0) \\
&= \begin{bmatrix} Y_{k+1} & Y_{k+2} & \cdots & Y_{k+\beta} \\ Y_{k+2} & Y_{k+3} & \cdots & Y_{k+\beta+1} \\ \vdots & \vdots & \ddots & \vdots \\ Y_{k+\alpha} & Y_{k+\alpha+1} & \cdots & Y_{k+\alpha+\beta-1} \end{bmatrix} \begin{bmatrix} Y_1 & Y_2 & \cdots & Y_\beta \\ Y_2 & Y_3 & \cdots & Y_{\beta+1} \\ \vdots & \vdots & \ddots & \vdots \\ Y_\alpha & Y_{\alpha+1} & \cdots & Y_{\alpha+\beta-1} \end{bmatrix}^T \\
&= \begin{bmatrix} \sum_{i=1}^{\beta} Y_i Y_i^T & \sum_{i=1}^{\beta} Y_i Y_{i+1}^T & \cdots & \sum_{i=1}^{\beta} Y_i Y_{\alpha+i-1}^T \\ \sum_{i=1}^{\beta} Y_i Y_{i+1}^T & \sum_{i=1}^{\beta} Y_{i+1} Y_{i+1}^T & \cdots & \sum_{i=1}^{\beta} Y_{i+1} Y_{\alpha+i-1}^T \\ \vdots & \vdots & \ddots & \vdots \\ \sum_{i=1}^{\beta} Y_{\alpha+i-1} Y_i^T & \sum_{i=1}^{\beta} Y_{\alpha+i-1} Y_{i+1}^T & \cdots & \sum_{i=1}^{\beta} Y_{\alpha+i-1} Y_{\alpha+i-1}^T \end{bmatrix}
\end{aligned}
\tag{4.28}
$$

For the case when $k = 0$, the correlation matrix $R_{hh}(0)$ becomes as following.

$$
\begin{aligned}
R_{hh}(0) &= H(0)H^T(0) \\
&= \begin{bmatrix} Y_1 & Y_2 & \cdots & Y_\beta \\ Y_2 & Y_3 & \cdots & Y_{\beta+1} \\ \vdots & \vdots & \ddots & \vdots \\ Y_\alpha & Y_{\alpha+1} & \cdots & Y_{\alpha+\beta-1} \end{bmatrix} \begin{bmatrix} Y_1 & Y_2 & \cdots & Y_\beta \\ Y_2 & Y_3 & \cdots & Y_{\beta+1} \\ \vdots & \vdots & \ddots & \vdots \\ Y_\alpha & Y_{\alpha+1} & \cdots & Y_{\alpha+\beta-1} \end{bmatrix}^T \\
&= \begin{bmatrix} \sum_{i=1}^{\beta} Y_i Y_i^T & \sum_{i=1}^{\beta} Y_i Y_{i+1}^T & \cdots & \sum_{i=1}^{\beta} Y_i Y_{\alpha+i-1}^T \\ \sum_{i=1}^{\beta} Y_i Y_{i+1}^T & \sum_{i=1}^{\beta} Y_{i+1} Y_{i+1}^T & \cdots & \sum_{i=1}^{\beta} Y_{i+1} Y_{\alpha+i-1}^T \\ \vdots & \vdots & \ddots & \vdots \\ \sum_{i=1}^{\beta} Y_{\alpha+i-1} Y_i^T & \sum_{i=1}^{\beta} Y_{\alpha+i-1} Y_{i+1}^T & \cdots & \sum_{i=1}^{\beta} Y_{\alpha+i-1} Y_{\alpha+i-1}^T \end{bmatrix}
\end{aligned}
\tag{4.29}
$$

As previously stated, $Y(k)$ is a $m \times r$ matrix whose rows are the Markov parameters corresponding to the each output. It can be recognized that the size of $H(k)$ and $H(0)$ is $\alpha m \times \beta r$, whereas the size of $R_{hh}(k)$ is $\alpha m \times \alpha m$. When the number of rows of the Hankel Matrix $H(k)$ is smaller than the number of columns, then the data correlation matrix $R_{hh}(k)$ is smaller in the size than the Hankel Matrix.

The matrix $R_{hh}(0)$ consists of auto-correlations of Markov parameters such as $\sum_{i=1}^{\beta} Y_i Y_i^T$ and cross correlations between the outputs such as $\sum_{i=1}^{\beta} Y_i Y_{i+1}^T$ accumulated over the r inputs. In case of correlated noise in the Markov Parameters, the correlation matrix $R_{hh}(0)$ will be containing less noise than the Hankel Matrix $H(0)$.

Substitution of Equation (4.15), into Equation (4.28) gives the following expression.

$$R_{hh}(k) = H(k)H^T(0) = P_\alpha A^k Q_\beta Q_\beta{}^T P_\alpha{}^T = P_\alpha A^k Q_c \qquad (4.30)$$

Where $Q_c = Q_\beta Q_\beta{}^T P_\alpha{}^T$. When the Correlation Matrix $R_{hh}(k) = P_\alpha A^k Q_c$ is compared with the Markov Parameter $Y(k) = CA^{k-1}B$, it can be observed that both matrices are the products of three matrices with discrete time state transition matrix in the middle. The ERA, explained in the above section, solves A, B, and C matrices based on the Hankel Matrices $H(0)$ and $H(1)$. Similarly, a block correlated Hankel Matrix can be constructed to solve for A, Q_c and P_α.

In fact, a $\xi \times \zeta$ block correlation Hankel Matrix can be formed as follows.

$$\aleph(k)=\begin{bmatrix} R_{hh}(k) & R_{hh}(k+\tau) & \dots & R_{hh}(k+\zeta\tau) \\ R_{hh}(k+\tau) & R_{hh}(k+2\tau) & \dots & R_{hh}(k+(\zeta+1)\tau) \\ \vdots & \vdots & \ddots & \vdots \\ R_{hh}(k+\xi\tau) & R_{hh}(k+(\xi+1)\tau) & \dots & R_{hh}(k+(\xi+\zeta)\tau) \end{bmatrix}$$

$$\aleph(k)=\begin{bmatrix} P_\alpha \\ P_\alpha A^\tau \\ \vdots \\ P_\alpha A^{\xi\tau} \end{bmatrix} A^k \begin{bmatrix} Q_c & A^\tau Q_c & \dots & A^{\zeta\tau} Q_c \end{bmatrix} \tag{4.31}$$

$$\aleph(k)=P_\xi A^k Q_\zeta$$

Again when $k=0$, the correlated Hankel matrix is obtained as

$$\aleph(0)=\begin{bmatrix} R_{hh}(0) & R_{hh}(\tau) & \dots & R_{hh}(\zeta\tau) \\ R_{hh}(\tau) & R_{hh}(2\tau) & \dots & R_{hh}((\zeta+1)\tau) \\ \vdots & \vdots & \ddots & \vdots \\ R_{hh}(\xi\tau) & R_{hh}((\xi+1)\tau) & \dots & R_{hh}((\xi+\zeta)\tau) \end{bmatrix}$$

$$\aleph(0)=\begin{bmatrix} P_\alpha \\ P_\alpha A^\tau \\ \vdots \\ P_\alpha A^{\xi\tau} \end{bmatrix} \begin{bmatrix} Q_c & A^\tau Q_c & \dots & A^{\zeta\tau} Q_c \end{bmatrix} \tag{4.32}$$

$$\aleph(k)=P_\xi Q_\zeta$$

where k is an integer chosen to avoid correlation terms that give rise to bias when noise is present in the data, and τ is an integer chosen to represent an interval to prevent significant overlapping of the adjacent R_{hh} blocks. The integers ξ and ζ are defined in order to define the amount of lag values included in the analysis. The matrices P_ξ and Q_ζ can be called block correlation observability and controllability matrices of dimension $m\alpha(\xi+1)\times n$ and $n\times m\alpha(\zeta+1)$ respectively, which are basically reflect the relationship between the system matrices A, B, C, and the Correlation Hankel Matrix $\aleph(0)$.

Similar to the ERA, the ERA/DC procedure continues with the factorization of the block Correlation Hankel Matrix $\aleph(0)$, using singular value decomposition as follows.

$$\aleph(0) = R\Sigma S^T \tag{4.33}$$

Where the columns of the matrices R and S are orthonormal, so that they satisfy $R^T R = I$, and $S^T S = I$ where I is the identity matrix. In addition to that, Σ is a rectangular matrix as

$$\Sigma = \begin{bmatrix} \Sigma_n & 0 \\ 0 & 0 \end{bmatrix} \tag{4.34}$$

where $\Sigma_n = \text{diag}[\sigma_1, \sigma_2, \ldots, \sigma_i, \sigma_{i+1}, \ldots, \sigma_n]$ and $\sigma_i (i = 1, 2, ..., n)$ are monotonically non increasing n (system order) number of eigenvalues as follows.

$$\sigma_1 \geq \sigma_2 \geq \ldots \geq \sigma_i \geq \sigma_{i+1} \ldots \sigma_n \geq 0 \tag{4.35}$$

Next, R_n and S_n matrices can be formed by using first n columns of R and S respectively. The columns of $R_n (m\alpha(\xi+1) \times n)$ and $S_n (m\alpha(\zeta+1) \times n)$ are orthonormal and Σ is a diagonal matrix containing the first n singular values that are considered as significant, based on the same truncation procedure explained in the ERA procedure. Here there is an important point to be highlighted that, when the noise is present in the data, the above factorization becomes approximate, because the discarded singular values becomes nonzero in the presence of noise.

Hence, the correlation Hankel Matrix $\aleph(0)$ and its pseudo inverse becomes as follows.

$$\aleph(0) = R_n \Sigma_n S_n^T \quad and \quad \aleph^{\dagger} = S_n \Sigma_n^{-1} R_n^T \tag{4.36}$$

Here Equation (4.36) can be proven by investigating the following expression.

$$\aleph(0)\,\aleph^{\dagger}\,\aleph(0) = \aleph(0) \tag{4.37}$$

Then using Equation (4.31) and (4.37), the above relationship can be rewritten as follows.

$$P_{\xi}Q_{\zeta}\aleph^{\dagger}P_{\xi}Q_{\zeta} = P_{\xi}Q_{\zeta} \quad or \quad P_{\xi}[Q_{\zeta}\underbrace{Q_{\zeta}^{\dagger}P_{\xi}^{\dagger}}_{\aleph^{\dagger}}P_{\xi}]Q_{\zeta} = P_{\xi}Q_{\zeta} \tag{4.38}$$

$$Q_{\zeta}\aleph^{\dagger}P_{\xi} = I_n \tag{4.39}$$

Here the condition is that both P_{ξ} and Q_{ζ} are of rank n, so that they are invertible. In order to obtain correct size of the correlation matrix, O_{γ} as a null matrix, I_{γ} as an identity matrix of order γ, and $E_{\gamma}^{T} = [I_{\gamma} \quad 0_{\gamma} \quad \dots \quad 0_{\gamma}]$ shall be defined. Then following a similar approach to that is given in the ERA section, a minimum order realization of dimension n can be derived as follows.

$$\begin{aligned}
R_{hh}(k) &= E_{\gamma}^{T}\,\aleph(k)E_{\gamma} \\
R_{hh}(k) &= E_{\gamma}^{T}P_{\xi}[Q_{\zeta}\aleph^{\dagger}P_{\xi}]A^{k}[Q_{\zeta}\aleph^{\dagger}P_{\xi}]Q_{\zeta}E_{\gamma} \\
R_{hh}(k) &= E_{\gamma}^{T}[P_{\xi}\,Q_{\zeta}]\aleph^{\dagger}[P_{\xi}A^{k}Q_{\zeta}]\aleph^{\dagger}\aleph(0)E_{\gamma} \\
R_{hh}(k) &= E_{\gamma}^{T}[R_n\Sigma_n S_n^{T}]S_n\Sigma_n^{-1}R_n^{T}[P_{\xi}A^{k}Q_{\zeta}]S_n\Sigma_n^{-1}R_n^{T}[R_n\Sigma_n S_n^{T}]E_{\gamma} \\
R_{hh}(k) &= E_{\gamma}^{T}R_n\Sigma_n^{1/2}[\Sigma_n^{-1/2}R_n^{T}[P_{\xi}A^{k}Q_{\zeta}]S_n\Sigma_n^{-1/2}]\Sigma_n^{1/2}S_n^{T}E_{\gamma} \\
R_{hh}(k) &= E_{\gamma}^{T}R_n\Sigma_n^{1/2}[\Sigma_n^{-1/2}R_n^{T}\aleph(1)S_n\Sigma_n^{-1/2}]^{k}\Sigma_n^{1/2}S_n^{T}E_{\gamma}
\end{aligned} \tag{4.40}$$

Indeed, this is the basic formulation of minimum realization for the ERA/DC. Therefore observability and controllability matrices can be computed as follows.

$$P_{\alpha} = E_{\gamma}^{\ T}R_n\Sigma_n^{1/2} \tag{4.41}$$

$$H(0) = P_\alpha Q_\beta = \begin{bmatrix} C \\ CA \\ CA^2 \\ \vdots \\ CA^{\alpha-1} \end{bmatrix} \begin{bmatrix} B & AB & A^2B & \dots & A^{\beta-1}B \end{bmatrix} \tag{4.42}$$

$$Q_\beta = P_\alpha^\dagger H(0) = [E_\gamma^T R_n \Sigma_n^{1/2}]^\dagger H(0) \tag{4.43}$$

Here it is clear that the output matrix C and the input matrix B can be obtained from Equation (4.42) by using first m rows of P_α and the first r columns of Q_β respectively. Hence a realization for the system triplet $[\hat{A},\ \hat{B},\ \hat{C}]$ can be found as follows.

$$\begin{aligned} \hat{A} &= \Sigma_n^{-1/2} R_n^T \aleph(1) S_n \Sigma_n^{-1/2} \\ \hat{B} &= [E_\gamma^T R_n \Sigma_n^{1/2}]^\dagger H(0) E_r \\ \hat{C} &= E_m^T R_n \Sigma_n^{1/2} \end{aligned} \tag{4.44}$$

As in the case of ERA, the natural frequencies and damping values belongs to system can be computed from the realized state transition matrix. In addition to that, with suitable transformation matrix, eigenvectors can be transformed into modal space so that, damped mode shapes and initial modal amplitudes can be determined.

Here another important point to note is that, ERA/DC involves a fit to the output, auto-correlations and cross-correlations over a defined number of lag values and measurement noise can be eliminated by properly selecting k integer number of lag values in Equation (4.31). On the other hand, ERA provides a least-squares fit so that, it is vulnerable to bias terms and measurement noise.

4.3.1 Performance Measures of System Realization with ERA or ERA/DC

In order to distinguish realized true system modes from false modes, two performance measures are introduced by Juang and Pappa [10]. These are the Modal Amplitude Coherence (MAC) and the Mode Singular Value (MSV). In order to compute performance measures, first identified discrete time state space in modal form shall be considered as

$$\begin{aligned} x_m(k+1) &= \hat{\Lambda} x_m(k) + \hat{B}_m u(k) \\ y(k) &= \hat{C}_m x_m(k) + Du(k) \end{aligned} \tag{4.45}$$

here $\hat{\Lambda}$ is a diagonal matrix, containing eigenvalues of discrete state transition matrix, $\hat{B}_m$ and $\hat{C}_m$ are the modal input-state and state-output matrices respectively. In this case the modal matrices can be computed as follows.

$$\begin{aligned} &\hat{A} = \Psi \hat{\Lambda} \Psi^{-1} \rightarrow \hat{\Lambda} = \Psi^{-1} \hat{A} \Psi \\ &\hat{B}_m = \Psi^{-1} \hat{B} \\ &\hat{C}_m = \hat{C} \Psi \end{aligned} \tag{4.46}$$

Then the complex modal system matrices can be partitioned as follows.

$$\hat{\Lambda} = \begin{bmatrix} \hat{\lambda}_1 & & & 0 \\ & \hat{\lambda}_2 & & \\ & & \ddots & \\ 0 & & & \hat{\lambda}_n \end{bmatrix} \quad \hat{B}_m = \begin{bmatrix} \hat{b}_1 \\ \hat{b}_2 \\ \vdots \\ \hat{b}_n \end{bmatrix} \quad \hat{C}_m = \begin{bmatrix} \hat{c}_1 & \hat{c}_2 & \cdots & \hat{c}_n \end{bmatrix} \tag{4.47}$$

Therefore, the identified modal amplitude time history for each mode can be obtained as follows.

$$\hat{q}_i = \begin{bmatrix} \hat{b}_i & \hat{\lambda}_i \hat{b}_i & \hat{\lambda}_i^2 \hat{b}_i & \cdots & \hat{\lambda}_i^{l-2} \hat{b}_i \end{bmatrix} \tag{4.48}$$

In order to asses, how good modal amplitude time history is identified, the real modal time history belonging to system must be computed. In this case, the real modal time history can be computed from controllability. For this purpose the Hankel matrix can be partitioned as

$$
\begin{aligned}
H(0) &= \bar{P}\bar{Q} \\
H(0) &= \begin{bmatrix} C_m B_m & C_m \Lambda B_m & \cdots & C_m \Lambda^{l-\alpha-1} B_m \\ C_m \Lambda B_m & C_m \Lambda^2 B_m & \cdots & C_m \Lambda^{l-\alpha} B_m \\ \vdots & \vdots & \ddots & \vdots \\ C_m \Lambda^{\alpha-1} B_m & C_m \Lambda^{\alpha} B_m & \cdots & C_m \Lambda^{l-2} B_m \end{bmatrix} \\
H(0) &= \begin{bmatrix} C_m \\ C_m \Lambda \\ \vdots \\ C_m \Lambda^{\alpha-1} \end{bmatrix} \begin{bmatrix} B_m & \Lambda B_m & \cdots & \Lambda^{l-\alpha-1} B_m \end{bmatrix}
\end{aligned}
\tag{4.49}
$$

Here it should be noted that actual system matrices Λ, B_m, and C_m are expressed in modal coordinates. Therefore, the actual modal time history can be computed from controllability matrix as follows.

$$
\begin{aligned}
\bar{Q} &= \begin{bmatrix} \bar{q}_1 \\ \bar{q}_2 \\ \vdots \\ \bar{q}_n \end{bmatrix} = \begin{bmatrix} B_m & \Lambda B_m & \cdots & \Lambda^{l-\alpha-1} B_m \end{bmatrix} \\
\bar{Q} &= \begin{bmatrix} \bar{q}_1 \\ \bar{q}_2 \\ \vdots \\ \bar{q}_n \end{bmatrix} = \begin{bmatrix} \begin{bmatrix} b_1 & \lambda_1 b_1 & \cdots & \lambda_1^{l-\alpha-1} b_1 \end{bmatrix} \\ \begin{bmatrix} b_2 & \lambda_2 b_2 & \cdots & \lambda_2^{l-\alpha-1} b_2 \end{bmatrix} \\ \vdots \\ \begin{bmatrix} b_n & \lambda_n b_n & \cdots & \lambda_n^{l-\alpha-1} b_n \end{bmatrix} \end{bmatrix}
\end{aligned}
\tag{4.50}
$$

Here when equations (4.48) and (4.50) are compared, it can be observed that the identified modal time history is equivalent to the real modal time history in the absence of noise.

After the real and identified modal time histories are obtained, performance measures, which are MAC and MSV can be computed.

MAC measures correspondence of identified modal time history to real modal time history. In its computation, it can be considered as a dot product of the real and identified modal time histories. In this case dot product in the MAC computation can also be considered as cosine of the angle between the identified and the real modal time histories which is computed for each mode as

$$MAC_i = \frac{\left|\bar{q}_i \hat{q}_i^*\right|}{\sqrt{\left|\bar{q}_i \bar{q}_i^*\right|\left|\hat{q}_i \hat{q}_i^*\right|}} \tag{4.51}$$

where * corresponds to transpose and complex conjugate operation.

Here it should be noted that, when the identified and real modal time histories are identical for a specific mode, MAC value is computed as 1, which is the limiting value for MAC.

On the other hand, MSV defines contribution of each identified mode to the realized impulse response history. Therefore a well identified mode has large contribution on the realized impulse response history and its MSV value is computed higher. Therefore, MSV values of each mode can be computed as

$$MSV_i = \sqrt{\left|\hat{c}_i\right|\left(1+\left|\hat{\lambda}_i\right|+\left|\hat{\lambda}_i^2\right|+\ldots+\left|\hat{\lambda}_i^{l-2}\right|\right)\left|\hat{b}_i\right|} \tag{4.52}$$

for sufficiently large number of data and when $\left|\hat{\lambda}_i\right|$ is less than 1, the MSV value can be approximated as follows.

$$MSV_i \cong \sqrt{\frac{\left|\hat{c}_i\right|\left|\hat{b}_i\right|}{\left(1-\left|\hat{\lambda}_i\right|\right)}} \tag{4.53}$$

Therefore for large number of data and when $\left|\hat{\lambda}_i\right|$ is less than 1, the limiting value of MSV can be computed by using Equation (4.53).

4.3.2 Damped Modal Realization from Output of ERA or ERA/DC

Here the realized model represented by $\hat{A}$, $\hat{B}$, and $\hat{C}$ is in the discrete time and it can be converted to continuous time, so that system frequencies and damping can be computed.

First transformation of the discrete system matrix $\hat{A}$ into its continuous case A can be performed by using the following relation as

$$\Psi^{-1}\hat{A}\Psi = e^{\Lambda\Delta t} \quad \Leftrightarrow \quad \Psi^{-1}A\Psi = \Lambda_c \tag{4.54}$$

where Ψ and Λ are the eigenvectors and eigenvalues of the matrix A. Then the continuous system eigenvalues, for zero order hold discretization assumption, can be obtained as

$$\Lambda_c = \ln(\Lambda)/\Delta t = diag\{\sigma_i \pm jw_i, i = 1,\ldots,n\} \tag{4.55}$$

here σ_i and w_i are the real and imaginary parts of the continuous state-space system characteristic roots. In addition to that, in Equation (4.55), imaginary roots represent the damped natural frequencies and by finding utilizing the following formulas the undamped natural frequencies (w_{ni}) and modal damping ratio (ζ_i) can be computed as follows.

$$w_i = w_{ni}\sqrt{1-\zeta_i^2} \tag{4.56}$$

$$\zeta_i = -\frac{\sigma_i}{w_{ni}} \tag{4.57}$$

Therefore the continuous state transition matrix can be obtained as follows.

$$A = \Psi \Lambda_c \Psi^{-1} \tag{4.58}$$

Secondly, it can be recalled that, as long as A is nonsingular, the discrete operator $\hat{B}$ can be computed as

$$\hat{B} = (\hat{A} - I) A^{-1} B \tag{4.59}$$

where I is a $n \times n$ identity matrix. From Equation(4.59), the following expression can be obtained by replacing $\hat{A}$ as follows.

$$\Psi^{-1} \hat{B} = (e^{\Lambda_c \Delta t} - I) \Lambda_c \Psi^{-1} B \tag{4.60}$$

Therefore the continuous input-state influence matrix can be computed from (4.59) as

$$B = A(\hat{A} - I)^{-1} \hat{B} \tag{4.61}$$

Moreover, it is known that the continuous and discrete forms of state-output influence matrix C and direct transmission matrix D are the same as they provide mapping between system states, inputs and outputs, which is not dependent on the time.

After the continuous time model is obtained, then continuous modal, state-space realization can also be obtained as follows

$$\begin{aligned} \dot{z}(t) &= \Lambda_c \, z(t) + B_\psi \, u(t) \\ y(t) &= C_\psi \, z(t) \end{aligned} \tag{4.62}$$

In Equation (4.62), it can be observed that internal variable $z(t)$ is associated with an arbitrary basis vector which can be obtained via $z(t) = \Psi x(t)$ transformation. On the other hand, the input vector $u(t)$, and output vector $y(t)$ are based on the same basis vector, which are measured from the experiments. Therefore the system

Therefore the modal excitation matrix B_ψ can be written as follows.

$$B_\psi = \Psi^{-1}B = \Lambda^{-1}(e^{\Lambda\Delta t} - I)^{-1}\Psi^{-1}\hat{B} \tag{4.63}$$

On the other hand, the modal measurement matrix C_ψ, can be obtained by using different sensor outputs as

$$C = [H_d\ 0] + [H_v\ 0]\,A + [H_a\ 0]A^2 \tag{4.64}$$

In practice, output of each sensor types are treated separately. This results that the modal output matrix becomes different according to sensor type as follows.

$$\begin{aligned} C_\psi &= \{H_d\Psi \text{ for displacement sensor output}\} \\ &= \{H_v\Psi\Lambda_c^{-1} \text{ for velocity sensor output}\} \\ &= \{H_a\Psi\Lambda_c^{-2} \text{ for acceleration sensor output}\} \\ &= \{\ldots \text{Real}(C_{\psi_i}) \pm \text{Imaginary}(C_{\psi_i})\ldots\} \text{ where } i = 1,\ldots n \text{ for each node} \end{aligned} \tag{4.65}$$

To sum up in this chapter, two powerful realization algorithms, which are ERA and ERA/DC are investigated in terms of their formulations and formulations of realized system matrices are stated. In addition to that, transformation from discrete realized system matrices, into continuous form are given in the last section. Finally, transformation to the continuous damped modal form is explained, which will be mainly used in the extraction of physical system parameters chapter.

CHAPTER 5

EXTRACTION OF PHYSICAL SYSTEM PARAMETERS

The first order modeling approach explained in the above sections are generally preferred and utilized by the researchers in the control field. In order to obtain first order state space models, methodologies like ERA and ERA/DC explained in the preceding sections are also sufficient. In those models or realizations, physical system properties like mass, stiffness or damping cannot be obtained directly. A transformation from the first order models, into second order models is required to determine mechanical system properties. The main idea behind obtaining the system properties is to whether find the best sensor locations for control purposes or validate finite element modeling of the system, or damage detection and localization for health monitoring purposes.

In literature, obtaining system properties from the measured input-output signals is called *the inverse vibration problem* [28], [29]. On the other hand obtaining first order models from the second order differential equations is a rather straightforward task and called the *forward vibration problem*. As expected, the inverse vibration problem is more complex such that, it attracted attention of various researchers with different methodologies. Some of those examples are published by Ibrahim(1983), Zhang and Lallement(1987), Yang and Yeh(1990), Alvin (1993), Alvin and Park(2003) [22] and De Angelis(2002) [28].

In this section a transformation based method for converting first order system model into second order structural dynamic model will be presented. The implemented methodology is called *Common Basis-Normalized Structural*

Identification (CBSI) which is developed by Alvin [25] and reformulated by Bernal and Güneş [30] and further examined by Luş et al. [28]. The main selection criterion among other methodologies are starting with the first order model obtained from the realization algorithms, being able to utilize all types of sensors (displacement, velocity and acceleration) and being able to of identify nonproportional damping properties as well.

Here there are two important points to be addressed. First, in the solution of inverse vibration problem, the number of sensors and actuators play crucial role in the size of identified physical system parameters. Different methodologies require, whether full set of actuators, or full set of sensors, or either an actuator or sensor at each degree of freedom. Actually CBSI method requires full set of sensors which means that, there must be a number of sensors at each degree of freedom of the system. However, utilizing lacking actuators is sufficient for CBSI implementation.

Second important issue is having at least one collocated (Having both sensor and actuator at the same degree of freedom) sensor and actuator pair. This requirement exists to obtain mass matrix from the mass normalized undamped modes or to scale complex eigenvectors. Actually, the collocated sensor and actuator requirement is general to all methodologies solving the inverse vibration problem. In the CBSI case as there exists sensors at all the degrees of freedom, by applying even a single input to the system satisfies the collocation requirement.

The CBSI procedure start with the realized discrete system model given in Equation (4.5).

$$\begin{aligned} z(k+1) &= \hat{A}z(k) + \hat{B}u(k) \\ y(k) &= \hat{C}z(k) + \hat{D}u(k) \end{aligned} \tag{5.1}$$

where $\hat{A}$, $\hat{B}$, $\hat{C}$, and $\hat{D}$ are the identified discrete system matrices obtained from any of the realization algorithms explained in the Chapter 4.

Similarly, the continuous counterpart of the Equation (5.1) can be obtained, as follows.

$$\begin{aligned} \dot{z}(t) &= A_c\, z(t) + B_c u(t) \\ y(t) &= C_c\, z(t) + D_c u(t) \end{aligned} \tag{5.2}$$

with A_c, B_c, C_c, and D_c are the continuous system matrices and here D can be omitted for displacement output representation.

Finally, the damped modal continuous form can be obtained by following the transformation $z(t) = \Psi \hat{z}(t)$ where $A_c = \Psi \Lambda_c \Psi^{-1}$ as follows.

$$\begin{aligned} \dot{\hat{z}} &= \Lambda_c\, z(t) + \Psi^{-1} B_c u(t) \\ y(t) &= C_c\, \Psi\, z(t) \end{aligned} \tag{5.3}$$

Here again it should be noted that, the D_c matrix is omitted because of the displacement-output equivalent model representation.

At this point, for a N degree of freedom system, in order to transform first order arbitrary based model given in Equation (5.3), into physical displacement-velocity model (PDV) described in Equation (3.18) which is again represented as

$$\begin{aligned} \dot{x}_I(t) &= A_I x_I(t) + B_I u(t) \\ y(t) &= C_I x_I(t) \end{aligned} \tag{5.4}$$

where

$$\begin{aligned} A_I &= \begin{bmatrix} 0 & I \\ -M^{-1}K & -M^{-1}D_{amp} \end{bmatrix} \\ B_I &= \begin{bmatrix} 0 \\ M^{-1}\hat{B} \end{bmatrix} \\ C_I &= \begin{bmatrix} H_d & 0 \end{bmatrix} \end{aligned} \tag{5.5}$$

There must be a transformation matrix T of dimension $2N \times 2N$ as

$$x(t) = \mathrm{T}\hat{z}(t) \tag{5.6}$$

provides the following relationship as

$$\begin{aligned} \mathrm{T}\Lambda_c &= A_1\mathrm{T} \\ \mathrm{T}^{-1}B_1 &= \Psi^{-1}B_c \\ C_1\mathrm{T}_1 &= C_c\Psi \end{aligned} \tag{5.7}$$

In the above expression, the transformation for matrix A_1 indicates that the transformation matrix must consist of the complex eigenvalues Λ_c and complex valued eigenvectors ψ^d, which are obtained from the eigensolution of the displacement velocity expression given in Equation(5.4)), and a diagonal matrix $\tilde{\mathrm{T}}$ which contains some scaling values for the eigenvectors as follows.

$$\mathrm{T} = \begin{bmatrix} \psi^d \\ \psi^d\Lambda_c \end{bmatrix}\tilde{\mathrm{T}} = \begin{bmatrix} \psi^d\tilde{\mathrm{T}} \\ \psi^d\Lambda_c\tilde{\mathrm{T}} \end{bmatrix} \tag{5.8}$$

Therefore the solution for the transformation matrix is developed by utilizing the transformation for the output matrix in the expression (5.7). As there exists full set of displacement sensors, H_d in C_I is an identity matrix with full rank (rank N) so the $\psi^d\tilde{\mathrm{T}}$ expression stated above can be evaluated as

$$C_1\mathrm{T}_1 = C_c\Psi = H_d\psi^d\tilde{\mathrm{T}} \;\Rightarrow\; \psi^d\tilde{\mathrm{T}} = H_d{}^{-1}C_c\Psi \tag{5.9}$$

In addition to that, as both Λ_c and $\tilde{\mathrm{T}}$ are diagonal, the following expression for the transformation matrix can be obtained as follows.

$$\mathrm{T} = \begin{bmatrix} \psi^d \\ \psi^d\Lambda_c \end{bmatrix}\tilde{\mathrm{T}} = \begin{bmatrix} H_d{}^{-1}C_c\Psi \\ H_d{}^{-1}C_c\Psi\Lambda_c \end{bmatrix} \tag{5.10}$$

Here all the expressions on the right hand side of the above equation are known, therefore the transformation matrix can be obtained easily but the eigenvectors ψ^d and diagonal scaling matrix $\tilde{\mathrm{T}}$ cannot be explicitly known at the moment and as will be stated below, they are not required to be known individually.

At this point, the state matrix A_I can be evaluated from eigensolution of the displacement velocity (DV) model, which is expressed as follows.

$$\begin{bmatrix} 0 & I \\ -M^{-1}K & -M^{-1}D_{amp} \end{bmatrix} \begin{bmatrix} \psi^d \\ \psi^d \Lambda_c \end{bmatrix} = \begin{bmatrix} \psi^d \\ \psi^d \Lambda_c \end{bmatrix} \Lambda_c \tag{5.11}$$

$$\begin{bmatrix} 0 & I \\ -M^{-1}K & -M^{-1}D_{amp} \end{bmatrix} = \begin{bmatrix} \psi^d \\ \psi^d \Lambda_c \end{bmatrix} \Lambda_c \begin{bmatrix} \psi^d \\ \psi^d \Lambda_c \end{bmatrix}^{-1} \tag{5.12}$$

$$\begin{bmatrix} 0 & I \\ -M^{-1}K & -M^{-1}D_{amp} \end{bmatrix} = \begin{bmatrix} \psi^d \\ \psi^d \Lambda_c \end{bmatrix} \tilde{\mathrm{T}} \Lambda_c \tilde{\mathrm{T}}^{-1} \begin{bmatrix} \psi^d \\ \psi^d \Lambda_c \end{bmatrix}^{-1} \tag{5.13}$$

Here the expression above still holds as the $\tilde{\mathrm{T}}$ matrix is diagonal. As stated before, the eigenvectors and scaling functions are not required to be determined individually. After the state matrix in Equation (5.13) is determined, the undamped eigenvalues and undamped eigenvectors of the second order system model can be obtained by solving the following eigenproblem as

$$M^{-1}K\hat{\Phi}_i = \Omega_i^{\,2}\hat{\Phi}_i \text{ where } i = 1,2,...,N \tag{5.14}$$

where $\hat{\Phi}_i$ is the arbitrarily scaled undamped eigenvectors and $M^{-1}K$ can be obtained from the partition of the A_I matrix given above. Finally, the collocation requirement is essential in order to obtain mass matrix M from displacement velocity model. Here the mass normalized eigenvectors Φ_i, can be obtained from

arbitrarily scaled undamped eigenvectors $\hat{\Phi}_i$, by utilizing the collocation requirement through a scaling matrix S as

$$\Phi = \hat{\Phi} S \tag{5.15}$$

where eigenvectors are constructed such that $\hat{\Phi} = \begin{bmatrix} \hat{\Phi}_1 & \hat{\Phi}_2 & \dots & \hat{\Phi}_N \end{bmatrix}$ and the scaling function is a diagonal matrix constructed such that $S = diag(s_1, s_2, \dots, s_N)$.

Therefore using the mass normalization property the inverse of the mass matrix M^{-1} can be obtained as follows.

$$M^{-1} = \Phi \Phi^T \tag{5.16}$$

$$M^{-1} = (\hat{\Phi} S)(S \hat{\Phi}^T) = \hat{\Phi} S^2 \hat{\Phi}^T = s_1^{\,2} \hat{\Phi}_1 \hat{\Phi}_1^{\,T} + s_2^{\,2} \hat{\Phi}_2 \hat{\Phi}_2^{\,T} + \dots + s_N^{\,2} \hat{\Phi}_N \hat{\Phi}_N^{\,T} \tag{5.17}$$

In addition to that, considering the scaling function for the input matrix in Equation (5.7), the $\mathrm{T}^{-1} B_1 = \Psi^{-1} B_c$ expression can be expanded as

$$\begin{bmatrix} \psi^d \\ \psi^d \Lambda_c \end{bmatrix} \tilde{\mathrm{T}} \Psi^{-1} B_c = \begin{bmatrix} H_d^{\,-1} C_c \Psi \\ H_d^{\,-1} C_c \Psi \Lambda_c \end{bmatrix} \Psi^{-1} B_c = \begin{bmatrix} 0 \\ M^{-1} \hat{B} \end{bmatrix} \tag{5.18}$$

where $\hat{B}$ is the binary input matrix given in Equation (3.1). Then lower partition of the above expression gives the following relation.

$$\begin{aligned} H_d^{\,-1} C_c \Psi \Lambda_c \Psi^{-1} B_c &= s_1^{\,2} \hat{\Phi}_1 \hat{\Phi}_1^{\,T} \hat{B} + s_2^{\,2} \hat{\Phi}_2 \hat{\Phi}_2^{\,T} \hat{B} + \dots + s_N^{\,2} \hat{\Phi}_N \hat{\Phi}_N^{\,T} \hat{B} \\ H_d^{\,-1} C_c \Psi \Lambda_c \Psi^{-1} B_c &= \begin{bmatrix} \hat{\Phi}_1 \hat{\Phi}_1^{\,T} \hat{B} & \hat{\Phi}_2 \hat{\Phi}_2^{\,T} \hat{B} & \cdots & \hat{\Phi}_N \hat{\Phi}_N^{\,T} \hat{B} \end{bmatrix} \begin{bmatrix} s_1^{\,2} \\ s_2^{\,2} \\ \vdots \\ s_N^{\,2} \end{bmatrix} \end{aligned} \tag{5.19}$$

Therefore, assuming only a single input is applied to the system, the solution of the scaling factors can be found as follows.

$$\begin{bmatrix} s_1^{\,2} \\ s_2^{\,2} \\ \vdots \\ s_N^{\,2} \end{bmatrix} = \left[\hat{\Phi}_1 \hat{\Phi}_1^{\,T} \hat{B} \quad \hat{\Phi}_2 \hat{\Phi}_2^{\,T} \hat{B} \quad \cdots \quad \hat{\Phi}_N \hat{\Phi}_N^{\,T} \hat{B} \right]^{-1} \times H_d^{\,-1} C_c \Psi \Lambda_c \Psi^{-1} B_c \qquad (5.20)$$

If there are more than one input, then the $\hat{B}$ and B_c matrices have r many columns, and as the above expression is valid individually for each column, Equation (5.20) is required to be solved for each input set, which imply that, there appears r set of scaling functions obtained, but one set of scaling function is sufficient and the rest will be equivalent to each other in the absence of noise.

After the scaling functions are obtained from the Equation (5.20), then the mass normalized eigenvectors $\Phi = \hat{\Phi} S$ can be obtained and then the mass matrix can be obtained as $M = (\Phi \Phi^T)^{-1}$. Therefore using the mass matrix and the $-M^{-1}K$ and $-M^{-1}D_{amp}$ expressions obtained from Equation (5.13), the stiffness and damping matrices can be obtained as

$$K = -M(-M^{-1}K) \qquad (5.21)$$

$$D_{amp} = -M(-M^{-1}D_{amp}) \qquad (5.22)$$

To sum up, the transformation based methodology described above successfully transforms the first order realized system model into second order system of equation and then mechanical system parameters which are composed of mass, stiffness and damping matrices can be obtained correctly. However, it should be noted that the above formulation is given for the displacement equivalent system model given in Equation (5.4). However, it can also be generalized for the other output measurements like, velocity or acceleration in the formulation of DV model.

For the case of velocity measurement, the output can be obtained as

$$y(t) = \begin{bmatrix} 0 & H_v \end{bmatrix} x_I(t) \tag{5.23}$$

then using the eigenvalue decomposition of the A_I, it is possible to express the transformation relation as follows.

$$\psi^d \tilde{\Gamma} = H_v^{-1} C_c \Psi \Lambda_c^{-1} \tag{5.24}$$

Similarly, for the acceleration measurement case, the output can be obtained as

$$y(t) = \begin{bmatrix} 0 & H_a \end{bmatrix} \dot{x}_I(t) = \begin{bmatrix} 0 & H_a \end{bmatrix} A_I x_I(t) + D_c u(t) \tag{5.25}$$

and similarly, the transformation relation for acceleration measurement becomes the following.

$$\psi^d \tilde{\Gamma} = H_a^{-1} C_c \Psi \Lambda_c^{-2} \tag{5.26}$$

Therefore, as the relationships of all types of measurements are obtained, any mixed kinds of sensors can be used during testing and the transformation methodology proceeds in the similar way with only changing the expressions for transformation matrix.

CHAPTER 6

SIMULATION AND TEST RESULTS

6.1 IDENTIFICATION IMPLEMENTATION FOR 1 DOF SIMULATED SYSTEM

In order to verify identification scheme described in the preceding sections, firstly simulations are used, as the model to be identified is known at the beginning, so that results can be easily compared and verified. For this purpose first a single degree of freedom model shown in Figure 6.1 is constructed.

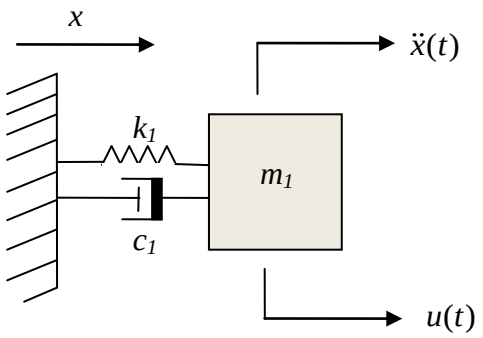

Figure 6.1 Single DOF System Model [1]

Here the system consists of a mass, spring, and damper and input and output is at the same location. In addition to that, acceleration is measured as the system output. The selected values for the mass, spring and damper are $M = 1kg$, $K = 1N/m$ and $\zeta = 0.01Ns/m$.

Therefore the second order equation of motion can be stated as follows.

$$\ddot{w}(t) + 0.01\dot{w}(t) + w(t) = u(t) \tag{6.1}$$

Then using physical displacement velocity model described in the Chapter 4, the equivalent first order state space formulation can be represented as

$$\begin{aligned} \dot{x} &= A_c x + B_c u \\ y &= Cx + Du \\ \begin{bmatrix} \dot{w} \\ \ddot{w} \end{bmatrix} &= \begin{bmatrix} 0 & 1 \\ -1 & -0.01 \end{bmatrix} \begin{bmatrix} w \\ \dot{w} \end{bmatrix} + \begin{bmatrix} 0 \\ 1 \end{bmatrix} u \\ y &= \begin{bmatrix} -1 & -0.01 \end{bmatrix} \begin{bmatrix} w \\ \dot{w} \end{bmatrix} + u \end{aligned} \tag{6.2}$$

In order to implement identification scheme, first system response is required to be determined and system model given above is simulated using Matlab/Simulink [31] environment with the model shown in Figure 6.2. As most of the modern data collection systems work in digital domain, the collected data is obtained in the discrete form with finite sampling intervals. In this study the sampling frequency is selected to be 1kHz unless otherwise stated.

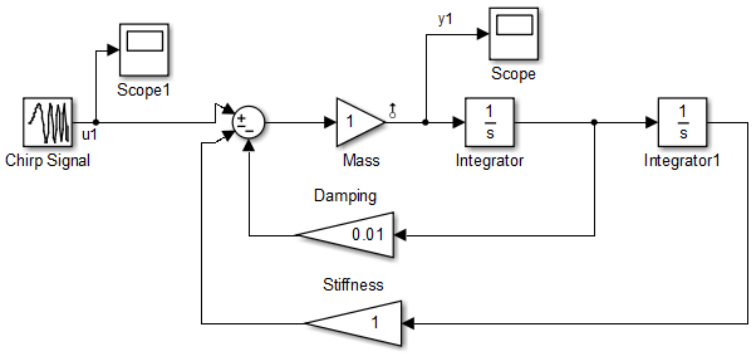

Figure 6.2 SDOF System Model in Simulink

In order to apply ERA and ERA/DC algorithms, first impulse response is required. As explained in Chapter 2, direct time domain methods may result in ill conditioned

input matrix, therefore rather than direct time domain approach, frequency domain and Wavelet transform techniques are implemented.

For the frequency domain approach, first a single tone input is applied to the system with knowing that frequency domain approach may yield bad results. After the analysis is carried out, as expected, results ended up with wrong system response, results of which are not presented here. Therefore in the second trial a chirp signal is applied to the system. In the second case a chirp signal with frequency range starting from 0.02 Hz up to 3 Hz in 100 seconds time interval is applied as the input. The input force signal applied to the system is shown in Figure 6.3 .a . Additionally in Figure 6.3.b the system response is shown for the applied chirp input.

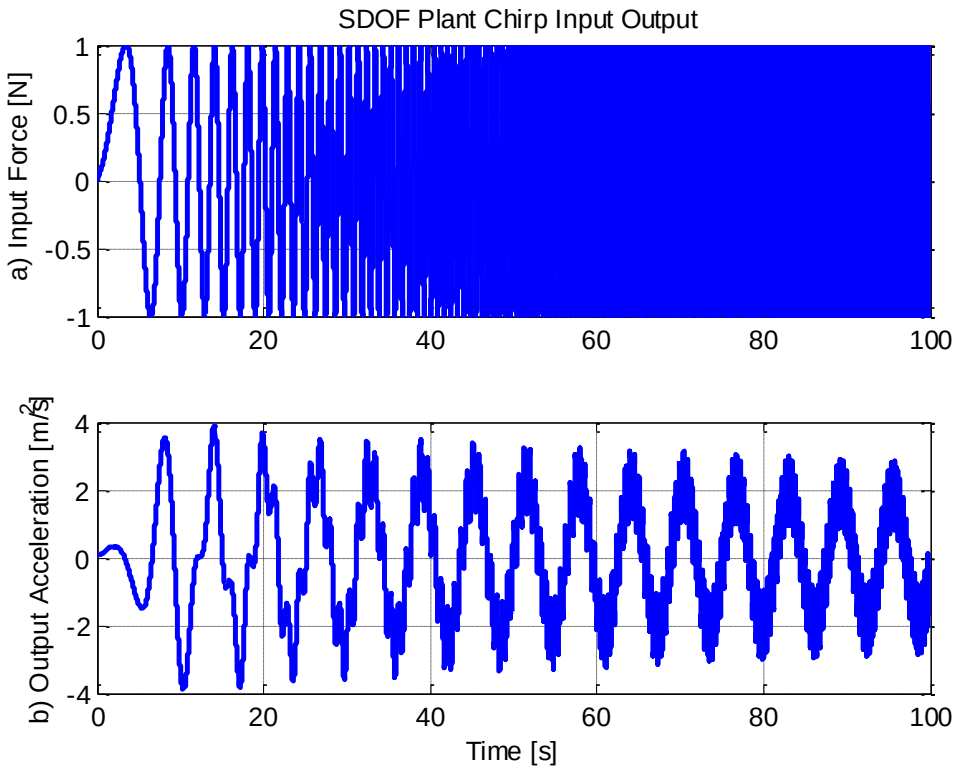

Figure 6.3 SDOF Plant Chirp Input / Output

Then the Fourier transform is applied to the input and output via Fast Fourier transform(FFT) method involved in Matlab's function library. After the Fourier

transforms of the input and output signals are obtained, the correlated input and output variables described in Chapter 2 are computed and by dividing output correlated variable to input correlated variable, the frequency response function shown in Figure 6.4 is obtained. After the frequency response function is obtained, the remaining task is to return back to time domain via inverse Fourier transform and when it is accomplished the impulse response of the single degree of freedom system is obtained as shown in the Figure 6.5. Here in order to capture system response, instead of a single tone frequency input, a chirp signal with a limited frequency range is applied with an educated guess on the range starting from very low frequencies. In addition to that as the system model is ideal and does not include measurement noise, ensembling is not applied in this case.

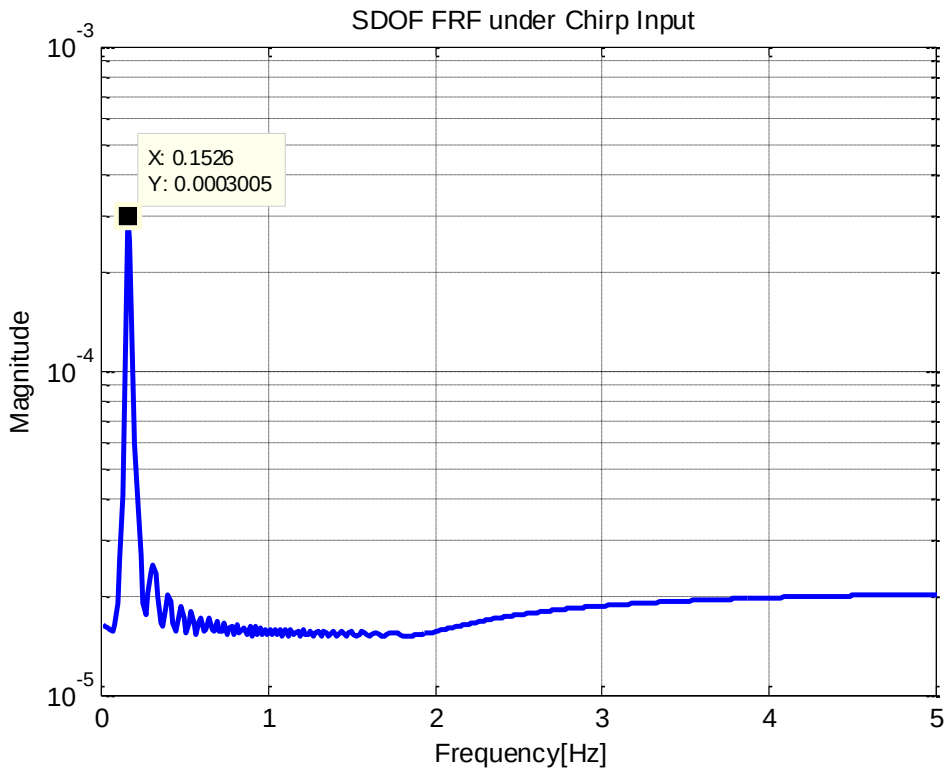

Figure 6.4 SDOF Plant Frequency Response Function

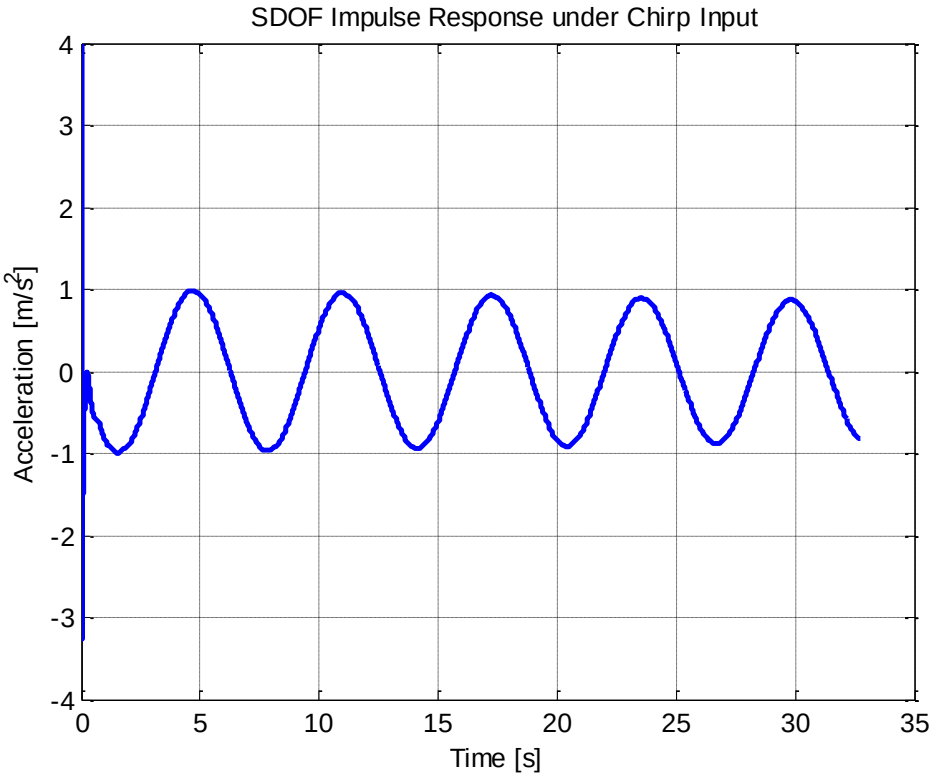

Figure 6.5 SDOF Plant with Chirp Input, IR Function obtained via Fourier Transform

As the second tool to extract impulse response function of the system is the Wavelet transform, Wavelet analysis is performed next. For the Wavelet analysis, as the computational time increases with the length of data, only first 4,1 seconds(indeed 4096 data points) of the input and output signals shown in Figure 6.3 are used in the computation of impulse response function. Again, as there is no noise or distortion on the data, ensembling is not used and Daubechies 4 wavelet, which has 8 coefficients shown in Figure 2.4 is used as the mother wavelet. The Daubechies 4 wavelet is selected because it resembles the expected system response and it requires less computation time as it has fairly less coefficients to be determined. After implementation of wavelet transform to the input signal and computation of the wavelet transform of the impulse response function, by taking its inverse wavelet

transform, the impulse response function of the single degree of freedom system is obtained as shown in Figure 6.6. Here the response is given up to 4,1 seconds, which is because the input and output signals are used with 4096 data points, which was the initial choice to decrease computation time and as 4096 is the 12^{th} power of 2 which is utilized for 12 level (full depth) wavelet analysis.

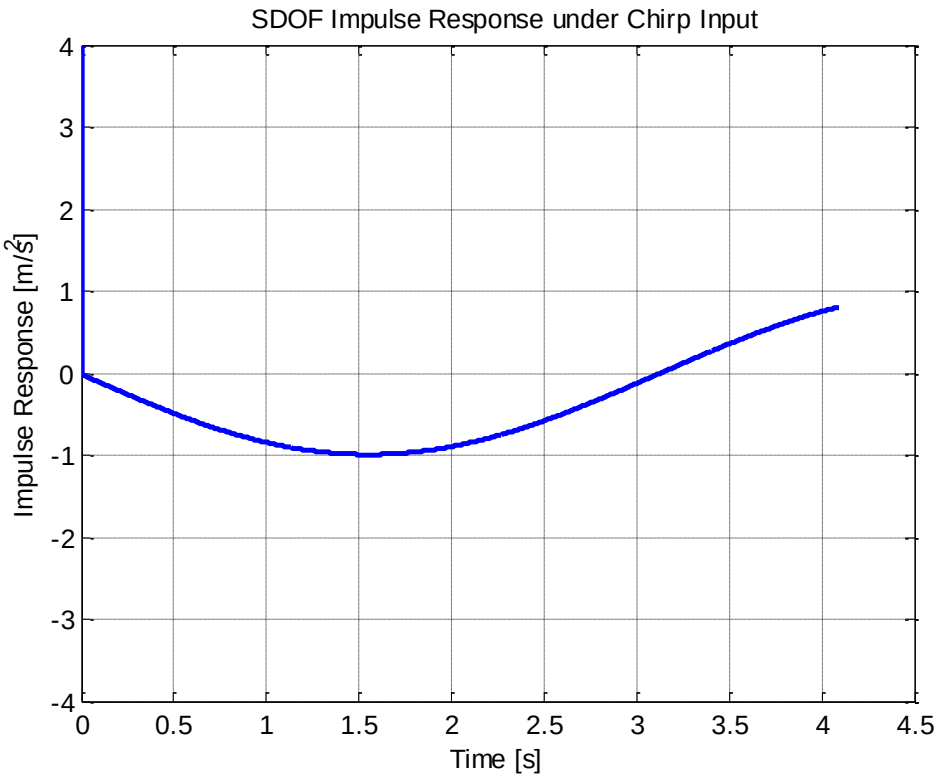

Figure 6.6 SDOF Plant with Chirp Input, IR Function obtained via Wavelet Transform

Here it should be noted that for a complex system, computation with 4 seconds of impulse response may not yield the exact system response, however, as in this case the system is simpler, the used short time response is sufficient to extract system response.

After the responses are obtained via Fourier and wavelet transforms, the ideal system response which is computed analytically from model given in Equation (6.2)

and responses computed via Fourier and wavelet analyses are compared as shown in Figure 6.7. Additionally, errors of the computed impulse responses, compared with the actual system response data are represented in Figure 6.7.b and Figure 6.7.c. Here the black line represents the analytical impulse response function computed from the state space model of the single degree of freedom system and the green, and red dashed lines are the impulse response functions obtained via Fourier and Wavelet analyses represented in Figure 6.5 and Figure 6.6 respectively.

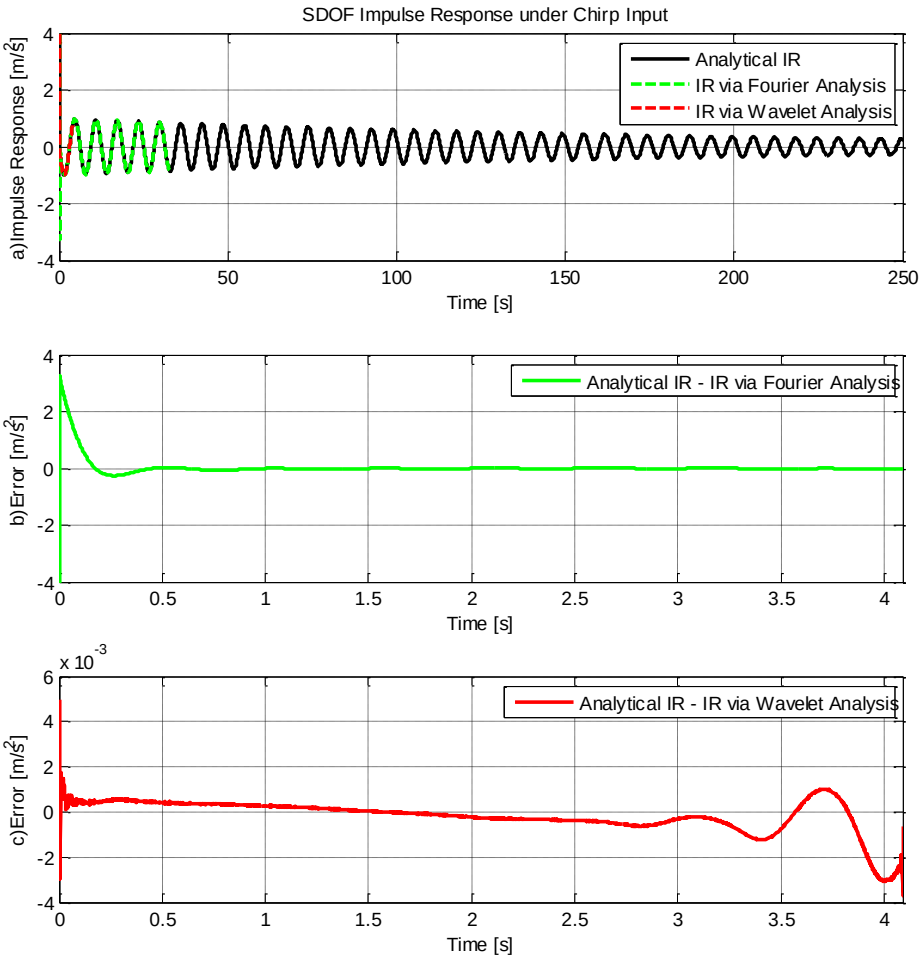

Figure 6.7 SDOF Plant Impulse Response Comparison

In Figure 6.7.b, from time range [0-1] seconds, it is observed that, the transient behavior of the impulse response is computed with high error via Fourier analysis. On the other hand, wavelet analysis captures the whole response characteristic, and it seems coherent with the analytical response function as seen in Figure 6.7.c. Another important advantage of the wavelet analysis is that, it captures true system response by using much lower data points than the Fourier analysis case.

In line with the results obtained from the comparison of Fourier and Wavelet analyses, the Wavelet analysis results are selected to be used in the remaining realization applications.

First the ERA is applied to the impulse response function results, obtained from Wavelet transforms. Moreover, the ERA analysis start with the formation of Markov parameters, which are obtained by using impulse response measurements of all system outputs at each sample time. Here in this system, as there is only one output, the system impulse response samples are equivalent to the Markov parameters. Then, by using Markov parameter, Hankel matrix will be constructed. The size of the Hankel matrix can be selected in order to include as much system response as possible, while keeping the computation time limited. Here as 4096 impulse response measurements (or Markov parameters) available from the results of Wavelet analysis, a 1000x1000 square Hankel matrix is formed for the realization analysis. After the Hankel matrix is formed using system Markov parameters, singular value decomposition is applied to the Hankel matrix and the singular values of the Hankel matrix are plotted against their values as shown in Figure 6.8. In this figure, non-zero singular values gives the rank information of the Hankel matrix, which is equivalent to the selected system order in the ERA analysis as well. As shown in Figure 6.8, the system order is computed as 2 from the SVD of the Hankel matrix, which is expected because the selected system is represented by one differential equation. Afterwards, according to the obtained system order, the left

and right unitary matrices are truncated and corresponding observability and controllability matrices are computed.

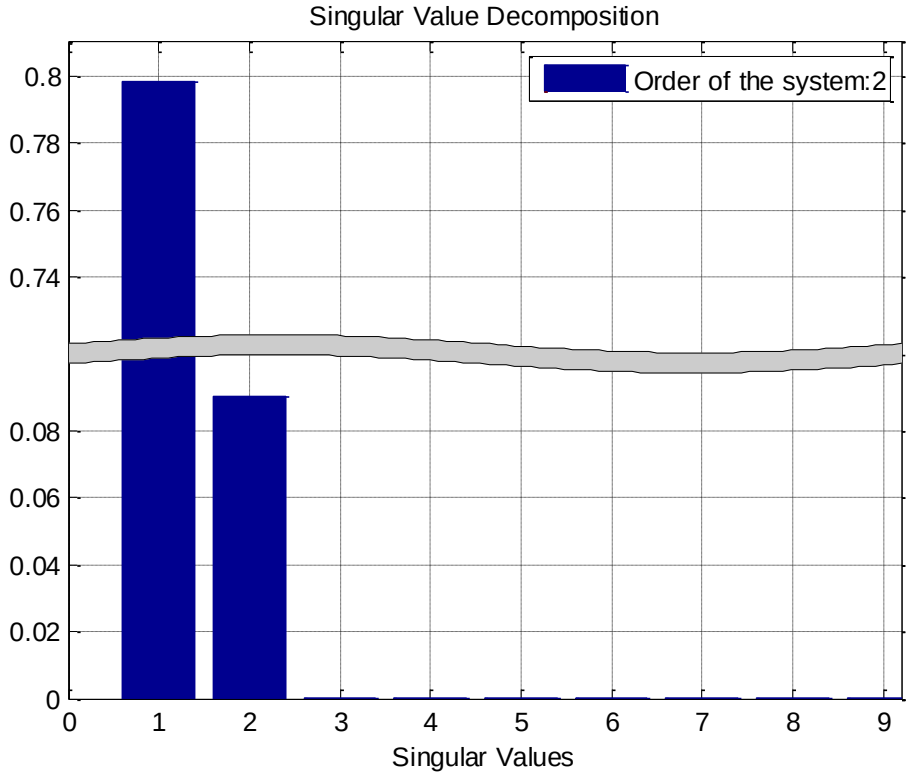

Figure 6.8 Singular Values of Hankel Matrix in ERA Analysis

Then using the formulation described in the ERA procedure, the discrete time system matrices $\hat{A}_0$, $\hat{B}_0$, $\hat{C}$, and $\hat{D}$ for the generalized discrete state space representation are computed as follows.

$$\begin{aligned} x(k+1) &= \hat{A}_0\, x(k) + \hat{B}_0 u(k) \\ y(k) &= \hat{C}\, x(k) + \hat{D} u(k) \end{aligned} \tag{6.3}$$

where

$$\hat{A}_0 = \begin{bmatrix} 1.001 & -0.001119 \\ 0.001119 & 0.9995 \end{bmatrix}$$
$$\hat{B}_0 = \begin{bmatrix} 0.01771 \\ -0.01741 \end{bmatrix} \tag{6.4}$$
$$\hat{C} = \begin{bmatrix} -0.01771 & -0.01741 \end{bmatrix}$$
$$\hat{D} = \begin{bmatrix} 1.000 \end{bmatrix}$$

Then the discrete system model given in Equation (6.3) is converted to continuous time by using Matlab's built in "d2c" conversion with zero order hold method, which is implementing the same discrete to continuous time conversion explained at the end of the Chapter 4. In addition to that, Matlab's "d2c" conversion is verified by comparing its results with analytical conversion described in Chapter 4. Then the resultant continuous time model is obtained as follows.

$$\begin{aligned} \dot{x}(t) &= \hat{A}x(t) + \hat{B}u(t) \\ y(t) &= \hat{C}x(t) + \hat{D}u(t) \end{aligned} \tag{6.5}$$

where

$$\hat{A} = \begin{bmatrix} 0.4978 & -1.119 \\ 1.119 & -0.5078 \end{bmatrix}$$
$$\hat{B} = \begin{bmatrix} 17.69 \\ -17.42 \end{bmatrix} \tag{6.6}$$
$$\hat{C} = \begin{bmatrix} -0.01771 & -0.01741 \end{bmatrix}$$
$$\hat{D} = \begin{bmatrix} 1.000 \end{bmatrix}$$

Here it should be noted that, as expected analytically the $\hat{C}$ and $\hat{D}$ matrices are the same for both discrete and continuous time models.

After discrete and continuous system models are realized, in order to assess how good ERA approximates the impulse response function of the system, two performance measures, the MAC and MSV are computed. Here as previously mentioned, MAC gives the correspondence between the identified pulse response

history and the pulse response used in the identification. When there is no noise included in the data, which is the case here, MAC is found as 1 and 1 for the two identified eigenvalues, which means these vectors are indeed identical to the pulse response history used in the identification. Whereas MSV gives the contribution of each mode to the identified impulse response function. In this case MSV is found as 0.9973 for the both eigenvalues out of 1. Which means very good approximation is obtained through the analysis and in order to visualize the performance of ERA, impulse response function of the SDOF system and the discrete model expressed in Equation (6.4) are compared in Figure 6.9. Therefore, as indicated by MAC and MSV, very good realization is obtained through the ERA analysis which is visually and analytically confirmed in Figure 6.9.a and Figure 6.9.b.

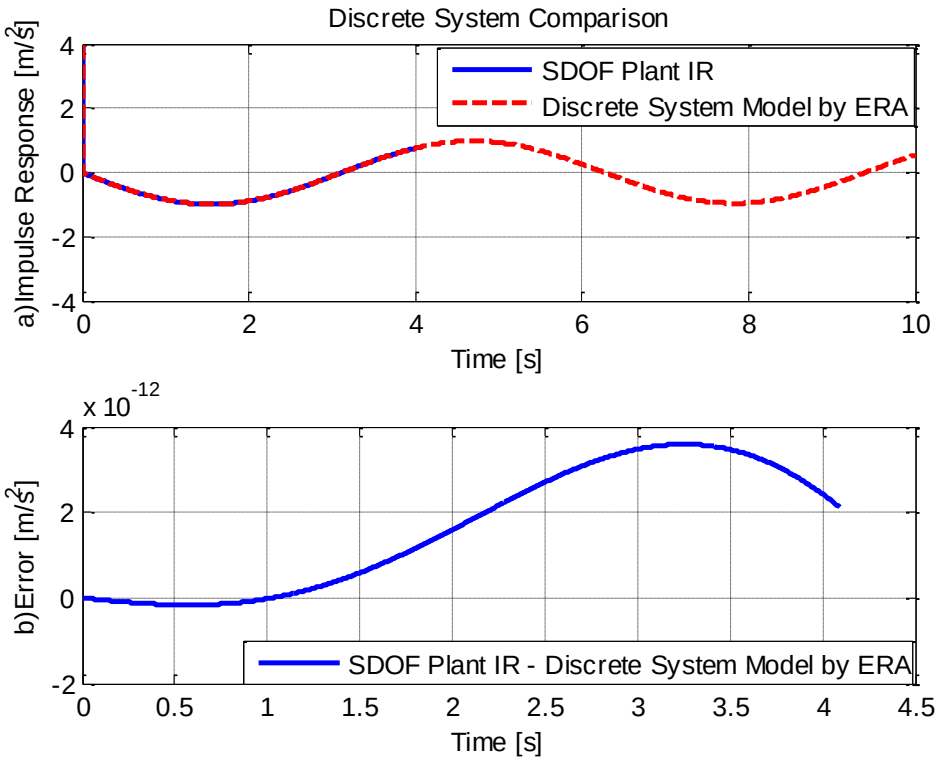

Figure 6.9 Comparison of SDOF System IR and Discrete System IR by ERA

At this point as the system of interest is a single degree of freedom, the transfer functions of the analytical system model and the one obtained from the realized continuous system model can be compared as following.

First the analytical transfer function between input and output can simply be obtained by taking Laplace transform of the differential equation given in Equation (6.1), or it can be computed from the state space model given in Equation (6.2) as following.

$$H_{analytical} = \frac{w(s)}{u(s)} = \frac{s^2}{s^2 + 0.01s + 1} \tag{6.7}$$

and the transfer function obtained from the continuous time state space realization obtained from ERA analysis can be obtained as follows.

$$H_{realized} = \frac{w(s)}{u(s)} = \frac{s^2 + 4.17*10^{-11}s - 1.87*10^{-12}}{s^2 + 0.01s + 1} \tag{6.8}$$

Comparison of the analytical transfer function and the one obtained from the ERA analysis shows that, the ERA computes the same characteristic polynomial, which conveys the resonances of the system, very accurately, however, it can be observed that there appeared roots of the numerator which are too close to the origin, in the ERA solution. These roots of the numerator appeared due to the residuals in the numerical analysis and application of sampling. Still the realized transfer function is acceptable as the roots of the numerator are too close to the origin.

Then, proceeding with the identification application, in order to obtain natural frequencies and system's physical parameters, the continues model must be converted to damped continuous modal displacement equivalent form, which is given below for the acceleration output case as

$$\begin{aligned} \dot{\hat{z}} &= \Lambda_c\, z(t) + B_z u(t) \\ y(t) &= C_z\, z(t) \end{aligned} \tag{6.9}$$

where

$$\Lambda_c = \begin{bmatrix} -0.005000 + 0.9999i & 0 \\ 0 & -0.005000 - 0.9999i \end{bmatrix}$$
$$B_z = \begin{bmatrix} -12.32 - 20.20i \\ -12.32 + 20.20i \end{bmatrix} \qquad (6.10)$$
$$C_z = \begin{bmatrix} 0.01804 + 0.01101i & 0.01804 - 0.01101i \end{bmatrix}$$

Therefore the damped natural frequencies are computed from the imaginary parts of the continuous eigenvalues as $w_{n1} = 0.9999\, rad/s$ and $w_{n2} = -0.9999\, rad/s$, this is because the two eigenvalues are the complex conjugates of the same mode and the only eigenvalue corresponding to the single mode can be stated as $w_n = 0.9999\, rad/s$. In this single-degree of freedom system case, as the natural frequency can be easily computed analytically, the results can be compared with the analytical ones easily. Therefore the analytical damped natural frequency for the single degree of freedom system can be computed as

$$\text{First, the undamped natural frequency } w_{ni} = \sqrt{\frac{K}{M}} = 1.000 \text{ rad/s}$$
$$\text{Secondly, the damped natural frequency } w_n = w_{ni}\sqrt{1-\zeta^2} = 0.9999 \text{ rad/s} \qquad (6.11)$$

Therefore the natural frequency computations match with the realized ones, and ERA results are verified to be correct.

Finally, physical system parameters, which are the mass, stiffness and damping matrices are obtained through a transformation procedure from the first order state space models into second order models, which is explained in Chapter 5. Here CBSI procedure is applied to the damped modal continuous form given above to extract physical system properties. For this purpose, as there is a single input applied to system, single scaling matrix is obtained through the analysis. Therefore, the extracted mass, stiffness and damping matrices are computed as following.

$$\begin{aligned} &\text{Mass: } \bar{M} = 1.000\ kg \\ &\text{Stiffness: } \bar{K} = 1.000\ N/m \\ &\text{Damping: } \bar{D} = 0.01000\ Ns/m \end{aligned} \tag{6.12}$$

Therefore the results exhibit excellent agreement with the physical system parameters with less than 1% error.

Second realization algorithm applied is the ERA/DC. This algorithm again uses the system impulse response function as the input and the same impulse response function, obtained from wavelet analysis, will be used for ERA/DC analysis. In this case the Hankel matrix formed by using Markov parameters is selected to be in the size of 500 x 500, because in this case the Correlation Matrices will be constructed by multiplication of each shifted Hankel matrix with the initial one ($R_{hh}(k) = H(k)H^T(0)$). After the Correlation Matrices are obtained, the Correlation Hankel Matrix is constructed by using 5 Correlation Matrices. After Correlated Hankel Matrices are constructed, the ERA/DC implementation continues with the similar factorization of the Correlated Hankel matrix via SVD. In this case again, the system order is obtained from the rank of the Correlated Hankel Matrix as 2, which is the number of nonzero singular values shown in Figure 6.10.

Afterwards, according to the obtained system order, the left and right unitary matrices are again truncated and corresponding observability and controllability matrices are computed in slightly different computation from the ERA method.

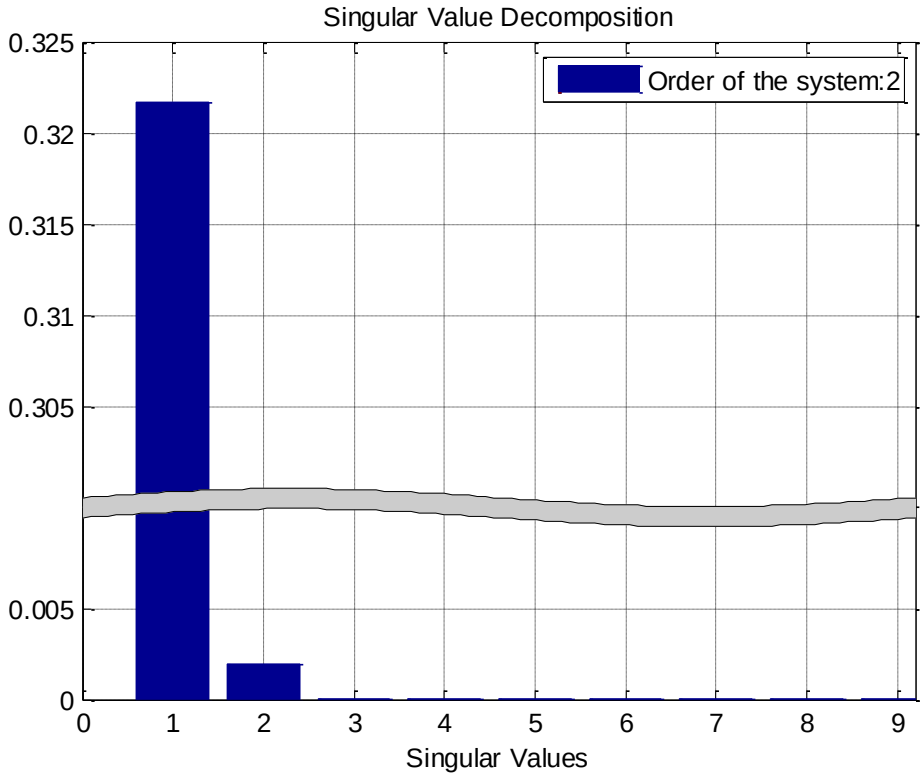

Figure 6.10 Singular Values of the Correlated Hankel Matrix in ERA/DC Analysis

Then using the formulation described in the ERA / DC procedure, the discrete time system matrices $\hat{A}_0$, $\hat{B}_0$, $\hat{C}$, and $\hat{D}$ for the generalized discrete state space representation, given in Equation (6.5), is computed as

$$\begin{aligned} x(k+1) &= \hat{A}_0\, x(k) + \hat{B}_0 u(k) \\ y(k) &= \hat{C}\, x(k) + \hat{D} u(k) \end{aligned} \tag{6.13}$$

where

$$\hat{A}_0 = \begin{bmatrix} 1.002 & -0.0005111 \\ 0.006471 & 0.9985 \end{bmatrix}$$
$$\hat{B}_0 = \begin{bmatrix} -0.02476 \\ 0.08515 \end{bmatrix} \tag{6.14}$$
$$\hat{C} = \begin{bmatrix} 0.006265 & 0.001698 \end{bmatrix}$$
$$\hat{D} = \begin{bmatrix} 1.000 \end{bmatrix}$$

The discrete system model found in Equation (6.13) is again converted to continuous time by using Matlab's built in "d2c" command with zero order hold method and the resultant continuous time model is obtained as follows.

$$\begin{aligned} \dot{x}(t) &= \hat{A}x(t) + \hat{B}u(t) \\ y(t) &= \hat{C}x(t) + \hat{D}u(t) \end{aligned} \tag{6.15}$$

where

$$\hat{A} = \begin{bmatrix} 1.513 & -0.5111 \\ 6.471 & -1.523 \end{bmatrix}$$
$$\hat{B} = \begin{bmatrix} -24.72 \\ 85.29 \end{bmatrix} \tag{6.16}$$
$$\hat{C} = \begin{bmatrix} 0.006265 & 0.001698 \end{bmatrix}$$
$$\hat{D} = \begin{bmatrix} 1.000 \end{bmatrix}$$

Again, it should be noted that, the $\hat{C}$ and $\hat{D}$ matrices are the same for both discrete and continuous time models.

This time, in order to assess how good ERA / DC approximates the system impulse response function, the two performance measures which are modal amplitude coherence(MAC) and mode singular value(MSV) are computed again. When there is no noise included in the data, which is the case in this example, MAC is found as 1 and 1 for the two identified eigenvalues, which means these vectors are indeed identical to the pulse response history used in the identification. Whereas MSV is computed as 0.4992 for the both eigenvalues out of 1. Here the MSV is found less

than the previous calculation found in the ERA, however this is expected as the Hankel Matrix size is selected to be smaller than the one used in the ERA analysis, in this case including more Markov parameters will increase the MSV but they will increase the computation time as well. Although modal singular value is found less in the ERA/DC case, still very good approximation is obtained through the analysis and in order to visualize the performance of ERA/DC, impulse response function of the SDOF system and the analytical impulse response function of the discrete model expressed in Equation (6.15) are shown in Figure 6.11. In addition to that the realization error between the analytical and realized impulse response functions are given in Figure 6.11.b.

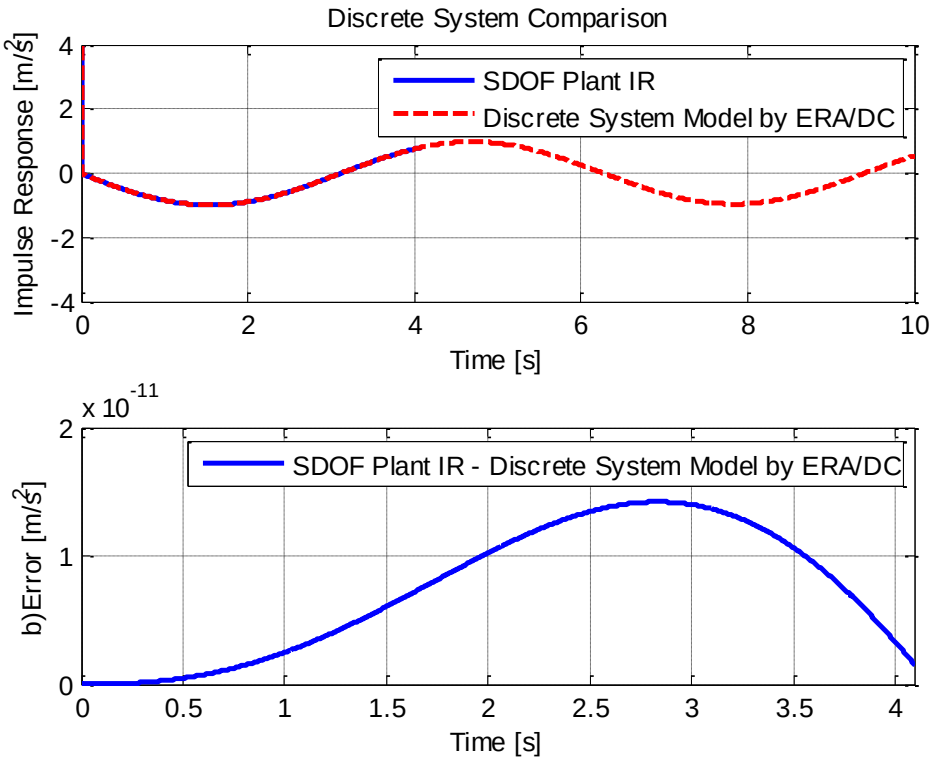

Figure 6.11 Comparison of SDOF System IR and Discrete System IR by ERA/DC

Here the transfer function obtained from the continuous time state space realization resulted from ERA/DC analysis can be obtained as

$$H_{realized} = \frac{w(s)}{u(s)} = \frac{s^2 + 3.85*10^{-11}s - 8.49*10^{-12}}{s^2 + 0.01s + 1} \qquad (6.17)$$

Comparing the transfer functions expressed in Equations (6.7), (6.8) and (6.17) yields that, the ERA/DC computes very similar results with the ERA analysis even in the case of half the size of Hankel matrix is utilized.

Then, proceeding with the identification application, in order to obtain natural frequencies and system's physical parameters, the continues model must be converted to damped continuous modal displacement equivalent form, which is given below for the acceleration output case as

$$\begin{aligned} \dot{\hat{z}} &= \Lambda_c\, z(t) + B_z u(t) \\ y(t) &= C_z\, z(t) \end{aligned} \qquad (6.18)$$

where,

$$\begin{aligned} \Lambda_c &= \begin{bmatrix} -0.005000 + 0.9999i & 0 \\ 0 & -0.005000 - 0.9999i \end{bmatrix} \\ B_z &= \begin{bmatrix} -44.30 - 150.4i \\ -44.30 + 150.4i \end{bmatrix} \\ C_z &= \begin{bmatrix} -0.003060 - 0.0009013i & -0.003060 + 0.0009013i \end{bmatrix} \end{aligned} \qquad (6.19)$$

therefore the damped natural frequencies are computed from the imaginary parts of the continuous eigenvalues as $w_{n1} = 0.9999\, rad/s$ and $w_{n2} = -0.9999\, rad/s$, this is because the two eigenvalues are the complex conjugates of the same mode and the only eigenvalue corresponding to the single mode can be stated as $w_n = 0.9999\, rad/s$.

Finally, physical system parameters, which are the mass, stiffness and damping matrices are obtained through a transformation procedure from the first order state space models into second order models, which is explained in Chapter 5. Here CBSI procedure is applied to the damped modal continuous form given above to extract physical system properties. For this purpose, as there is a single input applied to

system, single scaling matrix is obtained through the analysis. Therefore, the extracted mass, stiffness and damping matrices are computed as follows.

$$\begin{aligned} &\text{Mass: } \bar{M} = 1.000\ kg \\ &\text{Stiffness: } \bar{K} = 1.000\,N/m \\ &\text{Damping: } \bar{D} = 0.01000\,Ns/m \end{aligned} \tag{6.20}$$

which again exhibits excellent agreement with the physical system parameters with less than 1% error in.

To sum up, for a linear time invariant single degree of freedom system, in the absence of noise, the wavelet analysis is found to perform well on determining system impulse response history. In addition to that, for the single degree of freedom system, ERA and ERA/DC are found to be capable of realizing a state space system model well enough to capture system response. Finally the CBSI procedure performs the correct transformation such that, physical system properties for the identified proportionally damped system model are obtained correctly.

6.2 IDENTIFICATION IMPLEMENTATION WITH 3 DOF SIMULATED SYSTEM

In order to further investigate performance of the identification methods and transformations explained in the preceding chapters, a three degree of freedom system model shown in Figure 6.12 is constructed.

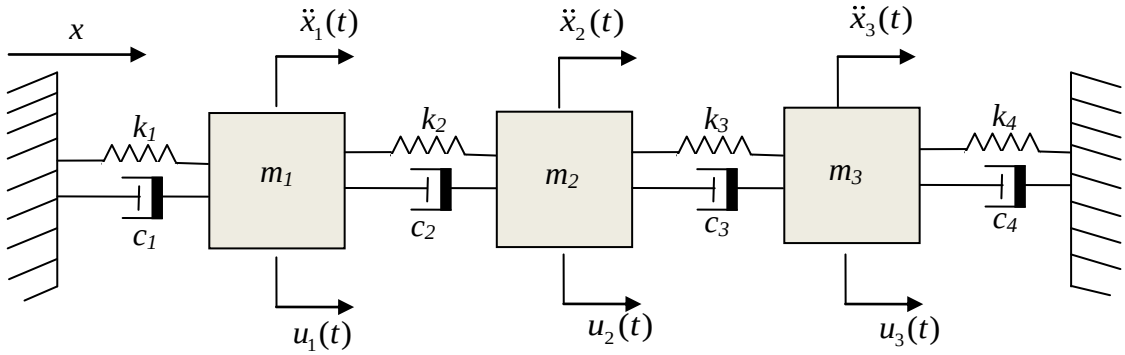

Figure 6.12 Three Degree of Freedom System Model

In this case, test system consists of three masses, four springs, and four dampers. In addition to that, three inputs are applied to each degree of freedom and three acceleration measurements are collected from each mass. The selected values for the mass, spring and damper parameters are as following.

$$\begin{bmatrix} m_1 \\ m_2 \\ m_3 \end{bmatrix} = \begin{bmatrix} 1 \\ 1 \\ 1 \end{bmatrix} kg \quad \begin{bmatrix} k_1 \\ k_2 \\ k_3 \\ k_4 \end{bmatrix} = \begin{bmatrix} 2 \\ 2 \\ 2 \\ 20 \end{bmatrix} N/m \quad \begin{bmatrix} c_1 \\ c_2 \\ c_3 \\ c_4 \end{bmatrix} = \begin{bmatrix} 0.1 \\ 0.1 \\ 0.1 \\ 1 \end{bmatrix} Ns/m$$

Therefore second order equation of motion can be stated as

$$[M]\ddot{x} + [D]\dot{x} + [K]x = Bu \tag{6.21}$$

$$\begin{bmatrix} 1 & 0 & 0 \\ 0 & 1 & 0 \\ 0 & 0 & 1 \end{bmatrix} \begin{Bmatrix} \ddot{x}_1 \\ \ddot{x}_2 \\ \ddot{x}_3 \end{Bmatrix} + \begin{bmatrix} 0.2 & -0.1 & 0 \\ -0.1 & 0.2 & -0.1 \\ 0 & -0.1 & 1.1 \end{bmatrix} \begin{Bmatrix} \dot{x}_1 \\ \dot{x}_2 \\ \dot{x}_3 \end{Bmatrix} + \begin{bmatrix} 4 & -2 & 0 \\ -2 & 4 & -2 \\ 0 & -2 & 22 \end{bmatrix} \begin{Bmatrix} x_1 \\ x_2 \\ x_3 \end{Bmatrix} = \begin{bmatrix} 1 & 0 & 0 \\ 0 & 1 & 0 \\ 0 & 0 & 1 \end{bmatrix} \begin{Bmatrix} u_1 \\ u_2 \\ u_3 \end{Bmatrix} \quad (6.22)$$

Then implementing the proper transformation, described in Chapter 4, physical displacement velocity model representation for first order state space model can be obtained. However, in this example this representation will not be presented here as this model does not contribute directly to find system response.

In order to start realization procedure, first system response must be obtained by simulating the system model in Matlab/Simulink. For this purpose, the Simulink model shown in Figure 6.14 is constructed and for each input point, chirp signals are applied sequentially, This sequential force application is required to determine output of the system for each input individually, which constructs the columns of the Markov Parameters Matrix. In order to obtain system response again chirp signal with frequency range of 0.1 to 10 Hz within 10seconds simulation time is used as the input to the system. From Figure 6.15-a to Figure 6.17-a, the sequential input applied to each node is shown in each figure. Additionally, in the b, c and d plots, the corresponding system outputs measured at each node is displayed. Combining outputs and inputs, system Markov parameters can be obtained by using Wavelet transform technique described in Chapter 2. In this case neither direct time domain techniques nor Fourier transforms will be used to determine system pulse response because, the superior performance of Wavelet transforms is verified even for a single degree of freedom system case. Here applying Wavelet transform to the input signal, with Daubechies 4 mother wavelet, which has 8 coefficients, then solving the convolution equation given in Equation (2.29), the Wavelet transform of the pulse response can be obtained. Then applying inverse Wavelet transform, the impulse response time histories can be obtained for 3 degree of freedom system.

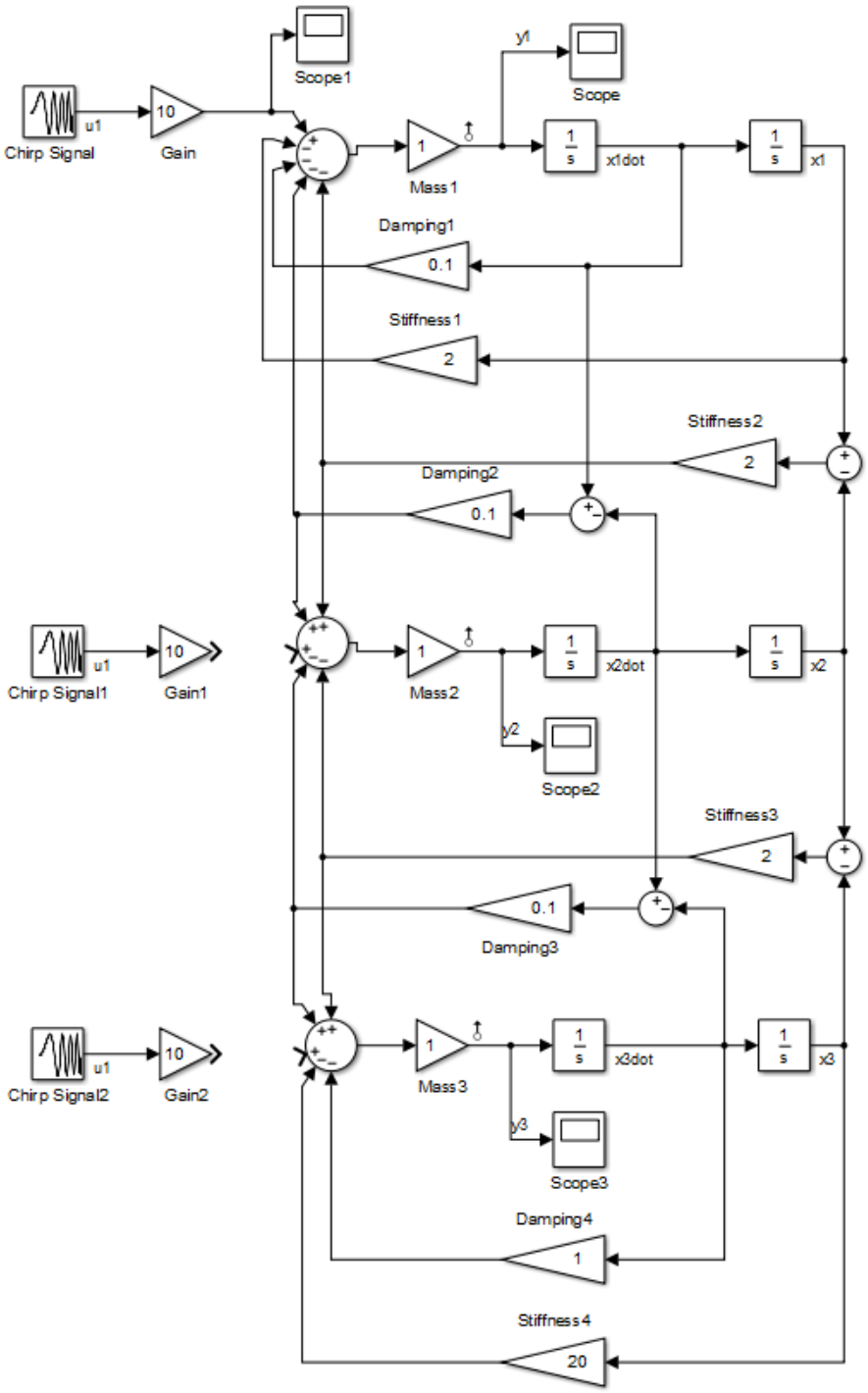

Figure 6.14 Three DOF System Model in Simulink

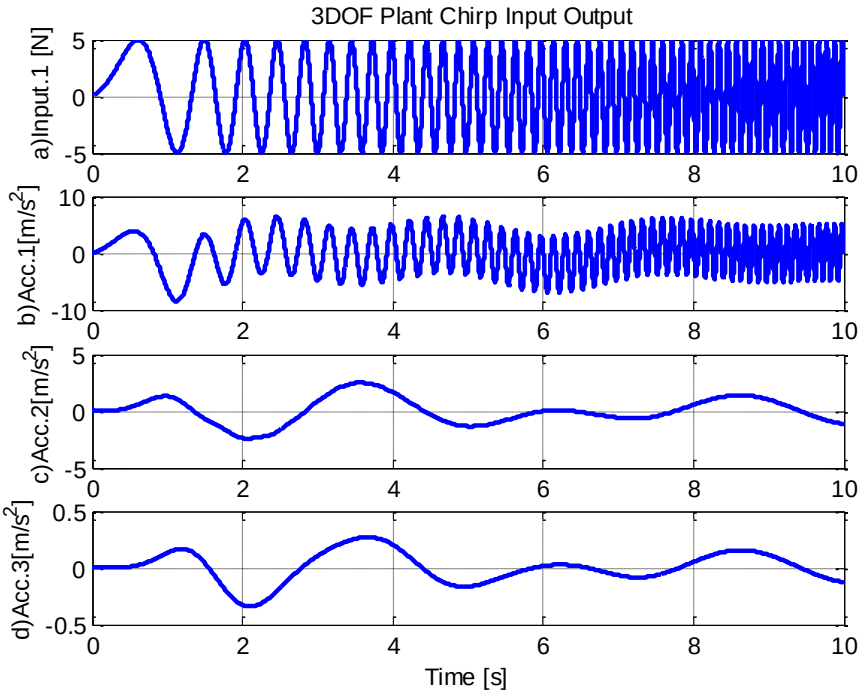

Figure 6.15 Three DOF System Output for Input 1

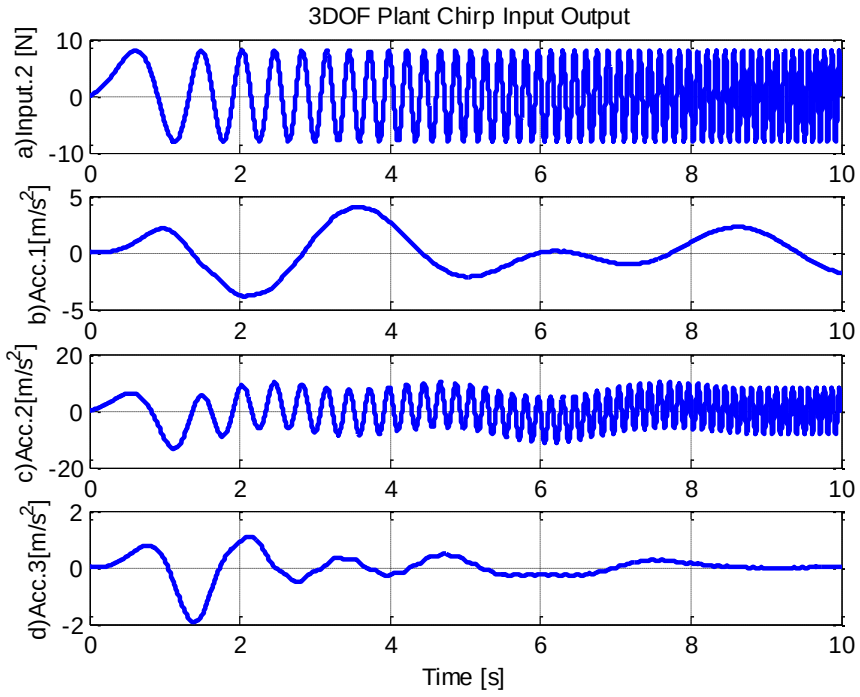

.

Figure 6.16 Three DOF System Output for Input 2

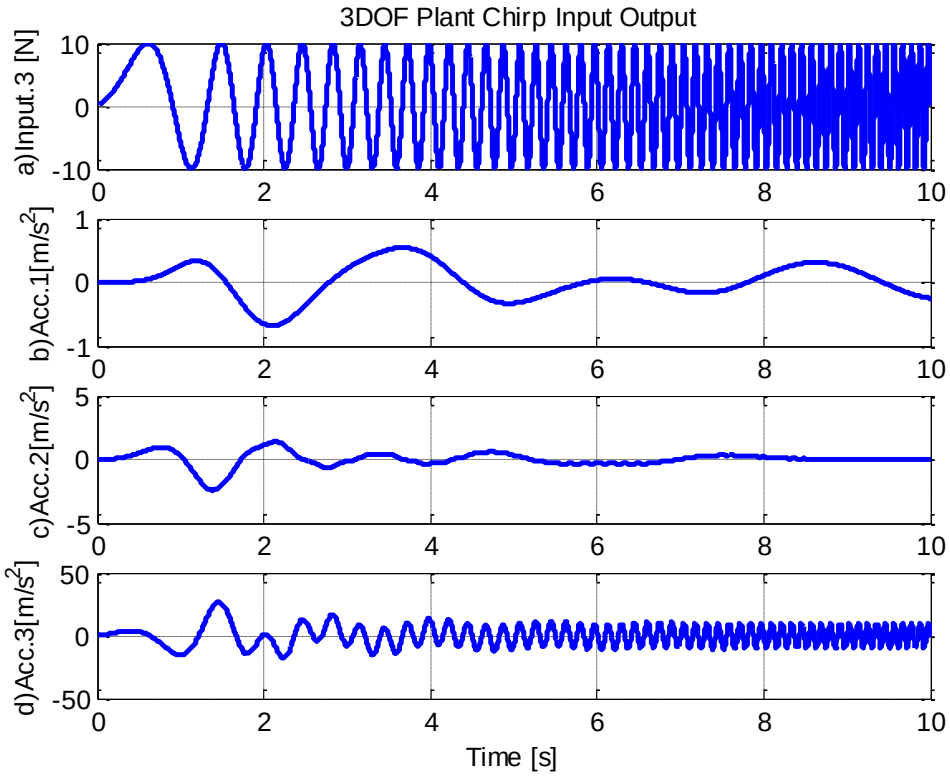

Figure 6.17 Three DOF System Output for Input 3

Here the Markov parameters obtained as a result of Wavelet analysis, are plotted in Figure 6.18 for 4 seconds, because the wavelet transform is applied over $2^{12} = 4096$ measurement points to decrease computation time. In the Figure 6.18, the response functions are named as $y_{i,j}$ where i stands for the output node and j stands for the input node. Therefore the columns of this figure gives response data for each individual input. After the Markov parameters are obtained, first the ERA can be applied to the impulse response data. In this case as the Markov Parameters for each time instant are in the dimension of 3×3 matrices, the Hankel constructed by using 1000×1000 square Markov Parameters becomes in the dimension of 3000×3000. After the Hankel matrix is constructed, the singular values decomposition is applied, and the singular values of the Hankel matrix are plotted against their values are shown in Figure 6.19. In this figure the nonzero singular values determines the rank

of the system which corresponds to the estimated order of the system, that will be modelled as a result of the ERA application.

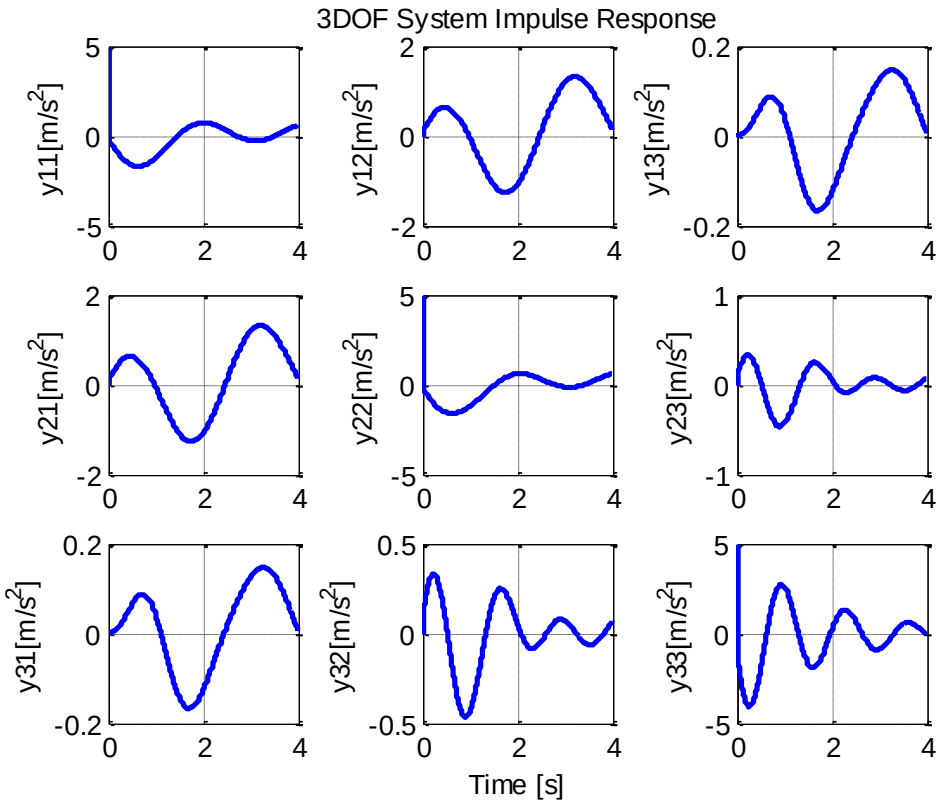

Figure 6.18 Three DOF System Impulse Response Determined via Wavelet Analysis

Here as the 3 degree of freedom system is expected to be represented by using 6 first order equations, the computed order of the system, shown in Figure 6.19 is correct. Then the left and right unitary matrices of the initial Hankel matrix are truncated according to the computed system order as the singular values beyond the calculated order of the system do not contribute to the solution.

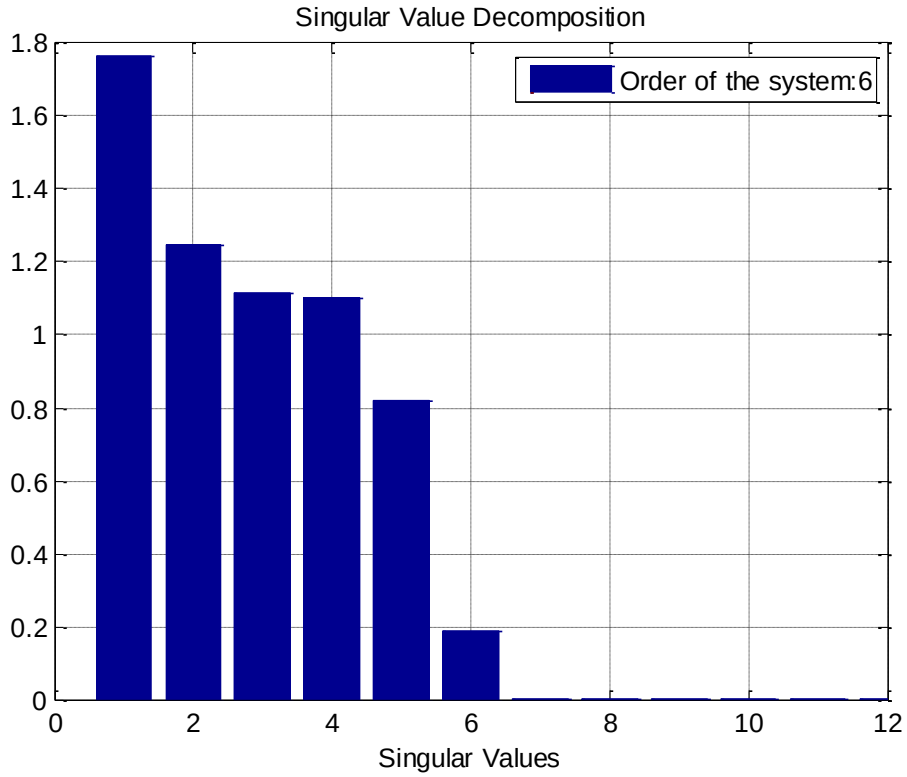

Figure 6.19 Singular Values of Hankel Matrix in ERA Analysis for 3DOF System

After the truncation, the ERA procedure is followed and the realized discrete time system matrices $\hat{A}_0$, $\hat{B}_0$, $\hat{C}$, and $\hat{D}$ for the generalized discrete state space representation are obtained as follows.

$$\begin{aligned} x(k+1) &= \hat{A}_0\, x(k) + \hat{B}_0 u(k) \\ y(k) &= \hat{C}\, x(k) + \hat{D} u(k) \end{aligned} \tag{6.23}$$

where

$$\hat{A}_0 = \begin{bmatrix} 0.9993 & 0 & 0 & -0.004680 & 0 & 0 \\ 0 & 0.9994 & 0 & 0 & -0.002464 & 0 \\ 0 & 0 & 1.000 & 0 & 0 & -0.001385 \\ 0.004680 & 0 & 0 & 0.9995 & 0 & 0 \\ 0 & -0.002464 & 0 & 0 & 1.000 & 0 \\ 0 & 0 & 0.001385 & 0 & 0 & 0.9998 \end{bmatrix}$$

$$\hat{B}_0 = \begin{bmatrix} 0.0006624 & -0.006035 & 0.0543 \\ 0.02919 & -0.02743 & -0.003404 \\ 0.01776 & 0.01866 & 0.001857 \\ -0.0005235 & 0.004770 & -0.04294 \\ 0.02637 & -0.02479 & -0.003075 \\ -0.01643 & -0.1727 & -0.001718 \end{bmatrix}$$

$$\hat{C} = \begin{bmatrix} -0.0006624 & -0.02919 & -0.01776 & -0.0005236 & 0.02637 & -0.01643 \\ 0.006035 & 0.02743 & -0.01866 & 0.004770 & -0.02479 & -0.01727 \\ -0.05433 & 0.003403 & -0.001867 & -0.04294 & -0.003076 & -0.001718 \end{bmatrix}$$

$$\hat{D} = \begin{bmatrix} 1.000 & 0 & 0 \\ 0 & 1.000 & 0 \\ 0 & 0 & 1.000 \end{bmatrix} \tag{6.24}$$

Then the system model realized in the discrete time domain is transformed into continuous time domain. The discrete system model found in Equation (6.23) is converted to continuous time by using Matlab's built in "d2c" command with zero order hold method, which represents the sampling used to collect system outputs. Therefore, the resultant continuous time model is obtained as follows.

$$\begin{aligned} \dot{x}(t) &= \hat{A}x(t) + \hat{B}u(t) \\ y(t) &= \hat{C}x(t) + \hat{D}u(t) \end{aligned} \tag{6.25}$$

where

$$\hat{A}=\begin{bmatrix} -0.6650 & 0 & 0 & -4.682 & 0 & 0 \\ 0 & -0.6113 & 0 & 0 & 2.465 & 0 \\ 0 & 0 & 1.001 & 0 & 0 & -1.385 \\ 4.682 & 0 & 0 & -0.4461 & 0 & 0 \\ 0 & -2.465 & 0 & 0 & 0.3173 & 0 \\ 0 & 0 & 1.385 & 0 & 0 & -0.1958 \end{bmatrix}$$

$$\hat{B}=\begin{bmatrix} 0.6614 & -6.026 & 54.24 \\ 29.17 & -27.41 & -3.401 \\ 17.75 & 18.65 & 1.856 \\ -0.5252 & 4.785 & -43.08 \\ 26.41 & -24.82 & -3.079 \\ -16.45 & -17.29 & -1.720 \end{bmatrix}$$

$$\hat{C}=\begin{bmatrix} -0.0006624 & -0.02919 & -0.01776 & -0.0005236 & 0.02637 & -0.01643 \\ 0.006035 & 0.02744 & -0.01866 & 0.004770 & -0.02479 & -0.01727 \\ -0.05433 & 0.003404 & -0.001857 & -0.04294 & -0.003075 & -0.001718 \end{bmatrix}$$

$$\hat{D}=\begin{bmatrix} 1.000 & 0 & 0 \\ 0 & 1.000 & 0 \\ 0 & 0 & 1.000 \end{bmatrix} \qquad (6.26)$$

Here in order to assess how good ERA approximates the system impulse response function, the two measures which are the MAC and MSV are computed. As previously mentioned, MAC gives the correspondence between the identified pulse response history and the pulse response used in the identification and when there is no noise included in the data, which is the case in this example, MAC is computed as 0.83, 0.83 ; 0.34 ,0.34; and 0.35, 0.35 out of 1 for each identified eigenvectors. Here the MAC values appear in pairs, this is expected because the eigenvectors corresponding to each mode appear as complex conjugate pairs and each pair has the same MAC value. Here for the first mode, the eigenvector correspondence appears good, however, for the second and third eigenvector pairs their correspondence appear a little lower and it can be further improved by increasing the number of Markov parameters used in the Hankel Matrix construction. Whereas MSV gives the contribution of each mode to the identified impulse response function. In this case, MSV value of the first eigenvector pair is computed as 0.0163 for the both eigenvectors out of 0.025. For the second and third eigenvector pairs, the MSV

values are computed as 0.57 and 0.77 out of 1. Which yields fairly good approximation is obtained through the analysis. Additionally, in order to visualize the performance of ERA, impulse response function of the 3DOF system and impulse response function of the analytical discrete model expressed in Equation (6.23) are shown in Figure 6.20. In Figure 6.20, the dashed red line represented the impulse response of the system, computed from wavelet analysis and blue solid line represents the analytical impulse response function of the discrete state space model realized via ERA analysis. Therefore, as indicated by MAC and MSV, good realization is obtained through the ERA analysis. In addition to that, the realization error between the analytical and realized impulse response functions are computed to be low as given in Figure 6.21.

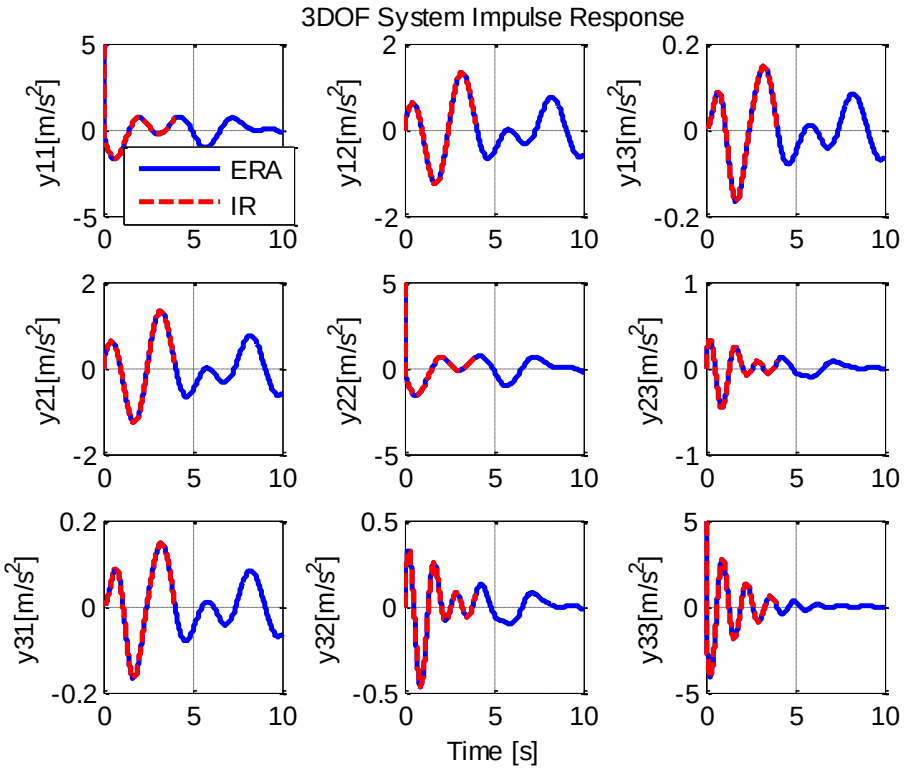

Figure 6.20 Comparison of 3DOF System IR and Discrete System IR obtained by ERA

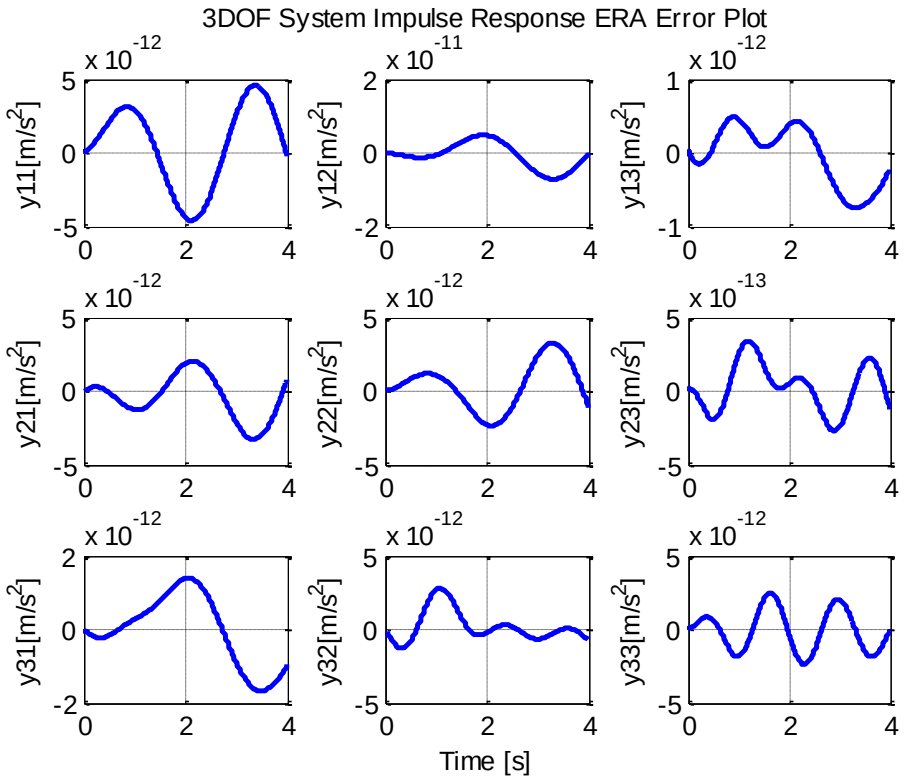

Figure 6.21 Realization Error for 3DOF Discrete System IR obtained by ERA

At this point in order to obtain natural frequencies and system's physical parameters, the continues model must be converted to damped continuous modal displacement-equivalent form as stated in Equation (5.3), which is given below for the acceleration output case as

$$\begin{aligned} \dot{\hat{z}} &= \Lambda_c\, z(t) + B_z u(t) \\ y(t) &= C_z\, z(t) \end{aligned} \tag{6.27}$$

where

$$\Lambda_c = \begin{bmatrix} -0.5556 + 4.681i & 0 & 0 & 0 & 0 & 0 \\ 0 & -0.5556 - 4.681i & 0 & 0 & 0 & 0 \\ 0 & 0 & -0.0475 + 1.377i & 0 & 0 & 0 \\ 0 & 0 & 0 & -0.0475 - 1.377i & 0 & 0 \\ 0 & 0 & 0 & 0 & -0.1470 + 2.420i & 0 \\ 0 & 0 & 0 & 0 & 0 & -0.1470 -2.420i \end{bmatrix} \tag{6.28}$$

$$B_z = \Psi^{-1} B_c = \begin{bmatrix} 0.4677 - 0.3606i & -4.261 + 3.285i & 38.36 -29.57i \\ 0.4677 + 0.3606i & -4.261 - 3.285i & 38.36 +29.57i \\ -11.63 -13.87i & -12.22 -14.58i & -1.216 - 1.451i \\ -11.63 +13.87i & -12.22 +14.58i & -1.216 + 1.451i \\ -20.62 +15.06i & 19.38 -14.15i & 2.405 - 1.756i \\ -20.62 -15.06i & 19.38 +14.15i & 2.405 + 1.756i \end{bmatrix}$$

$$C_z = C_c \Psi \Lambda_c^{-2} = \begin{bmatrix} 0 & 0 & 0.007267 + 0.006092i & 0.007267 - 0.006092i & -0.002515 + 0.003445i & -0.002515 - 0.003445i \\ -1.477*10^{-4} + 1.917*10^{-4}i & -1.477*10^{-4} - 1.917*10^{-4}i & 0.007638 + 0.006402i & 0.007638 - 0.006402i & 0.002463 - 0.003238i & 0.002463 + 0.003238i \\ 0.001330 - 0.001725i & 0.001330 + 0.001725i & 7.599*10^{-4} + 6.370*10^{-4}i & 7.599*10^{-4} - 6.370*10^{-4}i & 2.932*10^{-4} - 4.017*10^{-4}i & 2.932*10^{-4} + 4.017*10^{-4}i \end{bmatrix}$$

Then the damped natural frequencies are obtained from the imaginary parts of the continuous eigenvalues, which are obtained above, as $w_{n1} = 4.681\, rad/s$, $w_{n2} = 1.377\, rad/s$, and the third one is $w_{n3} = 2.420\, rad/s$. As expected, the computed eigenvalues appear as complex conjugate pairs on the main diagonal of the given eigenvalues matrix. Therefore, finally, the physical system parameters, which are the mass, stiffness and damping matrices, are obtained through a transformation procedure from first order state space models into second order models, as explained in Chapter 5. Here CBSI procedure is applied to the damped modal continuous form given above to extract physical system properties. However in this example as there are three inputs, three corresponding scaling functions are obtained. As the system model is ideal, which is a linear and time invariant one, the computed scaling functions appear to be identical and using any of them, the extracted mass, stiffness and damping matrices are computed as follows.

$$\hat{M} = \begin{bmatrix} 1.000 & 0 & 0 \\ 0 & 1.000 & 0 \\ 0 & 0 & 1.000 \end{bmatrix}$$

$$\hat{K} = \begin{bmatrix} 4.000 & -2.000 & 0 \\ -2.000 & 4.000 & -2.000 \\ 0 & -2.0000 & 22.00 \end{bmatrix} \qquad (6.29)$$

$$\hat{D} = \begin{bmatrix} 0.200 & -0.100 & 0 \\ -0.100 & 0.200 & -0.100 \\ 0 & -0.100 & 1.100 \end{bmatrix}$$

When the estimated physical system parameters given in Equation (6.29) are compare with the initial selected system parameters given in Equation (6.22), perfect match with less than 1% error is obtained in terms of physical system parameters and good realization is obtained as visually and analytically verified.

Secondly, the ERA/DC is applied to the 3DOF system model. As stated previously, ERA/DC also uses system impulse response as the starting point, then Hankel matrices are constructed accordingly. In this three degree of freedom system case, as the number of input and output is large, constructing square Hankel matrix with large number of Markov parameters, increases computation time, for this reason as the Correlated Hankel matrices are constructed using $R_{hh}(k) = H(k)H^T(0)$, a non square Hankel matrix may decrease the size of the Correlated Hankel Matrices. For this specific reason, Hankel matrices are constructed using 5x3000 Markov parameters, each Hankel matrix is obtained in the dimension of 15x9000 and Correlation Matrices $R_{hh}(k)$ are obtained in the dimension of 15x15, and by doing so, computation time dramatically decreased rather than working with a square Hankel matrix. Here it can be noted that, as correlation variable are introduce, obtaining smaller sized matrices still preserves the whole system response information. After 100 small sized Correlation Matrices are computed, Correlated Hankel Matrices are constructed. After the Correlated Hankel Matrices are obtained, singular value decomposition of the first Correlated Hankel matrix is obtained to

determine its effective rank, which corresponds to the estimated system order. In this case again, the estimated order of the system, which is obtained from the rank of the Correlated Hankel Matrix, is computed as 6, which is the number of nonzero singular values shown in Figure 6.22.

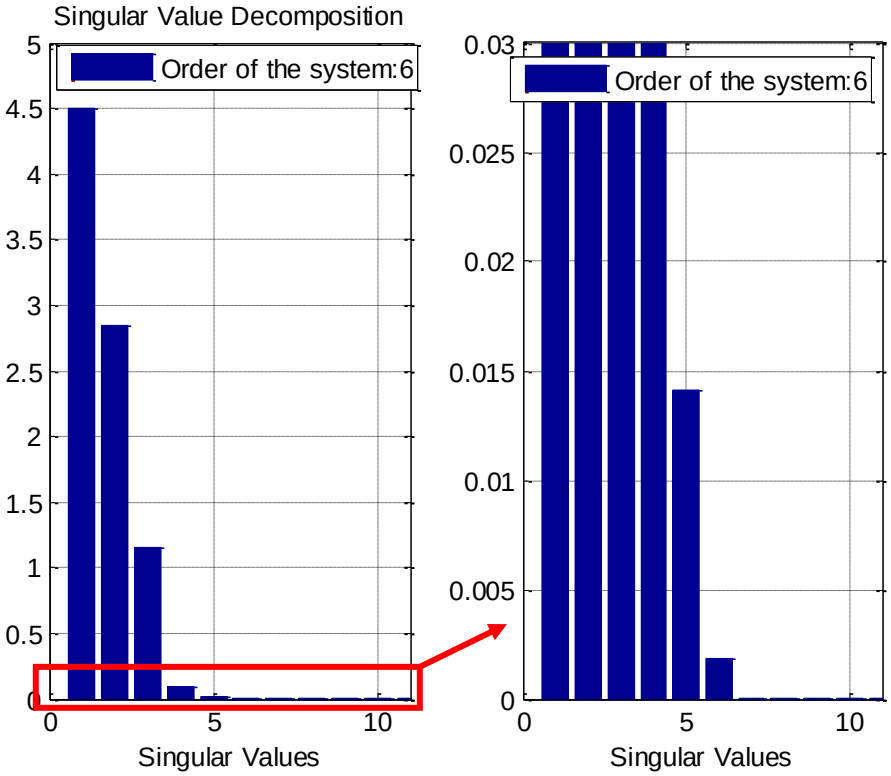

Figure 6.22 Singular Values of the Correlated Hankel Matrix in ERA/DC Analysis for 3DOF System

Then the left and right unitary matrices of the initial Correlated Hankel matrix are truncated according to the computed system order, as the singular values beyond the calculated order of the system do not contribute to the solution. After truncation, the ERA procedure is followed and the realized discrete time system matrices $\hat{A}_0$, $\hat{B}_0$, $\hat{C}$, and $\hat{D}$ for the generalized discrete state space representation, given in Equation (6.23), are obtained as follows.

$$\hat{A}_0 = \begin{bmatrix} 0.9993 & 0 & 0 & -0.004680 & 0 & 0 \\ 0 & 0.9994 & 0 & 0 & -0.002464 & 0 \\ 0 & 0 & 1.000 & 0 & 0 & -0.001385 \\ 0.004680 & 0 & 0 & 0.9995 & 0 & 0 \\ 0 & -0.002464 & 0 & 0 & 1.000 & 0 \\ 0 & 0 & 0.001385 & 0 & 0 & 0.9998 \end{bmatrix}$$

$$\hat{B}_0 = \begin{bmatrix} 0.0006624 & -0.006035 & 0.05430 \\ 0.02919 & -0.02743 & -0.003404 \\ 0.01776 & 0.01866 & 0.001857 \\ -0.0005235 & 0.004770 & -0.04294 \\ 0.02637 & -0.02479 & -0.003075 \\ -0.01643 & -0.1727 & -0.001718 \end{bmatrix}$$

$$\hat{C} = \begin{bmatrix} -0.0006624 & -0.02919 & -0.01776 & -0.0005236 & 0.02637 & -0.01643 \\ 0.006035 & 0.02743 & -0.01866 & 0.004770 & -0.02479 & -0.01727 \\ -0.05433 & 0.003403 & -0.001867 & -0.04294 & -0.003076 & -0.001718 \end{bmatrix}$$

$$\hat{D} = \begin{bmatrix} 1.000 & 0 & 0 \\ 0 & 1.000 & 0 \\ 0 & 0 & 1.000 \end{bmatrix} \qquad (6.30)$$

Then the system model realized in the discrete time domain is transformed into continuous time domain. The discrete system model found in Equation (6.23) is converted to continuous time by using Matlab's built in "d2c" command with zero order hold method, which represents the sampling used to collect system outputs. Therefore, the system matrices of the resultant continuous time model, expressed in Equation (6.25), are obtained as follows.

$$\hat{A}=\begin{bmatrix} -2.1553 & 0 & 0 & -4.9464 & 0 & 0 \\ 0 & -0.4169 & 0 & 0 & -2.4354 & 0 \\ 0 & 0 & 0.0439 & 0 & 0 & -1.3800 \\ 4.9476 & 0 & 0 & 1.0442 & 0 & 0 \\ 0 & 2.4354 & 0 & 0 & 0.1229 & 0 \\ 0 & 0 & 1.3798 & 0 & 0 & -0.1388 \end{bmatrix}$$

$$\hat{B}=\begin{bmatrix} -0.2622 & 2.3891 & -21.5055 \\ -5.6148 & 5.2773 & 0.6547 \\ -2.7331 & -2.8724 & -0.2858 \\ 0.5776 & -5.2628 & 47.3723 \\ 22.9583 & -21.5783 & -2.6772 \\ 19.1963 & 20.1750 & 2.0073 \end{bmatrix}$$

$$\hat{C}=\begin{bmatrix} 0.0013 & 0.0556 & 0.0330 & 0.0003 & 0.0069 & 0.0024 \\ -0.0115 & -0.0523 & 0.0347 & -0.0026 & -0.0064 & 0.0025 \\ 0.1031 & -0.0065 & 0.0034 & 0.0236 & -0.0008 & 0.0002 \end{bmatrix}$$

$$\hat{D}=\begin{bmatrix} 1 & 0 & 0 \\ 0 & 1 & 0 \\ 0 & 0 & 1 \end{bmatrix} \qquad (6.31)$$

Again, it should be noted that $\hat{C}$ and $\hat{D}$ are the same for discrete and continuous models as they provide mapping between outputs, states and inputs, independent of the time.

In this case, in order to assess how good ERA/DC approximates the system impulse response function, the two measures, the MAC and MSV are computed. In this case MAC is computed as 0.94, 0.94 ; 0.86 ,0.86; and 0.52, 0.52 out of 1 for each identified eigenvectors. Here the MAC values appear as pairs, this is expected because the eigenvectors corresponding to each mode appear as complex conjugate pairs. Moreover, the MAC values for each complex conjugate pair is equivalent to each other. Here for the first two modes, the eigenvector correspondence appears good, however, for the third eigenvector pair their contribution appear a little lower and it can be further improved by increasing the number of Markov parameters used in the Hankel Matrix construction. Whereas MSV gives the contribution of each mode to the identified impulse response function. In this case eigenvector pair MSV

is computed as 0.024 for the both eigenvectors out of 0.025. For the second and third eigenvector pairs, the MSV values are computed as 0.72 and 1 out of 1. Which yields that good approximation is obtained through the analysis. Additionally, in order to visualize the performance of ERA/DC, impulse response function of the 3DOF system and the discrete model with parameters expressed in Equation (6.30) are shown in Figure 6.23. In Figure 6.23, the dashed red line represented the impulse response of the system computed from Wavelet analysis and blue solid line represents the analytical impulse response function of the discrete state space model realized via ERA analysis. Therefore, as indicated by MAC and MSV, good realization is obtained through the ERA analysis. In addition to that, the realization error between the analytical and realized impulse response functions are computed to be low as given in Figure 6.24.

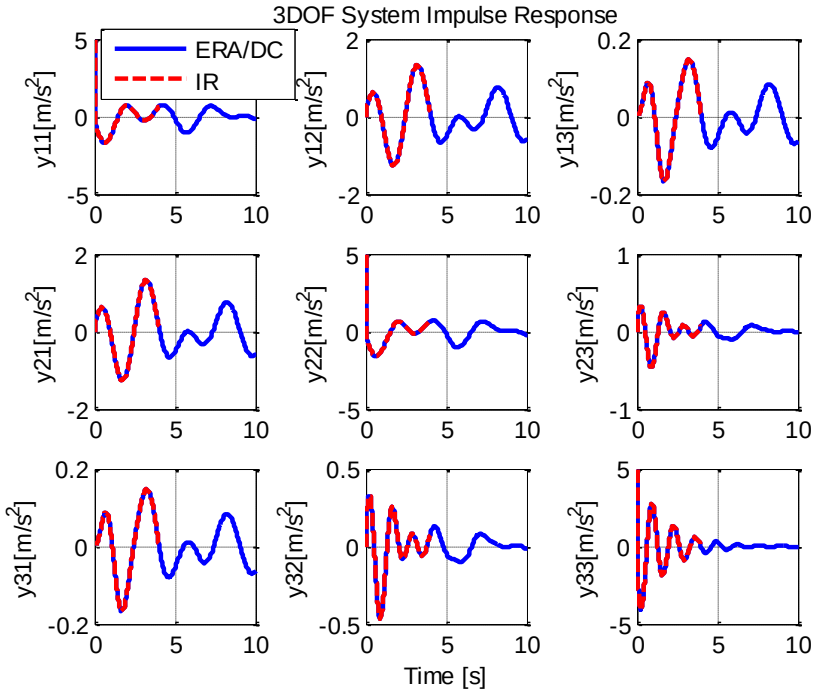

Figure 6.23 Comparison of 3DOF System IR and Discrete System IR obtained by ERA/DC

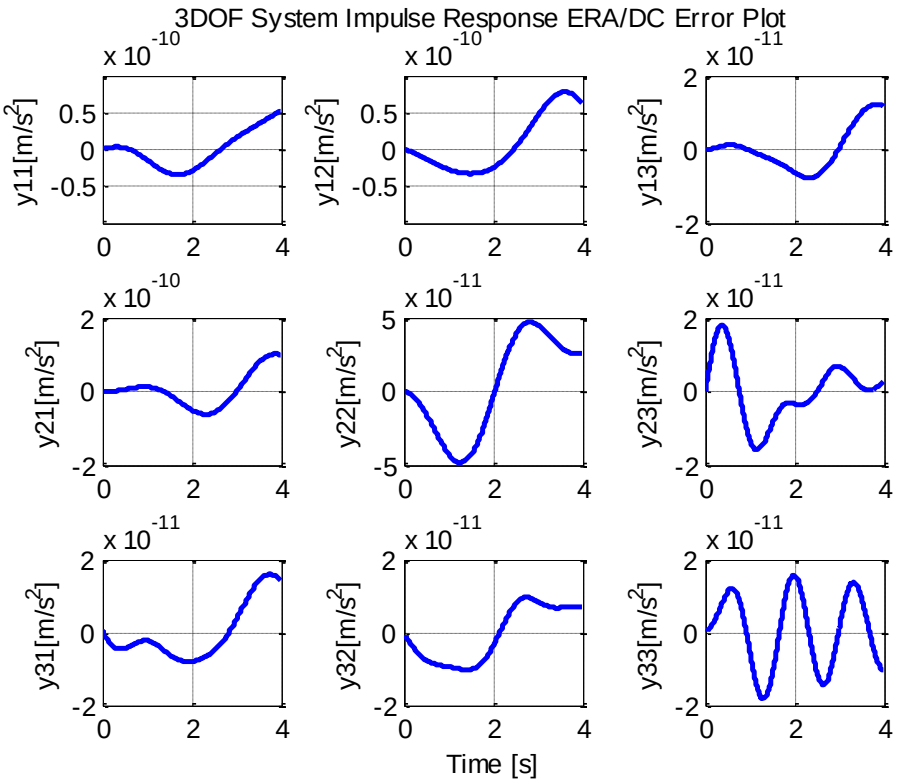

Figure 6.24 Realization Error for 3DOF Discrete System IR obtained by ERA/DC

Again, at this point in order to obtain natural frequencies and system's physical parameters, the continues model must be converted to damped continuous modal displacement-equivalent form as stated in Equation (5.3), which is given below for the acceleration output case

$$\begin{aligned} \dot{\hat{z}} &= \Lambda_c \, z(t) + B_z u(t) \\ y(t) &= C_z \, z(t) \end{aligned} \tag{6.32}$$

where

$$\Lambda_c = \begin{bmatrix} -0.5556 + 4.681i & 0 & 0 & 0 & 0 & 0 \\ 0 & -0.5556 - 4.681i & 0 & 0 & 0 & 0 \\ 0 & 0 & -0.04745 + 1.377i & 0 & 0 & 0 \\ 0 & 0 & 0 & -0.04745 - 1.377i & 0 & 0 \\ 0 & 0 & 0 & 0 & -0.1470 + 2.420i & 0 \\ 0 & 0 & 0 & 0 & 0 & -0.1470 -2.420i \end{bmatrix}$$

$$B_c = \Psi^{-1}B_C = \begin{bmatrix} 0.4084 + 0.05639i & -3.721 - 0.5138i & 33.50 + 4.625i \\ 0.4084 - 0.05639i & -3.721 + 0.5138i & 33.50 - 4.625i \\ -1.932 +13.73i & -2.031 +14.43i & -0.2021 + 1.436i \\ -1.932 -13.73i & -2.031 -14.43i & -0.2021 - 1.436i \\ 3.970 -15.90i & -3.732 +14.94i & -0.4630 + 1.853i \\ 3.970 +15.90i & -3.732 -14.94i & -0.4630 - 1.853i \end{bmatrix}$$

$$C_c = C_c \Psi \Lambda_c^{-2} = \begin{bmatrix} 0 & 0 & -0.01226 + 0.001725i & -0.01226 - 0.001725i & 6.450*10^{-3} - 1.611*10^{-3}i & 6.450*10^{-3} + 1.611*10^{-3}i \\ -0.0000 + 0.0003i & -0.0001 - 0.0003i & -0.01288 + 0.001813i & -0.01288 - 0.001813i & -6.062*10^{-3} + 1.515*10^{-3}i & -6.062*10^{-3} - 1.515*10^{-3}i \\ -4.741*10^{-4} - 3.091*10^{-4}i & -4.741*10^{-4} + 3.091*10^{-4}i & -0.001282 + 1.803*10^{-4}i & -0.001282 - 1.803*10^{-4}i & -0.7521*10^{-4} + 0.1879*10^{-4}i & -0.7521*10^{-4} - 0.1879*10^{-4}i \end{bmatrix} \quad (6.33)$$

Then the damped natural frequencies are obtained from the imaginary parts of the continuous eigenvalues obtained above as $w_{n1} = 4.681\,rad/s$, $w_{n2} = 1.377\,rad/s$ and the third one is $w_{n3} = 2.420\,rad/s$ which are exactly the same eigenvalues obtained in the ERA analysis. This is because, the natural frequencies are specific to the system and both algorithms realize the system with good approximation. As expected, the computed eigenvalues appear in complex conjugate pairs on the main diagonal of the given eigenvalue matrix. Finally, the physical system parameters, which are the mass, stiffness and damping matrices are obtained through a transformation procedure from the first order state space models into second order models, as explained in Chapter 5. Here CBSI procedure is applied to the damped modal continuous form given above, to extract physical system properties, but here as there are three inputs, three scaling functions are obtained. As the system model is ideal, linear and time invariant one, the computed scaling functions appear to be identical and using any of them, the extracted system parameters are computed as follows.

$$\hat{M} = \begin{bmatrix} 1.000 & 0 & 0 \\ 0 & 1.000 & 0 \\ 0 & 0 & 1.000 \end{bmatrix}$$

$$\hat{K} = \begin{bmatrix} 4.000 & -2.000 & 0 \\ -2.000 & 4.000 & -2.000 \\ 0 & -2.000 & 22.00 \end{bmatrix} \qquad (6.34)$$

$$\hat{D} = \begin{bmatrix} 0.2000 & -0.1000 & 0 \\ -0.1000 & 0.2000 & -0.1000 \\ 0 & -0.1000 & 1.100 \end{bmatrix}$$

When the estimated physical system parameters given in Equation (6.34) are compare with the initial selected system parameters given in Equation (6.22), perfect match is obtained in terms of physical system parameters and good realization is obtained as visually and analytically verified.

Finally, in order to observe performance of the whole identification process with a single input, the 3 DOF system model is investigated again. In this case only the input 1 is used to excite system and all the three system responses are utilized in the identification process. For this reason, the measurement data shown in Figure 6.15 is used. In a similar wavelet transform derivation, the impulse response of the system is the first column of Figure 6.18 indeed. Therefore, as the Markov parameters are predetermined, the Hankel matrix is constructed by using 1000×1000 square Markov Parameters becomes in the dimension of 3000×3000. After the Hankel matrix is constructed, the SVD is applied, and the singular values of the Hankel matrix are plotted against their values are shown in Figure 6.25. In this figure the nonzero singular values determines the rank of the system which corresponds to the estimated order of the system, that will be realized as a result of the ERA application.

Here as the 3 degree of freedom system is expected to be represented by using 6 first order equations, the computed order of the system, shown in Figure 6.25 is correct.

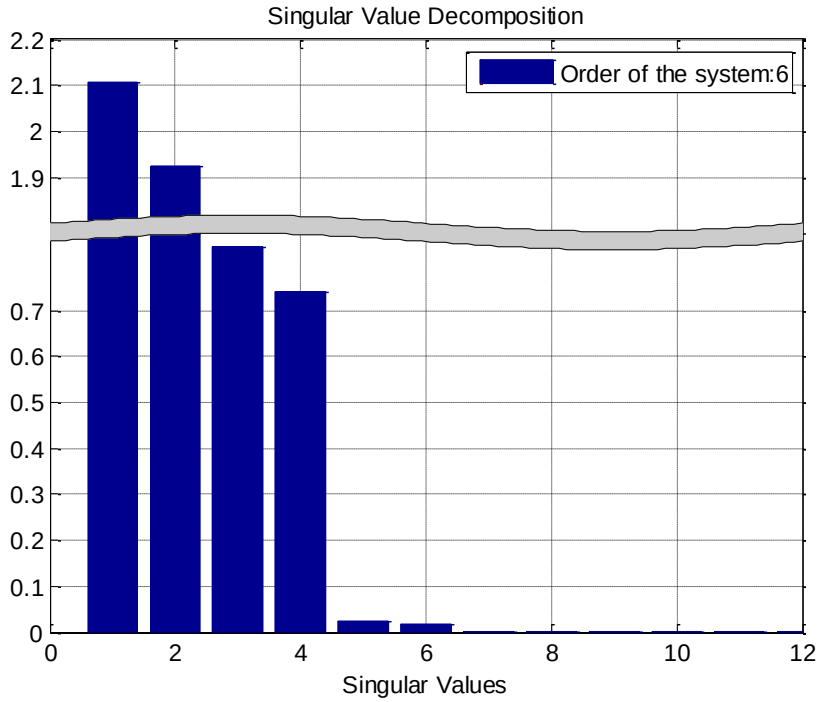

Figure 6.25 Singular Values of the Hankel Matrix in ERA Analysis with Single Input for 3DOF System

Then the left and right unitary matrices of the initial Hankel matrix are truncated according to the computed system order as the singular values beyond the calculated order of the system do not contribute to the solution.

After the truncation, the ERA procedure is followed and the realized discrete time system matrices $\hat{A}_0$, $\hat{B}_0$, $\hat{C}$, and $\hat{D}$ for the generalized discrete state space representation are obtained as follows.

$$\begin{aligned} x(k+1) &= \hat{A}_0\, x(k) + \hat{B}_0 u(k) \\ y(k) &= \hat{C}\, x(k) + \hat{D} u(k) \end{aligned} \tag{6.35}$$

where

$$
\hat{A}_0 = \begin{bmatrix}
0.9999 & -0.002039 & 6.741*10^{-4} & 5.067*10^{-4} & 0 & 0 \\
1.982*10^{-3} & 0.9999 & -4.549*10^{-4} & 0 & 0 & 0 \\
-9.992*10^{-4} & 8.250*10^{-4} & 0.9998 & 1.515*10^{-3} & 0 & 0 \\
-7.534*10^{-4} & 4.699*10^{-4} & 1.547*10^{-3} & 0.9999 & 0 & 0 \\
0 & 0 & -2.487*10^{-4} & -2.243*10^{-4} & 0.9998 & 4.525*10^{-3} \\
-1.259*10^{-4} & 1.031*10^{-4} & -1.596*10^{-4} & -1.188*10^{-4} & -4.863*10^{-3} & 0.9991
\end{bmatrix}
$$

$$
\hat{B}_0 = \begin{bmatrix}
0.03041 \\ -0.01965 \\ 0.03380 \\ 0.02538 \\ 0.004106 \\ 0.006743
\end{bmatrix}
$$

$$
\hat{C} = \begin{bmatrix}
-0.02567 & -0.2106 & -0.05737 & 0.01413 & 0 & 0 \\
0.02416 & -0.006839 & -0.02078 & -0.002472 & 4.103*10^{-4} & -6.759*10^{-4} \\
0.002758 & -3.479*10^{-4} & -0.002792 & -8.462*10^{-4} & -0.003468 & 0.005838
\end{bmatrix}
$$

$$
\hat{D} = \begin{bmatrix}
1.000 \\ 0 \\ 0
\end{bmatrix}
\tag{6.36}
$$

Then the system model realized in the discrete time domain is transformed into continuous time domain. The discrete system model found in Equation (6.23) is converted to continuous time by using Matlab's built in "d2c" command with zero order hold method, which represents the sampling used to collect system outputs. Therefore, the resultant continuous time model is obtained as follows.

$$
\begin{aligned}
\dot{x}(t) &= \hat{A}x(t) + \hat{B}u(t) \\
y(t) &= \hat{C}x(t) + \hat{D}u(t)
\end{aligned}
\tag{6.37}
$$

where

$$\hat{A}=\begin{bmatrix} -0.1427 & -2.039 & 0.6742 & 0.5064 & -7.731*10^{-4} & 0.002390 \\ 1.982 & -0.003121 & -0.4556 & 0.09887 & -3.572*10^{-4} & -0.001487 \\ -0.9923 & 0.8238 & -0.2186 & 1.515 & 0.005272 & 0.007182 \\ -0.7547 & 0.4698 & -1.546 & -0.02479 & 0.005874 & 0.006594 \\ -0.03774 & 0.01667 & -0.2486 & -0.2239 & -0.2092 & 4.527 \\ -0.1262 & 0.1031 & -0.1604 & -0.1192 & -4.866 & -0.9016 \end{bmatrix}$$

$$\hat{B}=\begin{bmatrix} 30.38 \\ -19.67 \\ 33.80 \\ 25.42 \\ 4.099 \\ 6.763 \end{bmatrix}$$

$$\hat{C}=\begin{bmatrix} -0.02567 & -0.2106 & -0.05737 & 0.01413 & 0 & 0 \\ 0.02416 & -0.006839 & -0.02078 & -0.002472 & 4.103*10^{-4} & -6.759*10^{-4} \\ 0.002758 & -3.479*10^{-4} & -0.002792 & -8.462*10^{-4} & -0.003468 & 0.005838 \end{bmatrix}$$

$$\hat{D}=\begin{bmatrix} 1.000 \\ 0 \\ 0 \end{bmatrix} \qquad (6.38)$$

Here in order to assess how good ERA approximates the system impulse response function, the two measures which are the MAC and MSV are computed. As previously mentioned, MAC gives the correspondence between the identified pulse response history and the pulse response used in the identification and when there is no noise included in the data, which is the case in this example, MAC is computed as 0.87, 0.87 ; 0.66 ,0.66; and 0.30, 0.30 out of 1 for each identified eigenvectors. Here the MAC values appear in pairs, this is expected because the eigenvectors corresponding to each mode appear as complex conjugate pairs and each pair has the same MAC value. Here for the first mode, the eigenvector correspondence appears good, however, for the second and third eigenvector pairs their correspondence appear a little lower and it can be further improved by increasing the number of Markov parameters used in the Hankel Matrix construction. Whereas MSV gives the contribution of each mode to the identified impulse response function. In this case, MSV value of the first eigenvector pair is computed as 0.023 for the both eigenvectors out of 0.025. For the second and third eigenvector pairs, the MSV values are computed as 0.75 and 0.95 out of 1. Which yields fairly good approximation is obtained through the analysis. Additionally, in order to visualize

the performance of ERA, for a single input case, impulse response function of the 3DOF system and impulse response function of the analytical discrete model expressed in Equation (6.35) are shown in Figure 6.26. In Figure 6.26, the dashed red line represented the impulse response of the system, computed from wavelet analysis and blue solid line represents the analytical impulse response function of the discrete state space model realized via ERA analysis. Therefore, as indicated by MAC and MSV, good realization is obtained through the ERA analysis. In addition to that, the realization error between the analytical and realized impulse response functions are computed to be low as given in Figure 6.27.

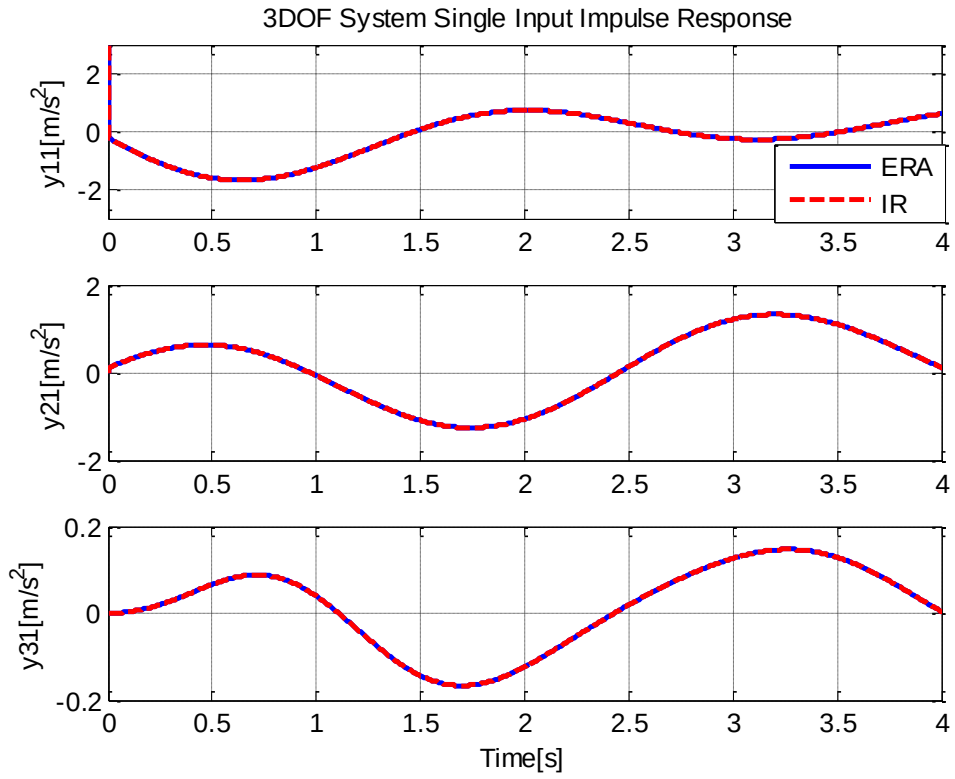

Figure 6.26 Comparison of Single Input 3DOF System IR and Discrete System IR obtained by ERA

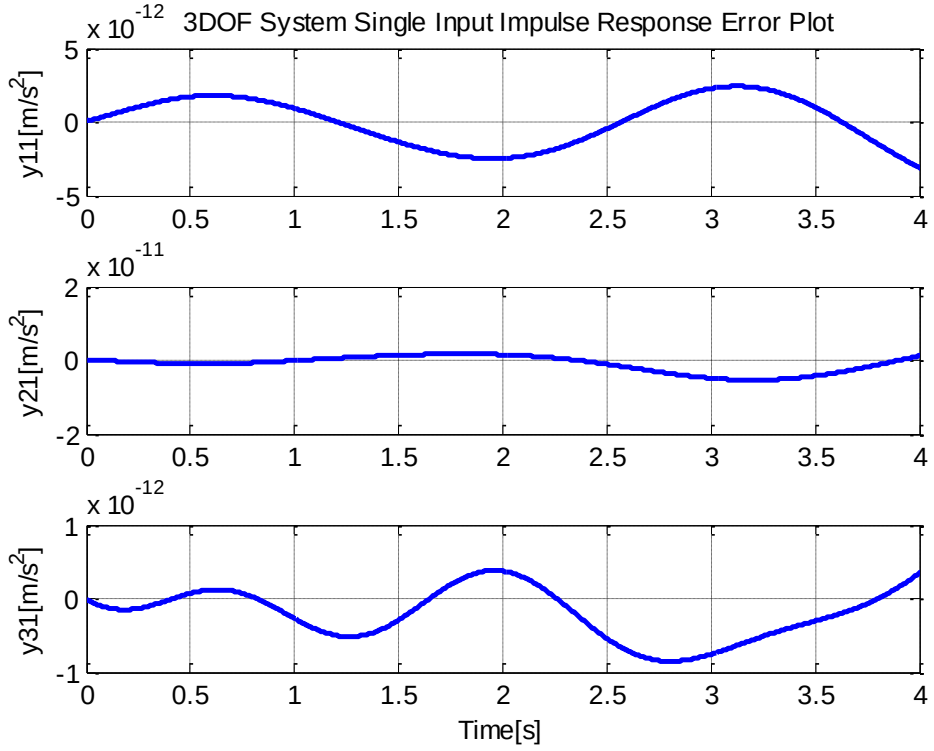

Figure 6.27 Realization Error for 3DOF Discrete System Single Input IR obtained by ERA

At this point in order to obtain natural frequencies and system's physical parameters, the continues model must be converted to damped continuous modal displacement-equivalent form as stated in Equation (5.3), which is given below for the acceleration output case as

$$\begin{aligned} \dot{\hat{z}} &= \Lambda_c\, z(t) + B_z u(t) \\ y(t) &= C_z\, z(t) \end{aligned} \tag{6.39}$$

where

$$\Lambda_c = \begin{bmatrix} -0.04745 + 1.377i & 0 & 0 & 0 & 0 & 0 \\ 0 & -0.04745 - 1.377i & 0 & 0 & 0 & 0 \\ 0 & 0 & -0.1470 + 2.420i & 0 & 0 & 0 \\ 0 & 0 & 0 & -0.1470 - 2.420i & 0 & 0 \\ 0 & 0 & 0 & 0 & -0.5556+4.681i & 0 \\ 0 & 0 & 0 & 0 & 0 & -0.5556 - 4.681i \end{bmatrix} \tag{6.40}$$

$$B_z = \Psi^{-1} B_c = \begin{bmatrix} 23.34 + 7.643i \\ 23.34 - 7.643i \\ -18.46 + 27.21i \\ -18.46 - 27.21i \\ 1.501 + 5.518i \\ 1.501 - 5.518i \end{bmatrix}$$

$$C_z = C_c \Psi \Lambda_c^{-2} = \begin{bmatrix} -0.002175 - 0.006642i & -0.002175 + 0.006642i & -0.002740 + 0.001859i & -0.002740 - 0.001859i & 0 & 0 \\ -0.002286 - 0.006981i & -0.002286 + 0.006981i & 0.002576 - 0.001747i & 0.002576 + 0.001747i & 0 & 0 \\ -2.2742*10^{-4} - 6.945*10^{-4}i & -2.2742*10^{-4} + 6.945*10^{-4}i & 3.195*10^{-4} - 2.168*10^{-4}i & 3.195*10^{-4}+2.168*10^{-4}i & -2.171*10^{-4}-5.903*10^{-5}i & -2.171*10^{-4}+5.903*10^{-5}i \end{bmatrix}$$

Then the damped natural frequencies are obtained, as $w_{n1} = 1.377 rad/s$, $w_{n2} = 2.420 rad/s$, and the third one is $w_{n3} = 4.681 rad/s$. Therefore, finally, the physical system parameters, which are the mass, stiffness and damping matrices, are obtained through CBSI procedure is applied to the damped modal continuous form given above to extract physical system properties. However in this example as there is a single input, corresponding scaling function is obtained, so that the physical system parameters are obtained as following.

$$\hat{M} = \begin{bmatrix} 1.000 & 0 & 0 \\ 0 & 1.000 & 0 \\ 0 & 0 & 1.000 \end{bmatrix}$$

$$\hat{K} = \begin{bmatrix} 4.000 & -2.000 & 0 \\ -2.000 & 4.000 & -2.000 \\ 0 & -2.0000 & 22.00 \end{bmatrix} \tag{6.41}$$

$$\hat{D} = \begin{bmatrix} 0.200 & -0.100 & 0 \\ -0.100 & 0.200 & -0.100 \\ 0 & -0.100 & 1.100 \end{bmatrix}$$

When the estimated physical system parameters are compare with the initial selected system parameters, perfect match with less than 1% error is obtained. Therefore, effectiveness of the selected identification methodologies are verified for a single input case as well.

6.3 IDENTIFICATION IMPLEMENTATION TO TEST SYSTEM

In order to investigate performance of the identification procedure described in the preceding sections, a test setup which represents a simplified version of the stabilized platforms, shown in Figure 6.28 is constructed.

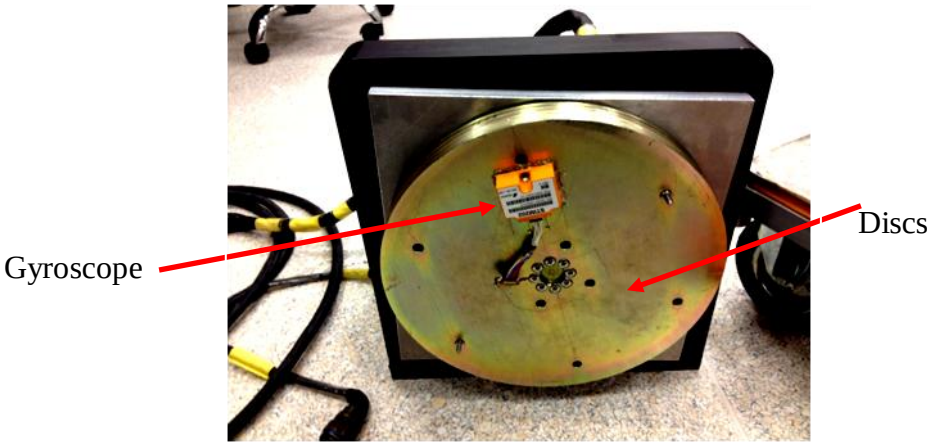

a) Front View

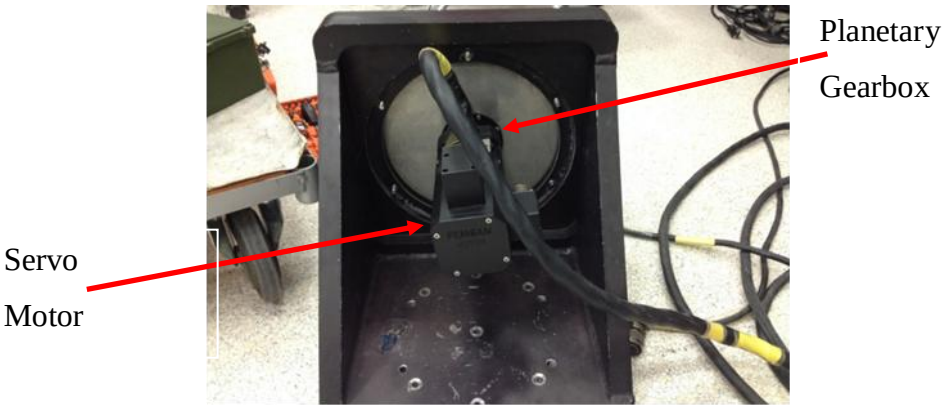

b) Rear View

Figure 6.28 Front(a) and Rear(b) View of The Test Setup

In this setup, an Apex AD064 planetary type zero backlash (< 1arcmin) gearbox with gear ratio 1:10 is connected to the end of the MOOG D323 servo motor and three discs with known inertia values are connected to the output of the gearbox.

Then the whole assembly is connected to the stationary black frame. In this setup, instead of working with a single spring between the motor and the discs, a real life problem is incorporated with using the gearbox, because the gearbox has its own stiffness and damping characteristics.

In this test setup, the MOOG D323 type servo motor is driven by using servo driver HERKUL-1D developed by ASELSAN. The torque control loop is running inside the HERKUL-1D driver so that the desired torque is developed at the motor with nearly 1 kHz torque loop bandwidth. In addition to that, servo motor used in the tests has a resolver sensor connected to its shaft, so that angular position and velocity of the shaft can be measured. In addition to that, STIM 202 type gyroscope is also connected onto disc, to measure angular velocity and it is connected to servo driver, for data collection. In this setup, the measurement signals are sampled at a frequency of 1kHz. Data Sheets of the used components are given in the Appendix .

The simplified representation of the test configuration can be shown in Figure 6.29.

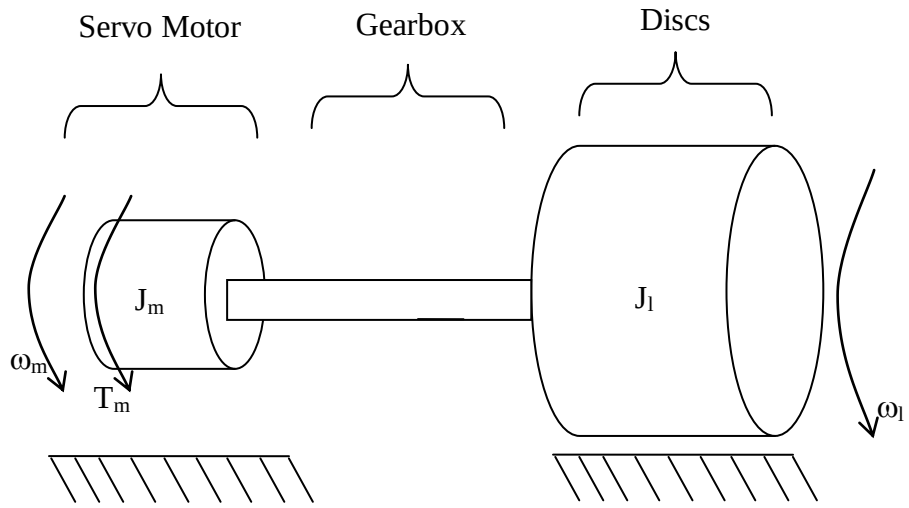

Figure 6.29 Equivalent Test System Representation

It should be noted that, this simplified representation is just to illustrate the test system and variables J_m and J_l are representing moment of inertia values of the

motor shaft and the discs respectively. The servo motor produces the desired torque on its shaft which is shown as T_m in Figure 6.29. In this setup, motor torque is not directly measured, however, from current feedbacks, effective torque developed by the motor is deduced by the servo driver and this torque value is utilized in the analysis. In addition to that, angular velocity of motor shaft, which is measured by using the resolver sensor is denoted by w_m and the load side angular speed, which is measured by gyroscope is denoted by w_l. At the beginning of the tests, only inertia values of the motor shaft and discs are known as $J_m = 0.004 kgm^2$ and $J_l = 0.18 kgm^2$ respectively, and in this setup due to the gear ratio, inertia value and measured response of the motor side are transformed to the load side with proper scaling. In addition to the motor and load inertia, the gearbox itself has a inertia value of $J_{gearbox} = 0.0013 kgm^2$, however as its exact contribution on which side is not known at the beginning, it is neglected. During testing, a frequency sweeping torque signal is commanded to the motor and the sweep signal with the frequency range starting from 20Hz and going up to 350Hz with 0.5Hz discrete frequency steps is generated inside the digital signal processor chip of the HERKUL-1D driver. During sweeping, for ensembling purposes, the sinusoidal signal at each frequency is repeated 16 times. Although test is repeated several times, only one of the measurement set is used in the analysis. During testing, the sweep signal shown in Figure 6.30 is applied to the system. In this figure, the sinusoidal torque signals are shown as a solid rectangle, however, zooming in to a specific time internal represents the true sinusoidal signal form as shown in Figure 6.31. In addition to that, in Figure 6.30, it is observed that actual torque has a disturbed section, which is because of coupling between the load and servo motor and it is detailed investigation can be find in [32]. In addition to the input applied to the system, the output measurements of motor and load side angular velocities are shown in Figure 6.32. Again in order to better visualize sinusoidal output velocities, a specific time interval is expanded in Figure 6.33.

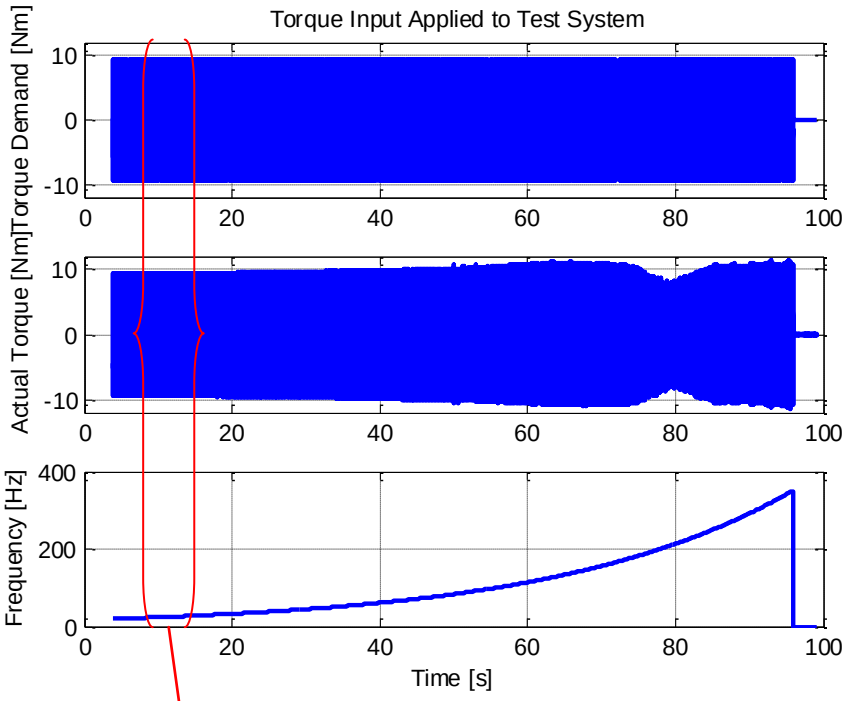

Figure 6.30 Torque Input Applied to Test System

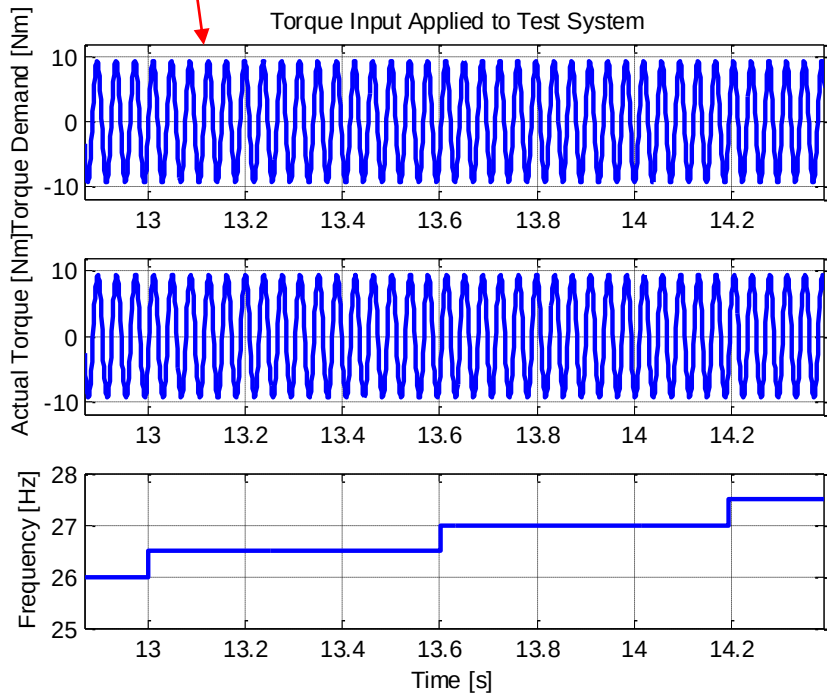

Figure 6.31 Detailed View of Torque Input Applied to Test System

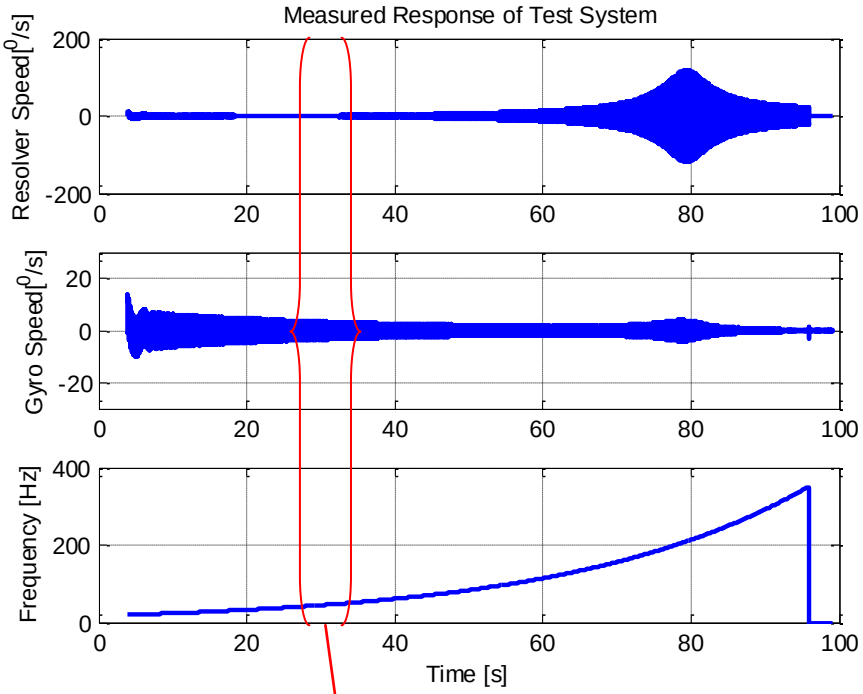

Figure 6.32 Measured Response of Test System

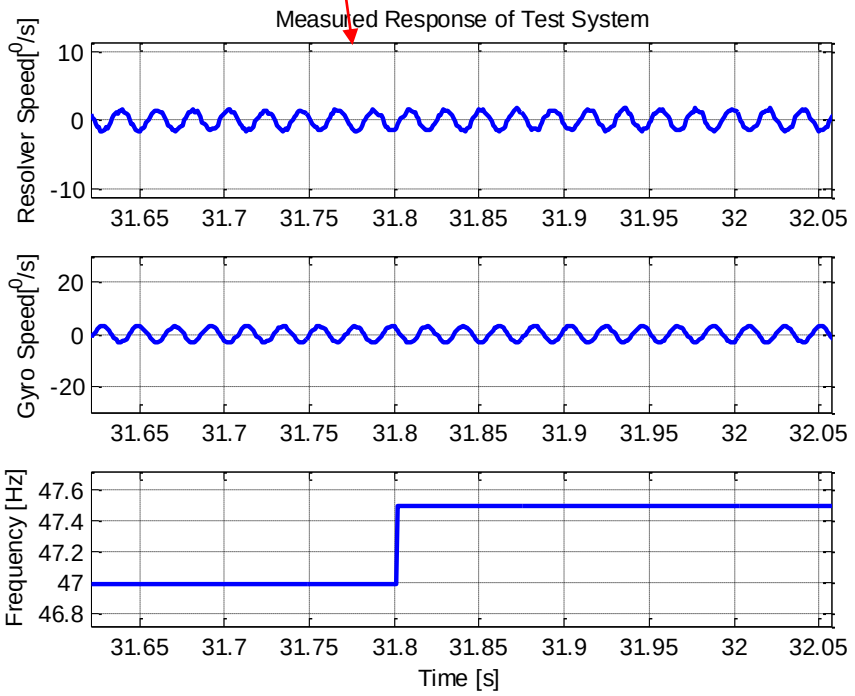

Figure 6.33 Detailed View of Measured Response of Test System

In order to start with the ERA, as stated in the previous examples, impulse response data must be obtained. In this case, Fourier transform method is utilized first to obtain system impulse response, in order to visualize performance of the Fourier transform method on real test data. In this case total number of 92108 data samples are recorded for each response measurement. As Fourier transform methods works with the data samples of powers of 2, the closest number of data sample is 2^{17}= 131072, therefore zeros are padded to the end of the measured data. After Fourier transform of the input and outputs are obtained, auto and cross correlated variables are obtained. After dividing cross correlated output to auto correlated input in the frequency domain and back transforming the frequency response function into time domain, the impulse response functions of the test system are obtained as shown in Figure 6.34.

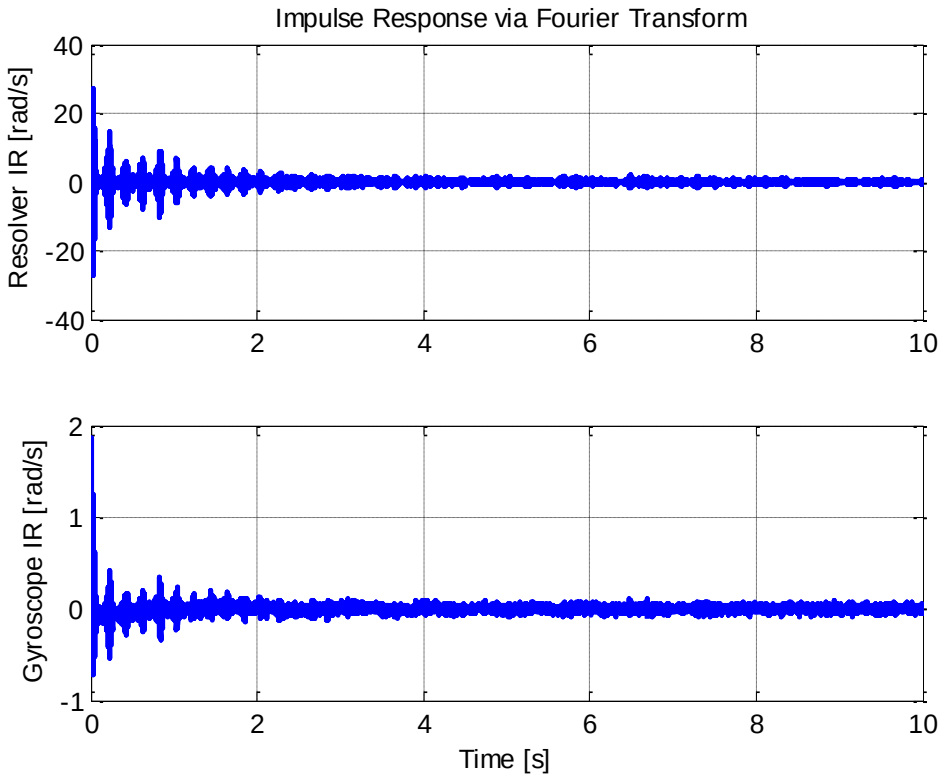

Figure 6.34 Impulse Response Functions of the Test Setup via Fourier Transform

In the Figure 6.34, it is observed that the noise becomes dominant in the impulse response data such that, Fourier transform could not convey the true Markov parameters of the test system.

As a second analysis tool to extract impulse response data, Wavelet transform will be utilized on the test data. Although there are 92108 number of measurement samples are recorded, in this case 2^{15} =32768 samples are used in the Wavelet analysis. Again Daubechies 4 wavelet is selected as the mother wavelet, which has 8 coefficient. In addition to that, full depth wavelet analysis with 15 levels are implemented to obtain Markov parameter of the test setup. After implementation of wavelet transform to the input and then solving convolution integral and applying inverse discrete Wavelet transform to the computed impulse response function, the obtained Markov parameters are plotted in Figure 6.35.

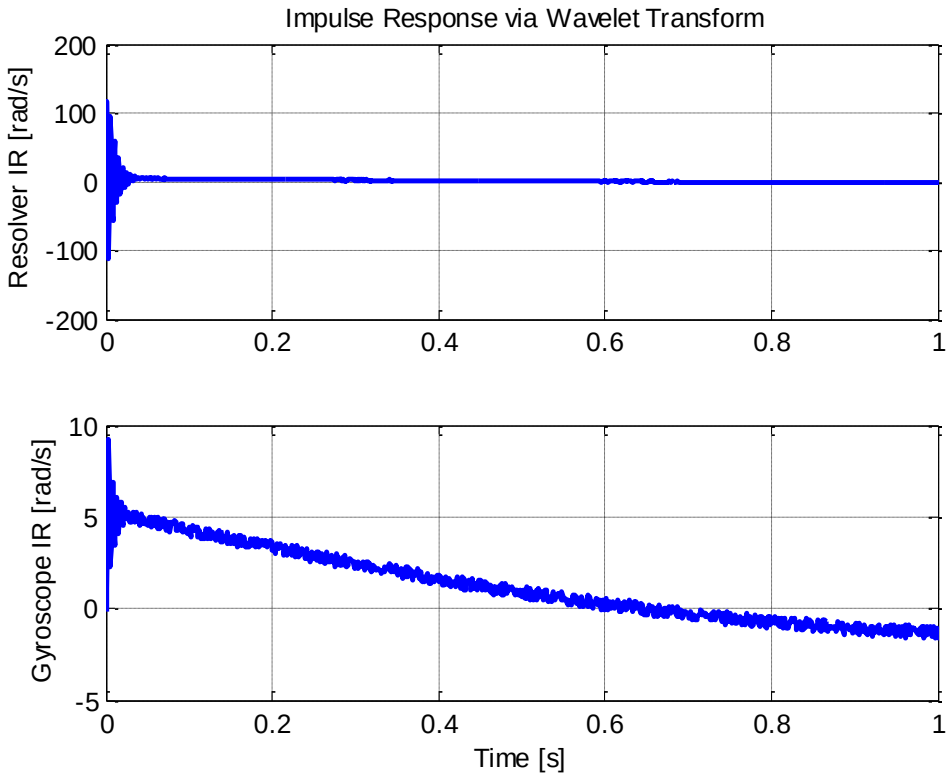

Figure 6.35 Impulse Response Functions of the Test Setup via Wavelet Transform

In Figure 6.35, although there exist a noise coupled on the extracted impulse response, the response of the system characteristics are captured mostly by the Wavelet transform method, although the computation time took long as the number of data samples are high. Therefore, in the realization application, the Markov parameters obtained as a result of the wavelet analysis will be used.

After impulse response functions are determined, then Eigensystem Realization algorithm can be implemented starting by forming Hankel matrices. In this case as there is a single input and two corresponding outputs, the Markov parameters at each time instant are in the size of 2x1, which is a column matrix. Therefore, in this case the Hankel matrices are constructed by using 500x500 square Markov parameters, which results in the dimension of 1000x500. After the Hankel matrix is constructed the singular values decomposition is applied, and the singular values of the Hankel matrix are plotted against their values are shown in Figure 6.36.

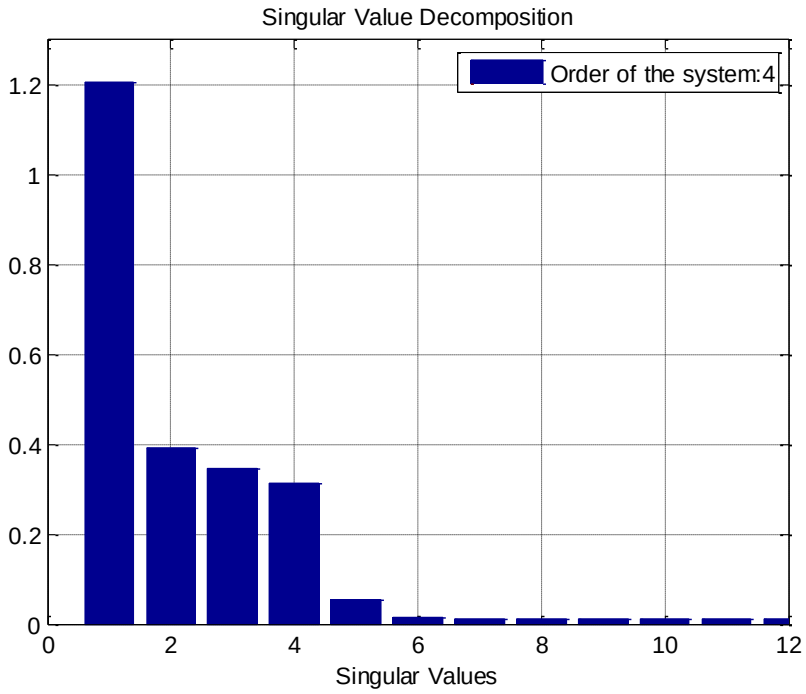

Figure 6.36 Singular Values of Hankel Matrix in ERA Analysis for Test System

In this figure, the nonzero singular values determines the rank of the system, which corresponds to the estimated order of the system as well. However, from Figure 6.36, it can be observed that none of the drawn singular values are not zero indeed, which resulted from the measurement noise involved in the impulse response functions. However, it can be observed that, after the 4^{th} singular value, the values drop significantly so that effective order of the system can be selected as 4 and the remaining singular values can be truncated as they appear due to measurement noise. Then the left and right unitary matrices of the initial Hankel matrix are truncated according to the estimated system order, as the singular values beyond the selected order are considered to be involved due to measurement noise.

After truncation, the ERA procedure is followed, and the realized discrete time system matrices $\hat{A}_0$, $\hat{B}_0$, $\hat{C}$, and $\hat{D}$ for the generalized discrete state space representation are obtained as follows.

$$\begin{aligned} x(k+1) &= \hat{A}_0\, x(k) + \hat{B}_0 u(k) \\ y(k) &= \hat{C}\, x(k) + \hat{D} u(k) \end{aligned} \tag{6.42}$$

where

$$\begin{aligned} \hat{A}_0 &= \begin{bmatrix} 0.9964 & -0.01628 & 0 & 0.003148 \\ -0.02688 & 0.1530 & -0.8366 & 0.2161 \\ -0.005123 & 0.8388 & 0.3637 & 0.1606 \\ -0.001495 & -0.2094 & 0.1747 & 0.9575 \end{bmatrix} \\ \hat{B}_0 &= \begin{bmatrix} -0.09301 \\ -0.3559 \\ -0.1222 \\ 0.005028 \end{bmatrix} \\ \hat{C} &= \begin{bmatrix} -0.06577 & -0.3559 & 0.1222 & -0.008700 \\ -0.06434 & 0.01290 & 0.001369 & 0.02116 \end{bmatrix} \\ \hat{D} &= \begin{bmatrix} 0 \\ 0 \end{bmatrix} \end{aligned} \tag{6.43}$$

Here it should be noted that the direct input-output influence matrix $\hat{D}$ is a null matrix as the utilized feedback on the test system are velocity measurements.

Then the system model realized in the discrete time domain is transformed into continuous time domain. The discrete system model computed in Equation (6.42) is converted to continuous time by using Matlab's built in "d2c" command with zero order hold method, which represents the sampling used to collect system outputs. Therefore, the resultant continuous time model is obtained as following.

$$\begin{aligned} \dot{x}(t) &= \hat{A}x(t) + \hat{B}u(t) \\ y(t) &= \hat{C}x(t) + \hat{D}u(t) \end{aligned} \tag{6.44}$$

where

$$\begin{aligned} \hat{A} &= \begin{bmatrix} -3.852 & -15.42 & -10.66 & 5.873 \\ -29.48 & -240.5 & -1268 & 324.6 \\ 13.31 & 1268 & 13.90 & -6.707 \\ -6.269 & -327.4 & 10.03 & -0.08619 \end{bmatrix} \\ \hat{B} &= \begin{bmatrix} -96.46 \\ -431.0 \\ 131.2 \\ -60.25 \end{bmatrix} \\ \hat{C} &= \begin{bmatrix} -0.06577 & -0.3559 & 0.1222 & -0.008700 \\ -0.06433 & 0.01290 & 0.001369 & 0.02116 \end{bmatrix} \\ \hat{D} &= \begin{bmatrix} 0 \\ 0 \end{bmatrix} \end{aligned} \tag{6.45}$$

After discrete and continuous system realizations are obtained, in order to assess how good ERA approximated the system impulse response function, the two measures, the MAC and MSV are computed. In this case MAC is computed as 1, 1 ; and 0.67 ,0.67 out of 1 for each identified eigenvectors. Here the MAC values appear as pairs, which is expected because the eigenvectors corresponding to each mode appear as complex conjugate pairs and, for each pair the MAC value is

equivalent. Here for the first and second mode, the eigenvector correspondence appears good. Whereas MSV gives the contribution of each mode to the identified impulse response function. In this case MSV is computed as 0.84 for the both eigenvectors out of 0.84 and for the second eigenvector pair, the MSV is computed as 1.1 out of 1.8, which yields that, very good approximation is obtained through the ERA analysis. Additionally, in order to visualize the performance of ERA, impulse response function of the test system and the impulse response function of the discrete model expressed in Equation (6.42) are shown in Figure 6.37. In Figure 6.37, the blue solid line represents the impulse response of the system computed from Wavelet analysis and dashed red line represents the analytical impulse response function of the discrete state space model realized via ERA analysis. Therefore, as indicated by MAC and MSV and verified in Figure 6.37 and Figure 6.38, very good realization is obtained through the ERA analysis.

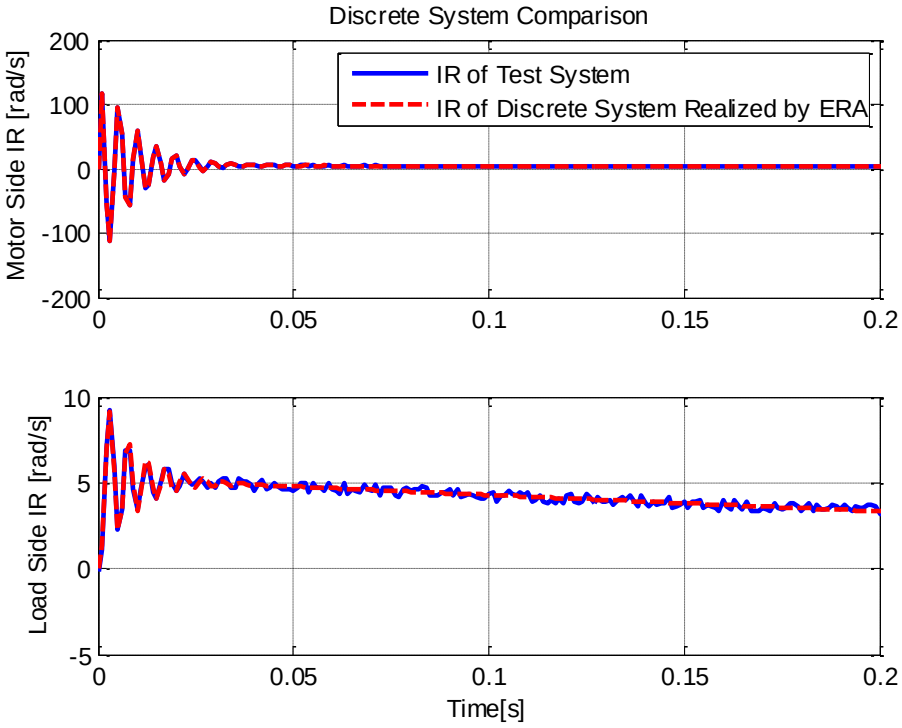

Figure 6.37 Comparison of Test System IR and Discrete System IR Realized by ERA

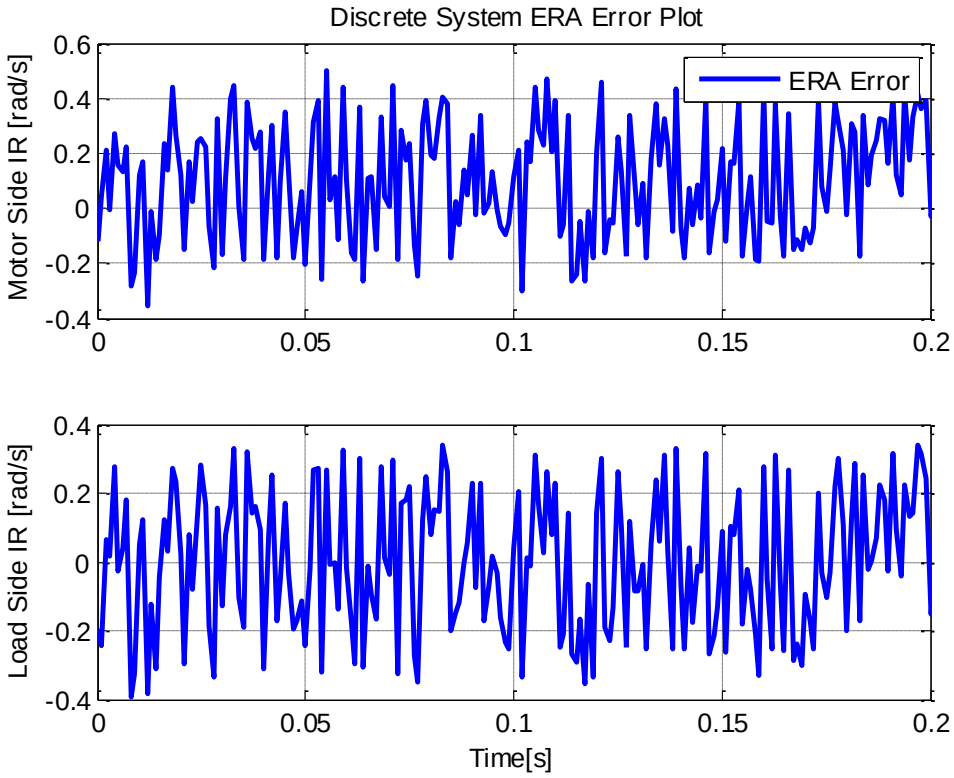

Figure 6.38 Realization Error of The Discrete System IR obtained by ERA

At this point in order to obtain, natural frequencies and system's physical parameters, the continues model must be converted to damped continuous modal displacement equivalent form, which is given below for the velocity output case as

$$\begin{aligned} \dot{\hat{z}} &= \Lambda_c\, z(t) + B_z u(t) \\ y(t) &= C_z\, z(t) \end{aligned} \tag{6.46}$$

where

$$\Lambda_c = \begin{bmatrix} -114.3 + 1303i & 0 & 0 & 0 \\ 0 & -114.3 - 1303i & 0 & 0 \\ 0 & 0 & -0.9428 + 1.680i & 0 \\ 0 & 0 & 0 & -0.9428 + 1.680i \end{bmatrix}$$

$$B_z = \begin{bmatrix} -305.5 + 69.87i \\ -305.5 - 69.87i \\ -64.50 - 58.42i \\ -64.50 + 58.42i \end{bmatrix} \qquad (6.47)$$

$$C_z = \begin{bmatrix} 0 + 2.104 * 10^{-4} i & 0 - 2.104 * 10^{-4} i & 0.002779 - 0.01300i & 0.002779 + 0.01300i \\ 0 & 0 & 0.002778 - 0.008812i & 0.002778 + 0.008812i \end{bmatrix}$$

Therefore, the damped natural frequencies are obtained from the imaginary parts of the continuous eigenvalues obtained as $w_{n1} = 1303 rad/s$ and the second one is $w_{n2} = 1.680 rad/s$. Here it should be noted that the second damped natural frequency does not correspond to any resonant mode of the system as the natural frequency value is too low and mode shapes for the second eigenvalue, shown in C_z are equivalent, which means rigid body movement rather than deflection. Moreover, in the test setup, as neither motor shaft, nor discs are connected to ground, actually the second eigenvalue corresponds to the rigid body mode of the test system.

Finally, the physical system parameters, which are the mass, stiffness and damping matrices are obtained through a transformation procedure as explained in the preceding sections. Here CBSI procedure is applied to the damped modal continuous form given above to extract physical system properties. For this purpose, as there is a single input applied to system, single scaling matrix is obtained through the analysis. As a result of the CBSI implementation, the extracted mass, stiffness and damping matrices are computed as follows.

$$[J]\ddot{\theta} + [D]\dot{\theta} + [K]\theta = \begin{bmatrix} 1 \\ 0 \end{bmatrix} u \qquad (6.48)$$

$$\hat{J} = \begin{bmatrix} 0.005673 & 4.689*10^{-4} \\ 4.689*10^{-4} & 0.1838 \end{bmatrix}$$
$$\hat{D} = \begin{bmatrix} 1.262 & -0.8268 \\ -0.8268 & 1.305 \end{bmatrix} \quad (6.49)$$
$$\hat{K} = \begin{bmatrix} 9363 & -9365 \\ -9365 & 9368 \end{bmatrix}$$

When the identified inertia matrix is investigated, it is observed that, there exists off diagonal inertia elements, which are not expected in any mechanical system. However, as their values are small, off diagonal inertia elements can be ignored as they may appear due to computational errors coupled through the noise and distortions on the measured input and output data. However, comparing the diagonal elements with the known inertia values of the motor and discs, there appears 42% error in the computation of motor inertia, and 2% error in the computation of the load inertia. In the motor inertia calculation, the error percentage may be seem too large; however, the actual amount of error is small, but as the inertia values is small too, the percent error becomes large. In this case indeed, the inertia of the gearbox, which was neglected at the beginning of the analysis, may be coupled to the motor inertia which explains the high percentage error and in this case the error gets down to 7%. Actually, when the internal structure of a planetary gearbox is considered contribution of gearbox inertia to motor side is reasonable, because the stiffness is in between the planet and sun gears, therefore, the input side always drives the input shaft and all the planet gears. In the stiffness matrix also a numerical error less than 0.04% is observed between diagonal and off-diagonal elements, which can be neglected by selecting the diagonal element is the equivalent stiffness value. In addition to that, damping matrix in this system is found to be proportional which is better to represent.

After finding mechanical system properties, the physical test system representation given in Figure 6.29, can be extended as shown in Figure 6.39.

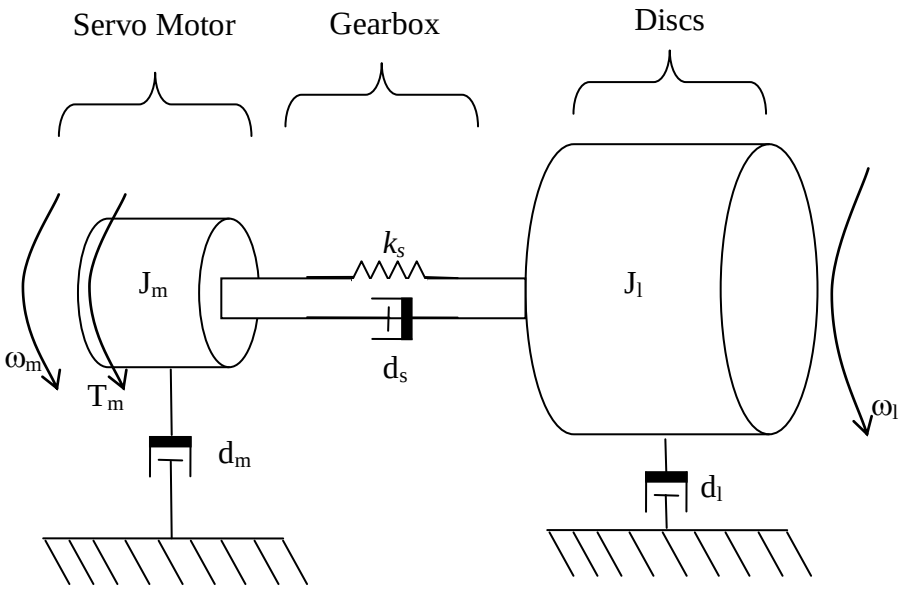

Figure 6.39 Realized Test System Representation

Here, the abbreviated symbols used in Figure 6.39 and their identified meanings are represented in Table 6.1.

Table 6.1 Equivalent Test Setup Parameters Realized via ERA

Variable Name	**Symbol**	**Value**
Motor Inertia	J_m	0.005673 kg.m^2
Load Inertia	J_l	0.1838 kg.m^2
Equivalent Gearbox Stiffness	k_s	9365Nm/rad
Equivalent Gearbox Damping	d_s	0.8268 Nm.s/rad
Motor Side Damping	d_m	0.4352 Nm.s/rad
Load Side Damping	d_l	0.4782 Nm.s/rad

After the identification procedure with ERA is completed, the second realization algorithm which is the Eigensystem Realization Algorithm with Data Correlation can be conducted to observe realization performance of the ERA/DC. In this case again, the impulse response function obtained via Wavelet analysis is used to form the Hankel Matrices. In this case the Hankel Matrices are again constructed using 500x500 Markov parameters, which results in 1000x500 dimension. Then the correlation matrices are obtained in the dimension of 1000x1000. After 100 Correlation Matrices are computed, Correlation Hankel Matrices are constructed. After the Correlated Hankel Matrices are obtained singular value decomposition is applied such that the singular values of the Correlated Hankel matrix are plotted against their values are shown in Figure 6.40.

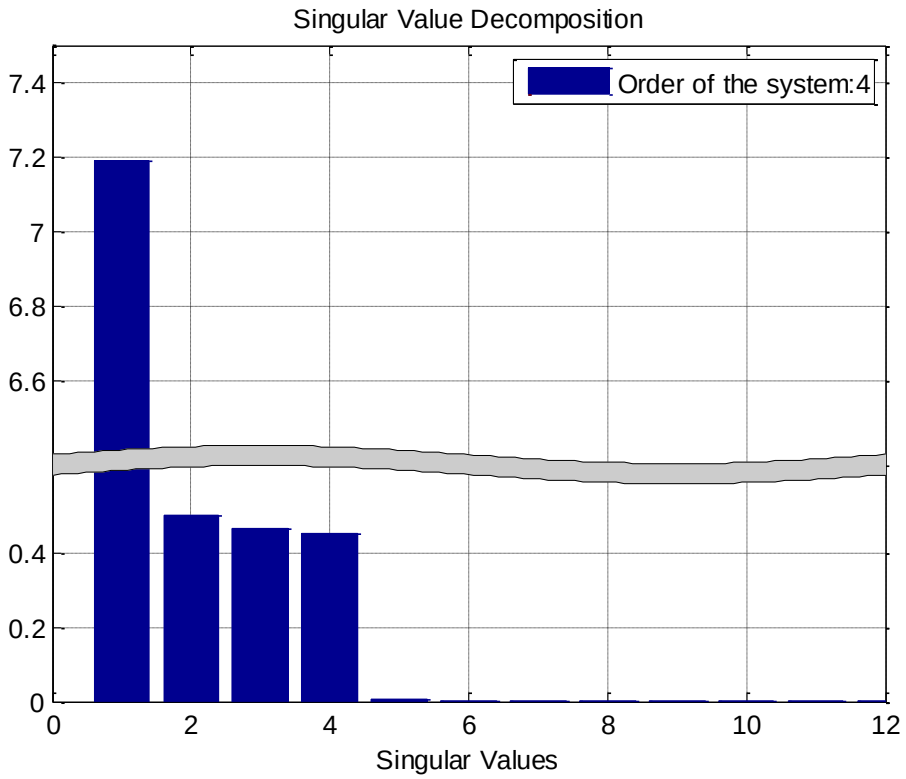

Figure 6.40 Singular Values of Correlated Hankel Matrix in ERA/DC Analysis for Test System

In Figure 6.40, although singular values above the 4th value, are not exactly 0, it can be observed that their values much lower than the ones obtained in the ERA analysis, which is expected as ERA/DC procedure tries to eliminate noise coupling by introducing correlation variables. Therefore again in this case, the effective order of the system is selected as 4. Then the left and right unitary matrices of the initial Correlated Hankel matrix are truncated according to the estimated system order.

After truncation, the ERA/DC procedure is followed and the realized discrete time system matrices $\hat{A}_0$, $\hat{B}_0$, $\hat{C}$, and $\hat{D}$ for the generalized discrete time state space representation are computed as follows.

$$\begin{aligned} x(k+1) &= \hat{A}_0\, x(k) + \hat{B}_0 u(k) \\ y(k) &= \hat{C}\, x(k) + \hat{D} u(k) \end{aligned} \tag{6.50}$$

where

$$\hat{A}_0 = \begin{bmatrix} 0.9965 & -0.001580 & -2.941*10^{-4} & 5.147*10^{-4} \\ -0.06036 & 0.9991 & 0.05778 & -0.02619 \\ -0.003034 & -0.03432 & 0.2251 & -0.8520 \\ -0.002588 & -0.05733 & 0.8656 & 0.2494 \end{bmatrix}$$

$$\hat{B}_0 = \begin{bmatrix} -0.08272 \\ -0.05502 \\ 0.5980 \\ 0.2057 \end{bmatrix} \tag{6.51}$$

$$\hat{C} = \begin{bmatrix} 0.07053 & -0.02057 & 0.2194 & -0.08757 \\ 0.07091 & -0.01152 & -0.007448 & 0.003256 \end{bmatrix}$$

$$\hat{D} = \begin{bmatrix} 0 \\ 0 \end{bmatrix}$$

Here again, it should be noted that $\hat{D}$ is a null matrix as the utilized feedbacks on the test system are velocity measurements.

Then the system model realized in the discrete time domain is transformed into continuous time domain. The discrete system model found in Equation (6.50) is converted to continuous time by using Matlab's built in "d2c" command with zero order hold method. Therefore, the resultant continuous time model is obtained as follows.

$$\begin{aligned} \dot{x}(t) &= \hat{A}x(t) + \hat{B}u(t) \\ y(t) &= \hat{C}x(t) + \hat{D}u(t) \end{aligned} \tag{6.52}$$

where

$$\begin{aligned} \hat{A} &= \begin{bmatrix} -3.467 & 1.573 & -0.6786 & 0.2437 \\ -5.894 & 1.196 & 71.16 & 15.08 \\ -4.777 & -70.12 & -131.3 & -1290 \\ -0.03073 & -28.42 & 1312 & -97.22 \end{bmatrix} \\ \hat{B} &= \begin{bmatrix} 83.04 \\ 31.25 \\ 671.5 \\ -221.9 \end{bmatrix} \\ \hat{C} &= \begin{bmatrix} 0.07053 & -0.02057 & 0.2194 & -0.08757 \\ 0.07091 & -0.01151 & -0.007448 & 0.003256 \end{bmatrix} \\ \hat{D} &= \begin{bmatrix} 0 \\ 0 \end{bmatrix} \end{aligned} \tag{6.53}$$

After discrete and continuous system realizations are obtained, in order to assess how good ERA/DC approximated the system impulse response function, the two performance measures which are modal amplitude coherence(MAC) and mode singular value(MSV) are computed. In this case MAC is computed as 1, 1 ; and 0.72 ,0.72 out of 1 for each identified eigenvectors. Here the MAC values appear as pairs, which is expected because the eigenvectors corresponding to each mode appear as complex conjugate pairs and for each pair the MAC value is equivalent. Here for the first and second mode, the correspondence between the identified modal time history and pulse response history exhibits perfect match and for the second mode, the

MAC value is computed slightly better than the ERA case. Whereas MSV gives the contribution of each mode to the identified impulse response function. In this case MSV is computed as 1.1, out of 1.8 for the first eigenvector pair and for the second eigenvector pair, the MSV is computed as 0.8 out of 0.8, which yields that very good approximation is obtained through the ERA/DC analysis. Additionally, in order to visualize the performance of ERA/DC, impulse response function of the test system, and the realized discrete model expressed in Equation(6.50), are shown in Figure 6.41. In Figure 6.41, the blue solid line represents the impulse response of the test system computed from Wavelet analysis and dashed red line represents the analytical impulse response function of the discrete state space model realized via ERA/DC analysis. Therefore, as indicated by MAC and MSV and verified in Figure 6.41 and Figure 6.42, very good realization is obtained through the ERA/DC analysis.

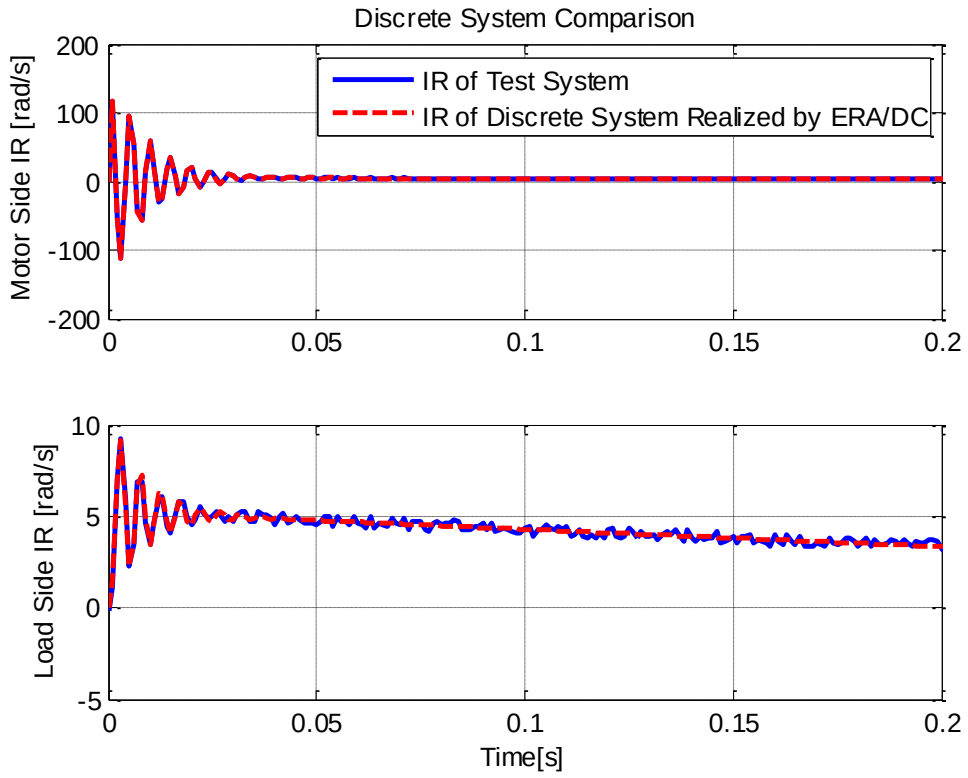

Figure 6.41 Comparison of Test System IR and Discrete System IR Realized by ERA/DC

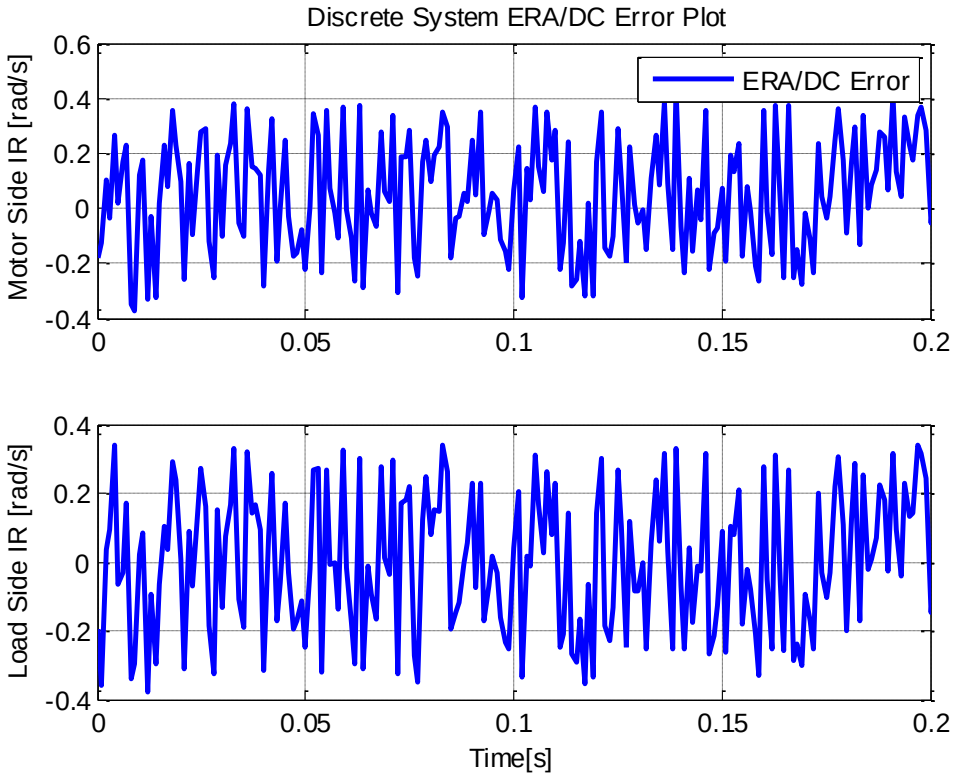

Figure 6.42 Error of The Discrete System IR obtained by ERA

At this point in order to obtain, natural frequencies and system's physical parameters, the continues model must be converted to damped continuous modal displacement equivalent form, which is given below for the velocity output case as

$$\begin{aligned} \dot{\hat{z}} &= \Lambda_c\, z(t) + B_z u(t) \\ y(t) &= C_z\, z(t) \end{aligned} \tag{6.54}$$

where

$$\Lambda_c = \begin{bmatrix} -0.9398 + 1.670i & 0 & 0 & 0 \\ 0 & -0.9398 - 1.670i & 0 & 0 \\ 0 & 0 & -114.5 + 1303i & 0 \\ 0 & 0 & 0 & -114.5 - 1303i \end{bmatrix}$$

$$B_z = \begin{bmatrix} 30.15 + 120.3i \\ 30.15 - 120.3i \\ -64.50 - 488.6i \\ -64.50 + 488.6i \end{bmatrix} \tag{6.55}$$

$$C_z = \begin{bmatrix} -0.01226 - 2.894*10^{-3}i & -0.01226 + 2.894*10^{-3}i & 1.221*10^{-4} + 3.898*10^{-5}i & 1.221*10^{-4} - 3.898*10^{-5}i \\ -0.01226 - 2.894*10^{-3}i & -0.01226 + 2.894*10^{-3}i & -4.0317*10^{-6} - 1.114*10^{-6}i & -4.0317*10^{-6} + 1.114*10^{-6}i \end{bmatrix}$$

Therefore, the damped natural frequencies are obtained from the imaginary parts of the continuous eigenvalues as $w_{n1} = 1.670 rad/s$ and the second one is $w_{n2} = 1303 rad/s$. Here it should be noted that, in this case the first damped natural frequency does not correspond to any resonant mode of the system as the natural frequency value is too low and mode shapes for the first eigenvalue pair, shown in C_z are equivalent, which means rigid body movement rather than deflection. Moreover, in the test setup, as neither motor shaft, nor discs are connected to ground, in this case the first eigenvalue corresponds to the rigid body mode of the test system.

Finally, the physical system parameters, which are the mass, stiffness and damping matrices are obtained through a transformation procedure as explained in the preceding sections. Here CBSI procedure is applied to the damped modal continuous form given above to extract physical system properties. For this purpose, as there is a single input applied to system, single scaling matrix is obtained through the analysis. Therefore, the extracted mass, stiffness and damping matrices are obtained as following.

$$[J]\ddot{\theta} + [D]\dot{\theta} + [K]\theta = \begin{bmatrix} 1 \\ 0 \end{bmatrix} u \tag{6.56}$$

$$\hat{J} = \begin{bmatrix} 0.005672 & 3.592*10^{-4} \\ 3.592*10^{-4} & 0.1840 \end{bmatrix}$$
$$\hat{D} = \begin{bmatrix} 1.279 & -0.8216 \\ -0.8216 & 0.8667 \end{bmatrix} \tag{6.57}$$
$$\hat{K} = \begin{bmatrix} 9378 & -9378 \\ -9378 & 9378 \end{bmatrix}$$

When the identified inertia matrix is investigated, it is observed that, there exists smaller off diagonal inertia elements, which are not expected in any mechanical system. However, as their values are small, off diagonal inertia elements can be

ignored as they may appear due to computational errors coupled through the measurement noise. However, comparing the diagonal elements with the known inertia values of the motor and discs, again there exists 43% error in the computation of motor inertia, and 2% error in the computation of the load inertia. In the motor inertia calculation, the error percentage may seem too large; however, the actual amount of error is small, but as the inertia values is small too, the percent error becomes large. Moreover, the inertia of the gearbox, which was neglected at the beginning of the analysis may be coupled to the motor inertia which explains the high percentage error and in this case the error gets down to 7%. Actually, when the internal structure of a planetary gearbox is considered contribution of gearbox inertia to motor side is reasonable, because the stiffness is in between the planet and sun gears, therefore, the input side always drives the input shaft and all the planet gears. In the stiffness matrix also, a numerical error less than 0.04% is observed between diagonal and off-diagonal elements, which can be neglected by selecting the diagonal element is the equivalent stiffness value. In addition to that, damping matrix in this system is found to be proportional which is better to represent, however as a result of ERA/DC analysis load side damping is computed less than the one found in the ERA analysis. In the reality, as the discs are directly connected to the output of the gearbox, excluding the equivalent damping of the gearbox, load side damping is expected to be low, which is consistent with identified damping value.

After finding mechanical system properties as a result of the ERA/DC analysis, parameters of the equivalent system representation given in Figure 6.39 can be tabulated in Table 6.2.

Table 6.2 Equivalent Test Setup Parameters Realized via ERA/DC

Variable Name	**Symbol**	**Value**
Motor Inertia	J_m	0.005672 kg.m^2
Load Inertia	J_l	0.1840 kg.m^2
Equivalent Gearbox Stiffness	k_s	9378Nm/rad
Equivalent Gearbox Damping	d_s	0.8216 Nm.s/rad
Motor Side Damping	d_m	0.4574 Nm.s/rad
Load Side Damping	d_l	0.04510 Nm.s/rad

To sum up, two different simulation models and a test setup are used to verify the performance of the realization and physical parameter determination algorithms explained in this study. When the results are investigated, it can be concluded that suggested algorithms and theories are working well on both simulation and test data. In the simulation case, as the system models are completely linear without any measurement noise, perfect match is obtained by the suggested realization and structural identification algorithms with less than 1% error. When the real test data is used, performance of the suggested methodologies are very good again for fairly low noise system measurements. It should be noted that, small deviation is observed on the physical system parameters computed as a result of ERA/DC when compared with the ones computed from ERA analysis, which is expected as ERA/DC provides slightly improved results.

CHAPTER 7

SUMMARY AND CONCLUSIONS

In this study, complete minimum order system identification application and physical parameter determination is investigated for linear and time-invariant system characteristics. The main idea behind obtaining system realization and physical system parameters is finding mass and stiffness distribution of the mechanical system, finding best possible sensor locations such that effective control action over the lumped masses can be determined. These requirements are resulted from both design and control of smaller and more agile stabilized mechanical platforms.

7.1 SUMMARY

For the specified purpose, system response determination methods are investigated in this study. As the realization algorithms applied in this study are both working in the time domain, methodologies obtaining time domain system characteristics are investigated. In time domain, system characteristics are represented by using impulse response functions and in the second chapter, direct time domain, Fourier transform method and Wavelet transform method are presented to obtain time domain impulse response function, from input and output measurements of the investigated system. In this chapter also basics and some properties of Wavelets are explained. However, although direct time domain approach is explained in this section, it is not actually implemented in this study as it is known to yield unstable impulse response function in most of the cases.

After impulse response determination algorithms are investigated, in the third chapter, second order system equations in matrix form is expressed for mechanical systems first. Then using proper transformation application, two specific first order state space model representations of the same system are obtained in the twice the size of the original second order representation. These two, first order models have their own special applications which are utilized both in system realization and control implementation. After state space models are obtained and their properties are represented, two more state space representations, which are in modal form, are expressed in chapter 3. Similarly, these two modal forms are obtained through proper transformations and these modal forms are especially used to determine modal characteristics of the system of interest, which are natural frequencies, modal damping and mode shapes.

After general models utilized in system identification are presented, in chapter 4, two minimum order, deterministic system realization algorithms which are ERA and its improved version, ERA/DC are expressed in details. These two realization algorithms, takes the discrete impulse response function of the system as their primary input and following through a numerically robust and straightforward procedure, they realize a minimum order discrete time state space representation on an arbitrary basis. In addition to that, transformation of discrete time domain state space system matrices, into continuous time domain are presented in this section as well.

Finally, in the fifth chapter, a transformation based procedure, which is called CBSI is presented to obtain physical system parameters from the realized first order state space models. In this application, full set of sensors are required at each degree of freedom of the system and at least one collocated sensor-actuator pair is required to obtain proper scaling matrix. This scaling matrix is important in the parameter extraction techniques, because realization algorithms computes arbitrary based normalized system models and in order to obtain actual system parameter,

transformation from arbitrary base into physical coordinated is a must and accomplished by the computed scaling matrix.

After the theory behind the minimum order, nonparametric and deterministic system identification is formulated, its performance and effectiveness is investigated first by two different simulation models. In the first model, a single degree of freedom translational system is investigated. In order to obtain impulse response function of the first model, both Fourier transform and Wavelet transform are implemented and in the transient response range, Fourier transform is found to yield wrong response whereas Wavelet transform technique yields the exact system impulse response characteristics. Therefore, the realization applications are performed by utilizing impulse response function obtained via Wavelet transform. Then, by constructing proper matrices with sufficient dimension, through singular value analysis, exact system order is obtain in a straightforward manner for both of the realization algorithms. After realized discrete state space models are obtained and transformed into continuous modal form, CBSI method is implemented to results of both of the realization algorithms. Finally, the results of the CBSI procedure, which are the physical system parameters, are found to perfectly match with the real system parameters used in simulation. In order to observe performance of the complete analysis, a second translational simulation model is constructed by with three degrees of freedom. In this case only Wavelet transforms is applied to extract impulse response functions. Then following the similar realization algorithms, true order of the system could obtained and from realized state space models, applying CBSI method, exact system properties are obtained. Within the simulations, no distortion or measurement noise was coupled to the input and output data and in this ideal case, the whole suggested identification procedure found to perform well.

On the other hand, in order to investigate performance of the identification procedure on real system data, a test setup, which is a simplified version of the stabilized machine gun platforms, is constructed. In the test setup, there is a single torque input applied by servo motor and two corresponding angular velocity outputs,

which are measured by resolver on the motor shaft and gyroscope on the discs. By using measured input and output data, first Fourier transform is utilized to obtain, impulse response of the test system; however, when the results are investigated noise and distortions on the pulse response identified by Fourier transform was found dominant, which resulted in wrong system impulse response characteristics. Then Wavelet transform is applied to the measure input and output signal to find impulse response characteristics. Moreover, the results of Wavelet transform technique are found good enough to represent actual impulse response characteristic of the test system. Although measurement noise is coupled to Wavelet generated impulse response histories, their magnitude is small compared with the responses obtained as a result of Fourier analysis. Then both Eigensystem Realization Algorithm and Then both Eigensystem Realization Algorithm with Data Correlations are applied to the impulse response function of the test system computed via Wavelet transforms, good realizations are obtained as numerically and visually inspected. During realizations, system order determination resulted slightly different from the simulation cases. As there exists measurement noise coupled to computed impulse response functions, from the results of the singular value decomposition, the system order is not directly obtained as the true value due to measurement noise, smaller valued singular values appear after correct number of nonsingular values. However, as there occurs big difference between the correct nonsingular values and the ones resulted due to noise, singular values are truncated after selected number of nonsingular values. After realizations are obtained, CBSI methodology is implemented to the realized models, and physical system parameters are obtained. In order to visualize system model, using identified mechanical system parameter, an equivalent system model is visualized and their identified parameters are represented for both realization algorithms. Although small discrepancy observed in the identified motor inertia value, it can be explained by taking the inertia of the gearbox into consideration. To sum up, when the results of the realization algorithms and physical parameter extraction method are investigated, it can be deduced that very good identification

performance is obtained through the suggested identification procedure. Finally, the whole identification process is visualized in the flowchart given in Figure 7.1.

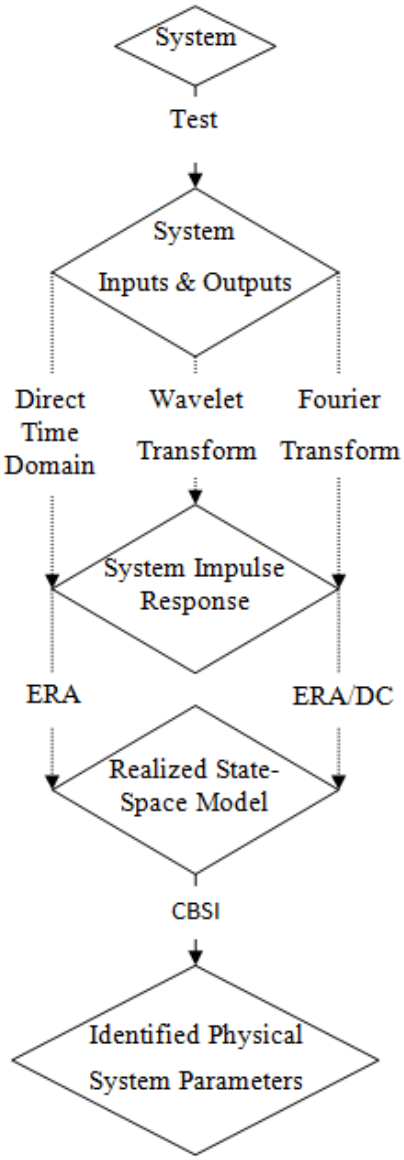

Figure 7.1 Identification Process Flowchart

7.2 CONCLUSION

When the overall identification process is considered, impulse response calculation is the key component to yield true system characteristics, however, Fourier analysis

and Direct time domain approach failed in this manner. On the other hand, the results of Wavelet transform technique are found good enough to represent impulse response characteristics of physical systems.

The selected realization algorithms, ERA and ERA/DC are computationally straightforward and superior in terms of determining true system order, as verified in both simulation and test systems. However noise is the primary distortion in a linear system identification application and ERA/DC is better at dealing with noise on the measurement data.

The selected physical system parameter determination method, CBSI performs true transformation from realized system models into physical system properties, however as it requires full set of sensors, in an actual large scale system, number of sensors must be high.

To sum up, whole identification procedure described in this study is evaluated as performing good enough to be used in real system development and verification application.

7.3 FUTURE WORK

In the future, the suggested identification methodology shall be applied to one of the actual stabilized platforms with incorporating enough number of measurement sensors. In addition to that, as high levels of measurement noise is one of the primary problem against linear system identification, by incorporating stochastic methods, characteristic of noise can be determined and noise suppression can be achieved by incorporating a proper Kalman Filter. Another improvement can be achieved by utilizing an observer to extract impulse response characteristics of the system rather than using Fourier or Wavelet analysis techniques. In real life as most of the mechanical systems exhibit nonlinear characteristic, incorporating nonlinearities into state space modeling and realizations is one of the major research topic that shall be studied in the future.

REFERENCES

[1] Juang, J., *Applied system identification*. Englewood Cliffs, NJ: Prentice Hall, 1994.

[2] Sincar, E., "Friction identification and compensation in stabilized platforms." *MS Thesis, Middle East Technical University*, 2013.

[3] Ljung,L., "Development of system identification," *Proceedings of the 13th IFAC world congress*, 1996, San Francisco, USA, pp. 141-146.

[4] Gevers, M., "A personal view of the development of system identification: a 30-year journey through an exciting field," *Control Systems, IEEE*, 2006, vol. 26, no. 6. pp. 93–105.

[5] Åström, K. J. and Eykhoff, P., "System identification—a survey," *Automatica*, vol. 7, no. 2, pp. 123–162, Mar. 1971.

[6] Åström, K. J. and Bohlin, T., "Numerical identification of linear dynamic systems from normal operating records," Theory of self-adaptive control systems, Teddington, Engl. In *Theory of Self-Adaptive Control Systems*, Plenum Press, New York, 1966.

[7] Ho, B. & Kalman, R., "Editorial: Effective construction of linear state-variable models from input/output functions." *at - Automatisierungstechnik*, 14(1-12), 1966, pp. 545-548.

[8] Akaike, H., "A new look at the statistical model ıdentification," *IEEE Trans., Autom. Control AC-19*, 1974, pp. 716-723.

[9] Box, G. E. P. and Jenkins, G. (1970), *Time Series Analysis, Forecasting and Control* (4th ed.), Hoboken, NJ: J. Wiley, 2008.

[10] Wahlberg, B. and Ljung, L., "Design variables for bias distribution in transfer function estimation," *IEEE Trans. Autom. Control.*, 31, 1986, pp. 169-192.

[11] Ljung, L., *System Identification : Theory for the User*. Upper Saddle River, NJ, USA: Prentice Hall PTR, 1987.

[12] Juang, J. and Pappa, R., "An eigensystem realization algorithm for modal parameter ıdentification and model reduction," *J. Guidance, Control and Dynamics*, Vol.8, 1985, pp. 620-627.

[13] J. Juang, "An overview of recent advances in system identification," *NASA Workshop on Distributed Parameter Modeling and Control of Flexible Aerospace Systems*, June 1994, pp. 279-289.

[14] Lew, J., Juang, J., and Longman, R., "Comparison of several system ıdentification methods for flexible structures," *Journal of Sound and Vibration 167*, 1993, pp.461-480.

[15] Chuang M., Chen, S., and Tsuei, Y., "Modal parameter identification by eigensystem realization algorithm," *Proceedings of SPIE, the International Society for Optical Engineering*, vol. 3089, 1997, pp.41-49.

[16] Sanchez-Gasca, J., "Computation of turbine-generator subsynchronous torsional modes from measured data using the eigensystem realization algorithm," *Power Engineering Society Winter Meeting, 2001. IEEE* , vol.3, pp.1272,1276.

[17] Petsounis, K. and Fassois, S., "Parametric time-domain methods for the identification of vibrating structures—a critical comparison and assessment," *Mechanical Systems and Signal Processing Vol.15,* November 2001, pp.1031-1060.

[18] Hill, M., "An Experimental Verification of the Eigensystem Realization Algorithm for Vibration Parameter Identification," *Student Research Accomplishments: Multidisciplinary Center for Earthquale Engineering Research University at Bufalo, NY*, 2004, pp. 29-37.

[19] Ulusoy, H. S., Feng, M. Q., & Fanning, P. J., "System identification of a building from multiple seismic records," *Earthquake Engineering & Structural Dynamics*, 2011, Vol.*40*(6), pp. 661-674.

[20] Amaddeo, C., Özçelik, Ö., Mısır, S., and Kahraman, S., "Identification of dynamic parameters of structures using earthquake data abstract," *E-Journal of New World Sciences Academy*, vol. 4, num. 3, 2009.

[21] Siringoringo, D., Abe, M., and Fujino, Y., "System Identification of Instrumented Bridge Using Earthquake-induced Record," *Proceedings of 22nd IMAC Conference and Exposition 2004: A Conference and Exposition on Structural Dynamics*, 26-29 Jan. 2004, Dearborn, MI, USA.

[22] Robertson A., Park. K., and Alvin. K., “Extraction of impulse response data via wavelet transform for structural system identification,” *Journal of Vibration and Acoustics*, Vol. 120, 1998, pp. 252-260.

[23] Polikar R., "The story of wavelets," *in Physics and Modern Topics in Mechanical and Electrical Engineering*, (ed. Mastorakis, N), World Scientific and Engineering Society Press, 1999, pp. 192-197.

[24] Daubechies, I., *Ten Lectures on Wavelets*. Montpelier, Vermont: Capital City Press, 1992.

[25] Newland, D. E., *An introduction to random vibrations, spectral and wavelet analysis*, 3rd Edition, Minelo, New York : Dover Publications, 1993.

[26] Alvin, K., Robertson, N., Reich, G., and Park, K., “Structural system identification: from reality to models,” *Computers & Structures*, 2003, vol. 81, no. 12, pp. 1149–1176.

[27] Misiti, M., Misiti Y., Oppenheim, G., and Poppi, J., “Wavelet Toolbox User Guide,”, Mathworks, 2014.

[28] Alvin, K. F., “Second-order structural identification via state-space-based system realizations,”, PhD Thesis, University of Colorado at Boulder, 1993.

[29] Ogata, K., *Modern Control Engineering*, 4th ed. Upper Saddle River, NJ, USA : Prentice Hall PTR, 2001.

[30] Lus, H., et al., “Constructing second-order models of mechanical systems from identified state space realizations. Part I: Theoretical discussions,” *Journal of Engineering Mechanics,2003, Vol.129, pp.477-488*.

[31] Lus, H., et al., “Constructing second-order models of mechanical systems from identified state space realizations. Part II: Numerical investigations,” *Journal of Engineering Mechanics,2003, Vol.129, pp. 489-501.*

[32] Bernal D. and Güneş B., “ Extraction of second order system matrices from state space realizations,” *Proceedings of 14th ASCE Engineering Mechanics Conference,* 2000, Austion, TX, USA.

[33] Mathworks, “Simulink getting started guide,” (r2014a), Retrieved May, 30, 2014 from http://www.mathworks.com/help/pdf_doc/simulink/sl_gs.pdf.

[34] Erdoğan O. C., Kılıç B., and Arı, E. O., "Dinamik Sistemlerin Modellenmesi," *Proceedings of 1st ASELSAN-SSTKON*, 2012, Ankara, TURKEY.

APPENDIX A

DATA SHEETS OF TEST SETUP COMPONENTS

SERVO DRIVER HERKUL-1D

HERKÜL-1D

HERKÜL – 1D, 24 VDC – 2 x 50 A, Dual Axis Servo Controller

- Servo controller developed for small to medium caliber gun and missile platforms, electro-optics and radar systems
- 100 A total current output in independently driven two lines
- Torque, speed and position control, integral stabilization control
- Adaptability to mission requirements owing to DSP technology
- Conformance to military specs (MIL-STD-810 & MIL-STD-461)
- Broad range of interface and sensor options
- Test interface and automated built-in test feature

Product Features

- High efficiency motor control using ASELSAN servo controller technology
- Torque, speed, position and stabilization control
- Application specific configuration (parametric motion limits, no-fire zone, maximum speed and acceleration)
- Extensive built-in self-test
- Over-heat and over-current protection
- Fanless cooling and silent operation

Technical Data

- Drives two 50 A brushless DC motors
- 18-32 VDC supply voltage
- Peripheral interfaces:
- Analog
- Serial (CAN, RS-232/422)
- Resolver
- Encoder (SSI/EnDat)
- Dimensions: 310 mm x 230 mm x 100 mm
- Weight: 7 kgf
- Conforms to MIL-STD-810 & MIL-STD-461
- Operating temperature: -40°C – +62 °C
- Storage temperature: -40 °C – +75 °C
- Vibration: 15 – 2000 Hz, 0.1 g^2/Hz
- Shock: 40 g, 11 ms MIL-STD-810
- EMC/EMI: MIL-STD-461

Figure A- 3 Data Sheet Of Servo Driver Herkul-1D

MOOG D323 SERVO MOTOR

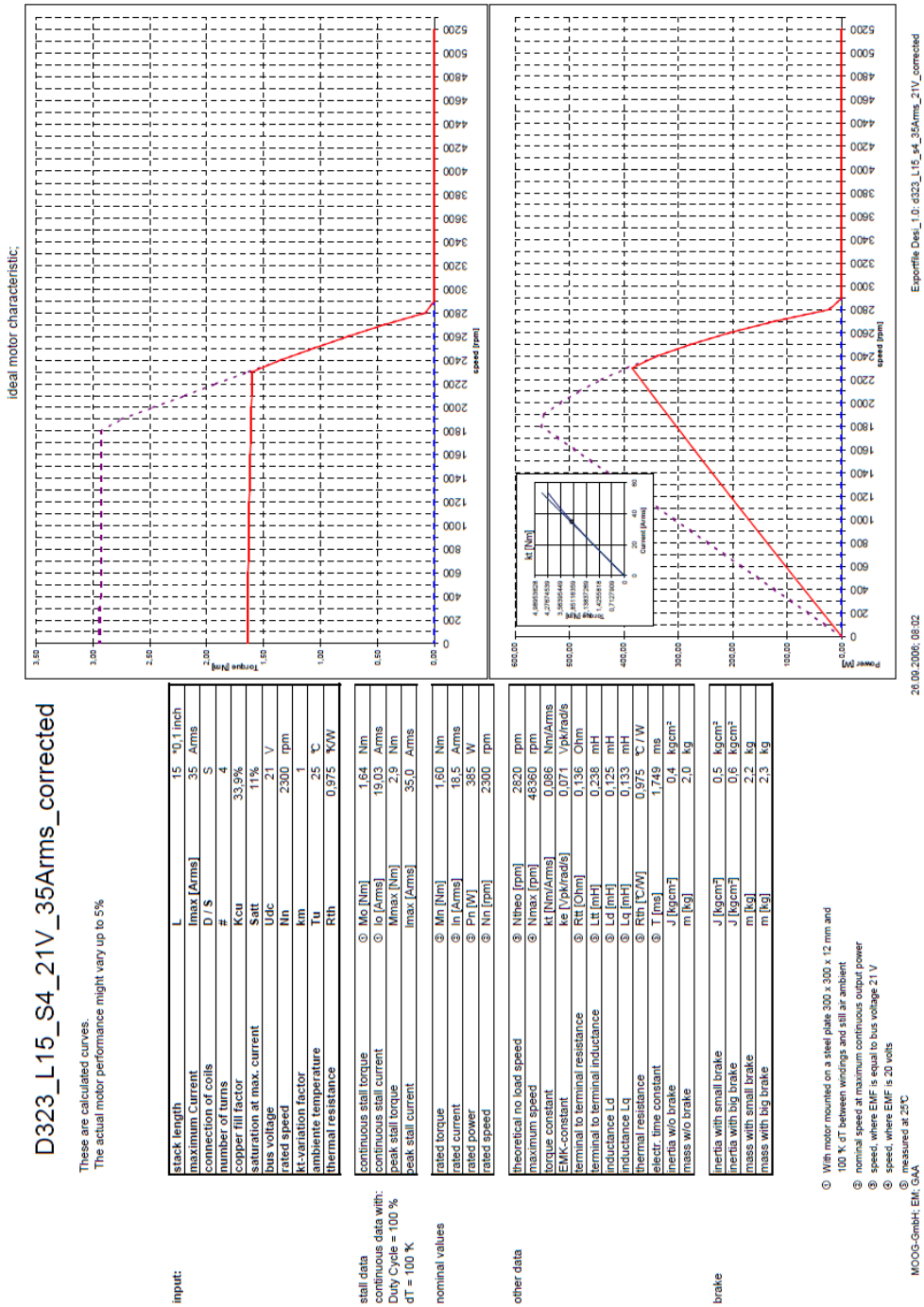

Figure A- 4 Data Sheet Of Moog D323 Servo Motor

APEX AD064 GEARBOX

Gearbox Performance

Model No.		Stage	Ratio[1]	AD047	AD064	AD090	AD110	AD140	AD200	AD255
Nominal Output Torque T_{2N}	Nm	1	5	22	60	160	330	650	1,200	2,000
			7	19	50	140	300	550	1,100	1,800
			10	14	40	100	230	450	900	1,500
		2	25	22	60	160	330	650	1,200	2,000
			35	19	50	140	300	550	1,100	1,800
			50	22	60	160	330	650	1,200	2,000
			70	19	50	140	300	550	1,100	1,800
			100	14	40	100	230	450	900	1,500
Max. Output Torque T_{2B}	Nm	1,2	5~100	3 times of Nominal Output Torque						
Nominal Input Speed n_{1N}	rpm	1,2	5~100	5,000	5,000	4,000	4,000	3,000	3,000	2,000
Max. Input Speed n_{1B}	rpm	1,2	5~100	10,000	10,000	8,000	8,000	6,000	6,000	4,000
Micro Backlash P0	arcmin	1	5~10	-	-	≤1	≤1	≤1	≤1	≤1
		2	25~100	-	-	-	≤3	≤3	≤3	≤3
Reduced Backlash P1	arcmin	1	5~10	≤3	≤3	≤3	≤3	≤3	≤3	≤3
		2	25~100	≤5	≤5	≤5	≤5	≤5	≤5	≤5
Standard Backlash P2	arcmin	1	5~10	≤5	≤5	≤5	≤5	≤5	≤5	≤5
		2	25~100	≤7	≤7	≤7	≤7	≤7	≤7	≤7
Torsional Rigidity	Nm/arcmin	1,2	5~100	3	7	14	25	50	145	225
Max. Bending moment M_{2B}[2]	Nm	1,2	5~100	42.5	125	235	430	1,300	3,064	5,900
Max. Axial Load F_{2r}[2]	N	1,2	5~100	1,080	2,110	2,310	4,800	6,200	5,450	10,600
Service Life	hr	1,2	5~100	30,000*						
Efficiency η	%	1	5~10	≥97%						
		2	25~100	≥94%						
Weight	kg	1	5~10	0.7	1.2	3.0	5.6	11.9	31.6	56.1
		2	25~100	1.0	1.6	3.7	7.3	15.9	36.9	70.4
Operating Temp	°C	1,2	5~100	-10°C~+90°C						
Lubrication		1,2	5~100	synthetic gear grease (NYOGEL 792D)						
Degree of Gearbox Protection		1,2	5~100	IP65						
Mounting Position		1,2	5~100	all directions						
Noise Level (n_1=3000rpm)	dB	1,2	5~100	≤56	≤58	≤60	≤63	≤65	≤67	≤70

Gearbox Inertia

Model No.		Stage	Ratio[1]	AD047	AD064	AD090	AD110	AD140	AD200	AD255
Mass Moments of Inertia J_1	kg • cm²	1	5	0.03	0.13	0.47	2.71	7.42	23.29	53.27
			7	0.03	0.13	0.45	2.62	7.14	22.48	50.97
			10	0.03	0.13	0.44	2.57	7.03	22.51	50.56
		2	25	0.03	0.03	0.13	0.47	2.71	7.42	23.29
			35	0.03	0.03	0.13	0.47	2.71	7.42	23.29
			50	0.03	0.03	0.13	0.44	2.57	7.03	22.51
			70	0.03	0.03	0.13	0.44	2.57	7.03	22.51
			100	0.03	0.03	0.13	0.44	2.57	7.03	22.51

1. Ratio ($i=N_1 / N_{out}$)
2. Applied to the output flange @ 100 rpm
*S1 service life 15,000 hrs

Figure A- 5 Data Sheet Of Apex AD064 Gearbox

STIM 202 GYROSCOPE

SPECIFICATIONS

Parameter	Min	Nom	Max	Unit
Weight		55		g
Input range		±400		°/s
Resolution		24		bit
Operating temperature	-40		85	°C
Power supply	4.5	5.0	5.5	V
Supply current		200		mA
Start-up time			10	s
Sampling frequency			1000	SPS
Storage temperature	-50		90	°C
Dynamic overload			5000	°/s
Mechanical shock			1500	g
In-run bias stability		0.5		°/h
Angular random walk		0.2		°/√h
Bandwidth (-3dB)			262	Hz
Non-linearity (BSL over +/- 200 °/s)			200	ppm
Scale Factor accuracy		±0.2		%
Bias temperature accuracy (1σ)		±30		°/h rms
Linear acceleration effect			18	°/h/g
RS422 bit rate			921600	bit/s
Input resistance (termination ON)		120		Ω
Input resistance (termination OFF)		125		Ω
RESET PIN (NRST)				
Logic levels		CMOS and TTL compatible		
Minimum hold time for reset	5			ms

MECHANICAL DIMENSIONS

All dimensions in mm.

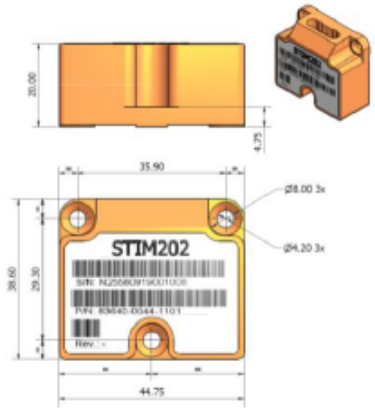

FUNCTIONAL BLOCK DIAGRAM

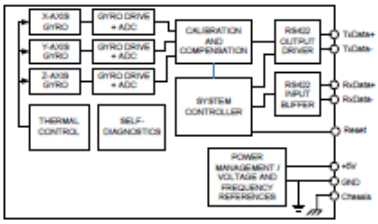

ALLAN VARIANCE

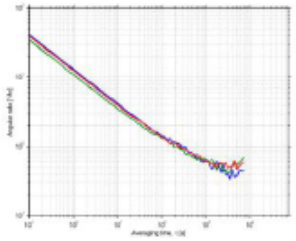

BIAS STABILITY

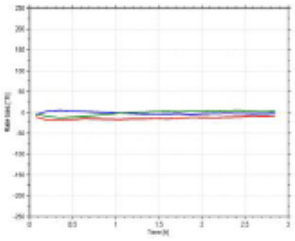

PIN OUT

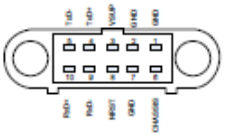

AXIS DEFINITIONS

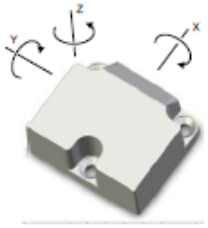

ELECTRICAL CONNECTIONS

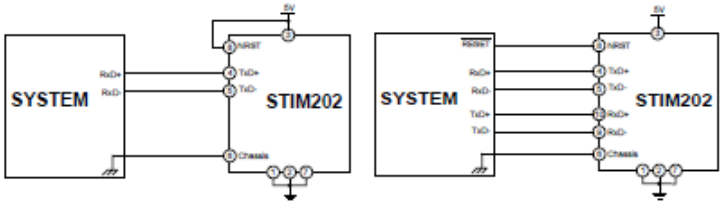

TRANSMIT ONLY

FULL FUNCTION

Figure A- 6 Data Sheet Of Stim 202 Gyroscope